

Copyright  
by  
William James Kelton  
2013

**The Dissertation Committee for William James Kelton Certifies that this is the  
approved version of the following dissertation:**

**Engineering Antibody Fc Domains for Improved Therapeutic Function**

**Committee:**

---

George Georgiou, Supervisor

---

Haley Tucker

---

Jennifer Maynard

---

Hal Alper

---

Lauren Ehrlich

# **Engineering Antibody Fc Domains for Improved Therapeutic Function**

**by**

**William James Kelton, B.E**

## **Dissertation**

Presented to the Faculty of the Graduate School of

The University of Texas at Austin

in Partial Fulfillment

of the Requirements

for the Degree of

**Doctor of Philosophy**

**The University of Texas at Austin**

**December 2013**

## **Dedication**

To all those who have made it possible for me to make it to this point, especially my parents Simon and Adrienne, my sister Catherine, and of course Nicole.

## **Acknowledgements**

I have been very fortunate to have the help of several people on my way to Texas including Prof Conan Fee and members of the Chemical and Process Engineering Department at the University of Canterbury. I thank them for all their encouragement and support. Likewise, I am deeply appreciative of the financial support I received from the J R Templin Trust, Fulbright New Zealand and the Tertiary Education Commission that made my study here possible.

At the University of Texas I have had the pleasure to work with and learn from many exceptional scientists including Dr Tom van Blarcom, Dr Sang Taek Jung, Dr Moses Donkor, Tae Hyun Kang and Jiwon Lee. My research has also been greatly aided by a number of very talented undergraduate researchers (Diya Liu, Nishuant Mehta and Rachel Yan) who have promising careers in science ahead of them. I am indebted to Prof George Georgiou who took a chance in hiring me and allowed me such an excellent opportunity to pursue my research with a large amount of academic freedom. Finally, I thank all the members of the BIGG lab who have made my time here in Texas most enjoyable, I hope to see you all in New Zealand someday.

# **Engineering Antibody Fc Domains for Improved Therapeutic Function**

William James Kelton, PhD

The University of Texas at Austin, 2013

Supervisor: George Georgiou

Therapeutic antibodies have achieved exceptional clinical success in the treatment of cancer and other human diseases. Now, new approaches are required to enhance the potency of antibodies to further increase the number of patients responding to therapy. By engineering the antibody Fc domain through mutation of the amino acid sequence, binding affinity to activating or inhibitory Fc receptors on effector cells can be increased to modulate the cellular immune response. However, attaining selectivity for closely related Fc receptors has proved challenging and the technique has not been applied to access the function of antibody isotypes other than IgG. Here we present new methods for enhancing antibody potency using both hybrid IgA/G and aglycosylated Fc domains. In the first instance, a chimeric antibody Fc domain has been created by combining residues from IgA with those from IgG. The new variant, MutD, introduces binding to Fc $\alpha$ RI while retaining affinity for certain members of the Fc $\gamma$ R family. ADCC assays show MutD, when part of a full length trastuzumab antibody against Her2 antigen, can kill Her2-overexpressing tumor cell lines as effectively as IgA antibodies. Moreover, MutD shows improved assembly compared to IgA and thus provides access to potent Fc $\alpha$ RI function while overcoming the expression and purification barriers that have limited the use of IgA as a therapeutic. Alternatively, aglycosylated antibodies may be

engineered for exceptional effector function. Glycans anchored to residue N297 of the antibody IgG Fc domain are typically critical in mediating binding toward the FcγRs. Yet, using a full length bacterial IgG display system, we have isolated aglycosylated Fc1004 with mutations that confer a 160-fold increase in the affinity toward the low affinity FcγRIIa-R131 allele as well as high selectivity against binding to the remarkably homologous inhibitory receptor, FcγRIIb. Incorporation of this engineered Fc into trastuzumab resulted in a 75% increase in tumor cell phagocytosis by macrophages compared to that of the parental glycosylated trastuzumab with medium Her2-expressing cancer cells. *In vivo* testing of Fc1004 using NOD/SCID mouse model, reconstituted by adoptive transfer of leukocytes from FcγRIIa-R131 homozygous donors, showed a promising reduction in tumor burden in SkBr-3 Her2+ xenografts.

## Table of Contents

List of Tables .....	xii
List of Figures .....	xiii
Chapter 1: Introduction .....	1
Antibodies as Therapeutics .....	1
Antibody Structure and Classes .....	2
Antibody Glycosylation .....	6
Antibody Biology and Function .....	7
Fc $\gamma$ R Mediated Function .....	9
Fc $\alpha$ RI Receptor Mediated Function .....	13
Fc Mediated Activation of the Classical Complement System .....	14
Monoclonal Antibodies In the Clinic .....	15
Next Generation Therapeutics by Antibody Engineering .....	17
Amino Acid Modification in Glycosylated Antibodies .....	18
Glycan Modification for Enhanced Therapeutic Effect .....	21
Aglycosylated Antibodies as Novel Therapeutics .....	22
Looking Beyond the IgG1 Isotype .....	28
Chapter 2: Engineering of an IgG/IgA Chimeric Fc Domain with Fc $\alpha$ RI and Fc $\gamma$ R Receptor Binding .....	29
Introduction .....	29
Materials and Methods .....	31
Alanine Mutagenesis .....	31
Construction and Expression of Fc Domain IgA/G Chimeras .....	32
Mammalian Expression of Fc receptors .....	32
Fc Receptor Binding ELISAs .....	33
Construction and Expression of Full Length IgA/G Chimeras and Control Antibodies .....	33
Mammalian Expression of Monomeric Fc $\gamma$ RIIa, Fc $\gamma$ RIIb and Fc $\alpha$ RI Receptors .....	34
SPR Affinity Measurements .....	35



ADCC Assays .....	36
Mammalian Expression of FcRn Peptide Fusion to MutD .....	37
FcRn Binding ELISA Assay .....	38
Results.....	39
Characterization of IgA interaction with the Fc $\alpha$ RI receptor .....	39
Construction and Receptor Binding Properties of Hybrid IgA/IgG Mutants .....	42
Evaluation of Full Length IgA/G Hybrid Binding to Fc Receptors and Complement Factors .....	43
<i>In vitro</i> Recruitment of Effector Cells by IgA/G Hybrid Antibodies for Tumor Cell Killing .....	48
Approaches for Half-life Extension of MutD Hybrid IgA/G antibodies .....	51
Discussion.....	54
Chapter 3: Effective Phagocytosis of Low Her2 Tumor Cell Lines with Engineered, Aglycosylated IgG Displaying High Fc $\gamma$ RIIa Affinity and Selectivity .....	57
Introduction.....	57
Materials and Methods.....	60
Library Construction .....	60
Culture and Spheroplasting of <i>E. coli</i> for Library Screening .....	60
Library Screening.....	61
SPR Analysis .....	61
ELISAs.....	62
HER2 Cell Surface Density .....	63
Preparation of Human Monocyte-derived Macrophages .....	63
Quantification of Fc $\gamma$ Rs on Macrophages.....	64
ADCP Assays.....	65
Results.....	66
Development and Characterization of a Full Length Antibody Display System in Bacteria.....	66

Isolation and Characterization of Aglycosylated IgG Fc Variants Displaying High Affinity and Binding Selectivity towards the FcγRIIa-R131 Allele.....	68
Enhanced ADCP of Low and Medium Her2 <sup>+</sup> Cell Lines .....	72
Mathematical Modeling of ADCP .....	76
Discussion.....	81
Chapter 4: An Engineered Aglycosylated Fc Variant with High FcγRIIa-R131 Selectivity over FcγRIIb Shows NK Cell-Independent Killing of Her2+ Tumors <i>in vivo</i> .....	83
Introduction.....	83
Materials and Methods.....	86
Construction and Expression of Full Length trastuzumab Fc1004 and Control Antibodies.....	86
Endpoint PCR Genotyping .....	87
Taqman Probe Genotyping .....	88
Preparation of Human Monocyte-derived Macrophages.....	89
ADCP Assays.....	90
Pharmacokinetic Study of Aglycosylated Fc1004 in Mice.....	90
SkBr-3 Tumor Xenograft Cancer Model .....	91
Results.....	93
Genotyping of Donors for FcγRIIa Polymorphism .....	93
Effect of FcγRIIa Polymorphism on Killing of Her2+ Tumor Cells by Fc1004 .....	95
<i>In vivo</i> Pharmacokinetics of Aglycosylated Fc1004.....	97
Enhanced Clearance of Her2+ Tumors in NOD/SCID Mice Reconstituted with Immune Cells from Human FcγRIIa- R131 Donors .....	99
Discussion.....	104
Chapter 5: Future Directions and Perspectives .....	106
Engineering New Fc Mutants .....	106
Investigating the Mechanism and Potential of Engineered Fc Variants .....	107
Applications for Aglycosylated Fc1004 .....	109

Appendix A.....	113
Appendix B .....	121
Materials and Methods.....	121
Molecular Biology Techniques.....	121
IgG Display in <i>E. coli</i> for FcγR Binding .....	124
Protein Expression and Purification.....	125
Construction and Parameterization of Mathematical Model .....	126
Appendix C .....	146
Appendix D.....	148
Materials and Methods.....	148
Transgenic Mouse ADCP Assay .....	148
References.....	149

## List of Tables

Table 1.1:	The Average Immunoglobulin Isotype Concentrations and Half-life in Human Sera. ....	4
Table 1.2:	The Distribution and Affinity of the Human Fc $\gamma$ Rs for IgG. ....	10
Table 1.3:	Aglycosylated Antibodies in Current or Past Clinical Trials.....	23
Table 2.1:	SPR Data for MutD Binding to Fc Receptors.....	45
Table 3.1:	SPR Analysis. ....	71
Table 4.1:	PCR Reaction Conditions for Endpoint Genotyping. ....	88
Table 4.2:	Half-life of Fc1004 and Clinical Grade Herceptin Antibodies in Mouse Serum. ....	99
Table A.1:	Plasmids Used in Chapter 2. ....	113
Table A.2:	Primers Used in Chapter 2. ....	113
Table A.3:	Oligonucleotides Used in Chapter 2. ....	115
Table B.1:	Plasmids Used in Chapter 3. ....	131
Table B.2:	Primers Used in Chapter 3. ....	133
Table B.3:	Kinetic On and Off Rates for Trastuzumab Fc Variant Binding to Fc $\gamma$ Rs as Determined by SPR Analysis. ....	135
Table B.4:	Parameters Used to Generate Fc $\gamma$ RIIa/b Activation Model.....	136
Table B.5:	Intrinsic Signaling Potencies of Fc $\gamma$ RIIa-H131, Fc $\gamma$ RIIa-R131, and Fc $\gamma$ RIIb.....	137
Table C.1:	Plasmids Used in Chapter 4. ....	146
Table C.2:	Primers Used in Chapter 4. ....	146
Table C.3:	Genotypes of Anonymous Donors and Frequencies of Observed Alleles .....	147

## List of Figures

Figure 1.1: Typical Antibody Structure.....	3
Figure 1.2: The Role of Antibodies in Mediating Inflammatory Responses by Bridging the Innate and Adaptive Arms of Immunity. ....	8
Figure 1.3: The Path to Developing Fully Human Antibodies.....	16
Figure 1.4: Strategies for Improving Antibodies by Engineering the Fc Domain.....	18
Figure 1.5: The Aglycosylated Fc5 Mutant.....	27
Figure 2.1: Residues Selected for Alanine Scanning in the Human IgA Fc Domain.....	40
Figure 2.2: ELISA Analysis of Binding between IgA Variants with Alanine Point Mutations.....	41
Figure 2.3: 4-20 % SDS-PAGE Analysis of Full Length Expression of Trastuzumab Antibodies. ....	44
Figure 2.4: ELISA Analysis of Variant Binding to Fc $\gamma$ RIIIa.....	46
Figure 2.5: ELISA Analysis Shows MutD can Simultaneously Bind to both Fc $\alpha$ RI and Fc $\gamma$ RI.....	47
Figure 2.5: MutD Binds C1q from the Classical Complement Pathway. ....	48
Figure 2.6: MutD Mediated Killing of Her2+ SkBR-3 Cells by ADCC.....	50
Figure 2.7: Characterization of MutD with C-terminal Peptide Fusion Binding to FcRn at pH 5.8 and 7.4. ....	52
Figure 2.8: Afucosylated IgG1 Fc Domain in Complex with Fc $\gamma$ RIIIa (PDB: 3ay4). ....	55
Figure 3.1: Overlaid Fc $\gamma$ RIIIa (PDB: 1H9V) and Fc $\gamma$ RIIb (PDB: 2FCB) have High Structural Homology and Sequence Identity. ....	58

Figure 3.2: Full Length Display of IgG Antibodies in Bacteria.....	66
Figure 3.3: Mutations Isolated in AglycoT-Fc1001 (A) and AglycoT-Fc1004 (B) are Shown on the 3D Structure of an Aglycosylated IgG1 Fc (PDB: 3S7G).....	69
Figure 3.4: Expression Level of Her2 and FcγR on Tumor Cell Lines and Macrophages for ADCP Assay.....	73
Figure 4.1: PCR Endpoint Genotyping of Anonymous Donor Pool.....	94
Figure 4.2: Genotyping Using Real-time PCR and Taqman Probes.....	95
Figure 4.3: Representative ADCP Data for Genotyped Individuals in the Killing of Her2+ MDA-MB-453 Breast Cancer Cells.....	97
Figure 4.4: Pharmacokinetic Profile of Serum Persistence of Fc1004 as Compared to Clinical Grade Herceptin.....	98
Figure 4.5: Experimental Design for Adoptive Transfer Tumor Xenograft Study.....	101
Figure 4.6: Adoptive Transfer Tumor Xenograft Study.....	102
Figure 5.1: Experimental Design for the Evaluation of Engineered Fc Domain Mediated Antigen Presentation for Enhanced T Cell Activation.....	109
Figure 5.2: Partial Mechanism of Ipilimumab Action.....	110
Figure 5.3: ADCP of Her2+ MDA-MB-453 Breast Cancer Cells by Transgenic FcγRIIa/b Mouse Macrophages.....	111
Figure A.1: SDS-PAGE Gel Showing Expression of IgA Fc Alanine Scanning Mutants Expressed in HEK293F Cells.....	117
Figure A.2: Characterization of Aglycosylated IgA Expressed in Bacteria.....	117
Figure A.3: Sequence Alignment of IgA/G Variants with Wild Type IgG.....	118

Figure A.4: Characterization of IgA/G Domain Swap Variants. ....	118
Figure A.5: SPR Analysis of MutD Affinity for FcγRIIa, FcγRIIb and FcαRI at Equilibrium. ....	119
Figure A.6: Kinetic Analysis of MutD Affinity for FcγRI by SPR. ....	120
Figure B.1: <i>E. coli</i> Bacterial Expression System for the Display of Full Length IgGs. ....	138
Figure B.2: Sequences and Corresponding FACS Signals for Isolated Fc Variants. ....	139
Figure B.3: Characterization of Isolated Aglycosylated Fc Variants. ....	140
Figure B.4: Biacore Sensorgrams for FcγRIIa-R131-GST, FcγRIIa-H131- GST and FcγRIIb-GST Binding to Aglycosylated Mutants. ....	141
Figure B.5: Expression Level of Her2 and FcγR on Tumor Cell Lines and Macrophages for ADCP Assay. ....	142
Figure B.6: ADCP Analysis for Ovarian Cancer Cells Expressing Medium HER2 Density (SKOV-3) and Low HER2 Density (MDA-MB- 453). ....	143
Figure B.7. The Model Returns Similar Predictions for Receptor Signaling Potency Independent of Experimental Data Used for Parameterization. ....	145

## **Chapter 1: Introduction**

### **ANTIBODIES AS THERAPEUTICS**

Antibodies are an essential part of the adaptive immune response that serves to protect a host against an immense diversity of disease causing agents. As a key aspect of antibody function, immune cells may be linked to pathogenic targets with exceptional specificity to enact a vast array of inflammatory and anti-inflammatory actions that modulate the immune response during the resolution of an infection. Harnessing these molecules as protein therapeutics has revolutionized the treatment of human disease over the last century by curing or extending survival times of patients with notoriously difficult to treat conditions such as cancer, bacterial infection and autoimmunity. The advent of recombinant DNA technology has rapidly improved the discovery of new antibodies with specificity against nearly any target desired. As of February 2013, 34 monoclonal antibodies have been approved for treatment in the US, generating over \$ 64 billion in sales in 2012 [1, 2]. This figure constituted more than 50 % of the total sales for all biologics in the same year. The success of antibodies in the clinic is the culmination of more than one hundred years of intensive investigation encompassing the fields of immunology, medicine and protein engineering. Antibodies were first used therapeutically, albeit unknowingly, in 1890 when Emil von Behring and Kitasato Shibasaburo first demonstrated the concept of ‘passive immunization’ [3]. This technique involved the transfer of serum from animals immunized with diphtheria, to animals with a current infection, in order to clear the disease. Later, the approach was adapted in the 1940’s for use in humans to treat patients with measles [4]. However, despite widespread use of this technology in the early 20<sup>th</sup> century little was known about the biochemical and molecular nature of the antibodies conferring protection. Breakthroughs in the late 1950’s and early 1960’s led to the discovery of antibody structure thus paving the way



for facile manipulation of the amino acid sequence and subsequent function that make these molecules so successful as drugs today [5, 6]. The following sections outline several new and novel approaches being developed to create next generation antibody therapeutics with enhanced potency.

## **ANTIBODY STRUCTURE AND CLASSES**

Largely due to the work of the Nobel laureates Edelman and Porter, antibodies were found to be tetramers comprised of two identical heavy and two identical light polypeptide chains (Figure 1.1). In addition to several intramolecular disulfide bonds within the antibody domains, the structure is further stabilized by intermolecular disulfide bonds between the heavy chains in the flexible hinge region as well as disulfide bonds that serve to link the light and heavy chains. This pairing of the heavy chain variable (VH) and light chain variable (VL) domains creates an antigen binding pocket that determines antibody specificity. Within the variable domains, contacts with cognate antigens are primarily mediated by regions of especially high sequence diversity termed the complementary determining regions (CDRs).

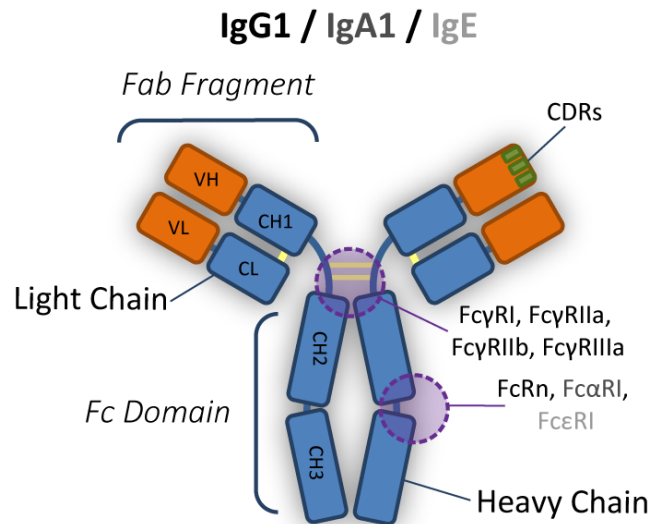


Figure 1.1: Typical Antibody Structure.

Antibodies are comprised of two heavy and two light chains assembled in a tetramer. Binding sites for Fc receptors are indicated in purple for each isotype. Interchain disulfide bonds are indicated yellow.

While antibody VH/VL specificity is essential in focusing the immune response towards a particular pathogen, the constant region of the antibody ultimately determines how the pathogen is cleared. Humans express five main antibody classes (IgG, IgA, IgM, IgD and IgE) each characterized by a unique constant region that can promote inflammatory or inhibitory responses by interaction with various components of the immune system. Critically important to this function is the Fc domain where the majority of receptor binding occurs, as shown in Figure 1.1. In addition to mediating the clearance of pathogens, the Fc domain is also responsible for controlling the pharmacokinetics of each antibody class through interaction with specialized receptors that recycle the antibodies from serum (Table 1.1).

Table 1.1: The Average Immunoglobulin Isotype Concentrations and Half-life in Human Sera.

Isotype	Allotype	Antibody Concentration (mg/mL)	Serum Half Life (days)
IgG	IgG1	7.2 – 7.8 [7]	21 [8]
	IgG2	2.4 – 3 [7]	21[8]
	IgG3	0.6 – 1.2 [7]	7.1[8]
	IgG4	0.36 – 0.72 [7]	21[8]
IgA	IgA1	1.12 – 2.90 [9]	5.9 [9]
	IgA2	0.12 – 0.47[9]	4.5 [9]
IgE	IgE	0.0003 [10]	2 [11]
IgM	IgM	1.47 ± 0.84 <sup>a</sup> [12]	10 [11]
IgD	IgD	0 – 0.061 [13]	2.8 [14]

<sup>a</sup> indicates ± 1 SD

In healthy human serum, IgG is represented at the highest concentrations and mediates potent immune function by binding to Fc gamma receptors (FcγRs), complement proteins or by direct neutralization of targets such as viruses. Within this isotype, 4 subclasses are found (IgG1, IgG2, IgG3 and IgG4) each with distinct binding profiles to the FcγRs and factors from the complement cascade. IgG1 and IgG3, which most strongly activate complement and bind the FcγRs, are typically produced in response to protein antigens whereas IgG2 and IgG4 more often respond to carbohydrate moieties [15]. IgG1 has been widely adopted for therapeutic purposes both for its potent Fc function and also because this antibody subclass is characterized by an extraordinarily long half-life of ~21 days as a result of the recycling action of FcRn receptors that are constitutively expressed on epithelial cells.

In some applications however, the use of other antibody isotypes might confer certain physiological advantages. For example, although no therapies have been approved to date, IgA antibodies have evolved to be well suited for immune defense at mucosal surfaces. In fact, due to the immense surface area of the mucosa, the average human

synthesizes 66 mg/kg/day of all forms of IgA, more than all the other immunoglobulin classes combined [16]. Several adaptations have emerged to allow for transport of such large quantities of antibody across the mucosal epithelial and to protect IgA from proteolytic challenge in the harsh mucosal environment. IgA first dimerizes by association with the J chain protein, thus creating a molecule with enhanced antigen affinity by avidity, before binding to the polymeric Ig receptor (pIgR). A transcytosis event follows and the pIgR is cleaved to release secretory IgA into the mucosa. The cleaved fragment of the pIgR (secretory component) remains bound to stabilize the IgA dimer as well as promote adherence to the surrounding mucous [17]. Furthermore, the predominant subclass secreted to the mucosa, IgA2, contains heavily glycosylated and very short hinge regions which offer further protection from proteases.

IgA is also curiously represented in monomeric form at higher serum concentrations in humans than in the sera of other animal species. As shown in Table 1.1, the allotypes of IgA can comprise up to 25% of the total serum immunoglobulins. The reasons for this uniquely high concentration are yet to be determined, but a leading hypothesis suggests humans can use serum IgA to reduce inflammation in the periphery by engagement to Fc receptors [18]. Mechanisms such as this could be important in reducing any undesirable inflammatory activity mediated by a therapeutic antibody.

In contrast to IgA and IgG much less is known about the therapeutic potential of the remaining human antibody isotypes. Holding nearly equal serum representation as IgA is IgM which is uniquely expressed as a pentamer by forming disulfide linkages between the CH4 domains of adjacent antibodies [19]. In pentameric form, the J chain can also associate with IgM to allow for secretion via the pIgR at mucosal surfaces. IgM antibodies typically have low somatic hypermutation and as a result are lower in affinity than their IgG or IgA counterparts. Avidity generated by the pentameric structure

provides a boost to raise the apparent affinity of the complex. The final two isotypes, IgE and IgD, have the lowest serum representation of all the antibodies and the shortest serum half-lives. IgE is most often implicated in allergy and in response to parasite infection [20]. IgD on the other hand is normally expressed in membrane bound form on B cells and the function it might fulfill in serum is not clear.

### **Antibody Glycosylation**

Post translational modification by the addition of glycans plays an essential role in fine-tuning antibody structure and interaction with the immune system. IgG function and immune cell recruitment is particularly dependent on N-linked glycosylation at residue N297 for promoting interaction with various Fc receptors. The loss of glycosylation either through enzymatic digestion or expression in systems lacking glycosyltransferase machinery results in the near complete loss of antibody mediated cell cytotoxicity (ADCC) [21]. Other antibody isotypes, such as IgA, contain additional O-linked and N-linked glycosylation sites and in humans close to 30% of Fab domains have N-linked glycosylation [22]. The biotechnology sector has spent considerable effort ensuring the glycan composition on therapeutic antibodies is consistent and well defined from batch to batch by engineering sophisticated expression systems and cell lines [23-25]. Inconsistency of the glycan composition can have a huge impact on the therapeutic effect of an antibody. The most notable example is the lack of fucosylation at the free terminus of the antibody glycan which improves the affinity of IgG for FcγRIIIa by 50 fold [26]. Conversely, the presence of high levels of terminal sialylation induces anti-inflammatory effects though stronger antagonism of the DC-SIGN receptor [27].

## ANTIBODY BIOLOGY AND FUNCTION

The mechanism of antibody generation is an ancient and highly conserved evolutionary adaptation. Understanding this process is essential in the design and discovery of new antibody therapeutics. *In vivo*, enormous antibody diversity is achieved through the mechanism of VDJ recombination in pre B cells in which genomic loci (V, D and J genes) are rearranged to form VH domains and spliced together with the IgM constant domain locus [28]. While combinatorial selection of V, D and J elements from a large genomic pool generates substantial antibody sequence variety, most of the diversity is concentrated in the CDR3 regions due to non-templated end joining of the D and J segments. The antibody VL domain undergoes a similar process but lacks the D segments of the VH. Some estimates put the potential number of unique antibodies that can be generated by this process (VH and VL domain diversity) in excess of  $1 \times 10^{13}$  [29]. Following rearrangement of the germline DNA, pre B cells egress from the bone marrow to germinal centers in the peripheral lymph tissue where IgD generated from alternative splicing of the IgM locus is up-regulated on B cell surfaces to form immature B cells [30]. The germinal center provides an ordered environment rich with the co-stimulatory signals required to mature B cells in with strict specificity for a single antigen. To ensure responses are mounted against potential pathogenic threats, circulating antigen presenting cells (APCs) return from surveying the periphery to display foreign antigens in peptide form on major histocompatibility complexes (MHCs) (Figure 1.2).

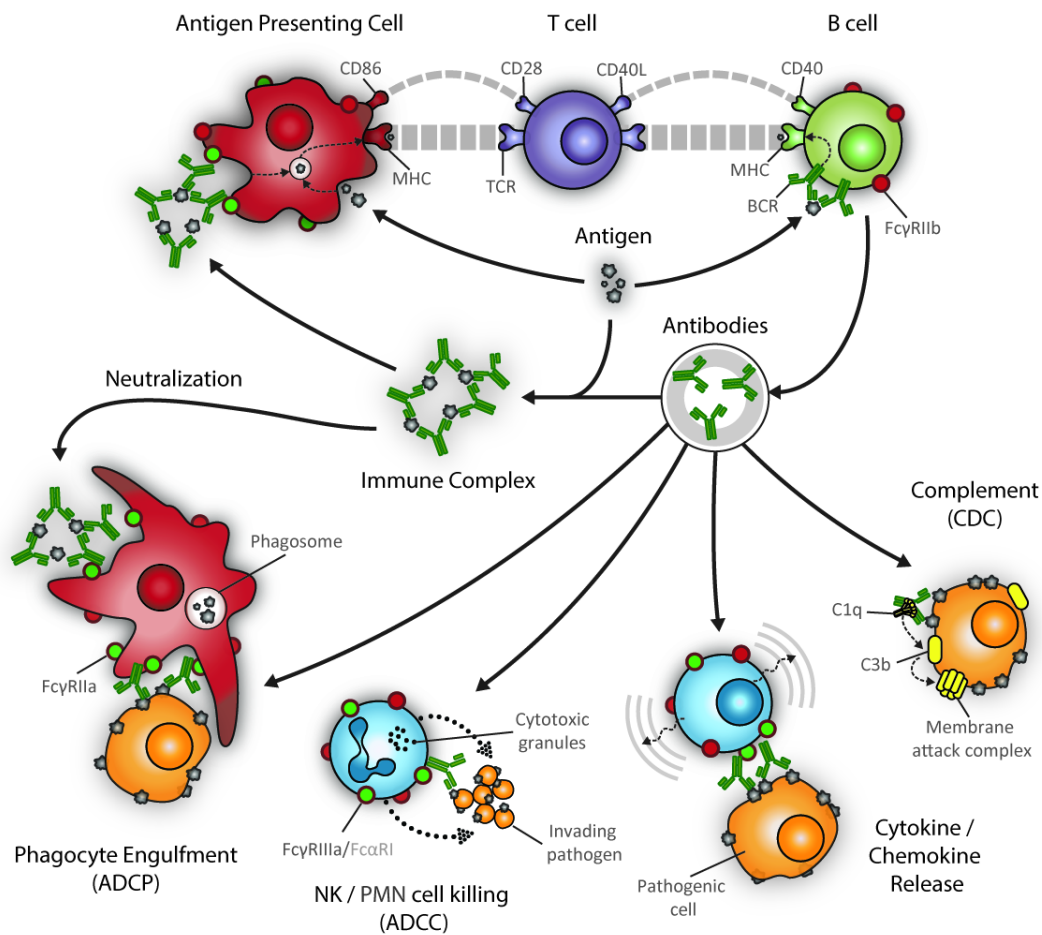


Figure 1.2: The Role of Antibodies in Mediating Inflammatory Responses by Bridging the Innate and Adaptive Arms of Immunity.

Antigen presenting cells sample circulating antigen to activate helper T cells which in turn activate antigen specific B cell responses. Coating of target pathogens by these antibodies elicits a wide range of killing responses including antibody dependent cell phagocytosis (ADCP), antibody dependent cell cytotoxicity (ADCC), the release of cytokines and chemokines to influence the local immune environment and the activation of the complement pathway.

MHCs on the surfaces of APCs are recognized by T cell receptors to activate the adaptive arm of immunity either through the generation of antigen specific CD4 T helper cells or by activation of potent cytotoxic CD8 T cells with direct cell killing ability. CD4 helper T cells provide strong activation and maturation signals for B cells expressing membrane

bound IgM (B cell receptor) of the correct specificity. In certain circumstances, such as multivalent polysaccharide antigens, B cells may also be activated in a T cell-independent manner when multivalent antigens binding directly to the B cell receptor [31]. This is especially important as it allows for antibodies to be generated to conformational epitopes rather than just linear peptides. In either case, once a B cell matures class switch recombination may be initiated, in which the constant domain sequences of IgM or IgD are replaced with those of IgG, IgA or IgE. The isotype of the antibody is determined by many complex factors including the nature of the T cell help if present, the nature of the antigen and the cytokine environment in the germinal center. After class switching, soluble antibody is secreted but further affinity and specificity refinement may be made by successive rounds of activation-induced (cytidine) deaminase (AID) mediated somatic hypermutation [32]. Once suitable VH and VL sequences have been generated, mature B cells can either terminally differentiate plasma cells that produce massive quantities of antibodies or become memory cells, ready to respond rapidly to new onsets of the same infection. The criteria by which the immune system controls antibody selection for memory is yet to be fully defined but it appears high affinity is not the sole governing factor.

### **FcγR Mediated Function**

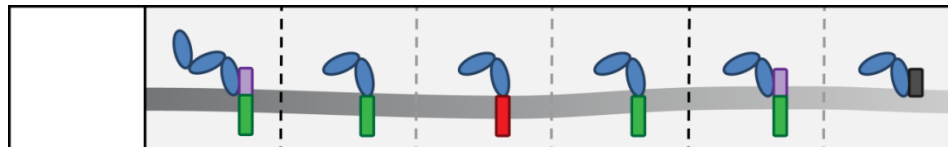
Both native antibodies generated during an immune response and recombinant therapeutic antibodies have an impressive array of mechanisms by which to destroy targets. Importantly, antibodies can facilitate activation of the innate or ‘non-specific’ immune system as well as the adaptive or ‘acquired’ immune system (Figure 1.2). Innate immunity provides a rapid frontline response to target commonly encountered pathogen motifs whereas the slower adaptive immune response described above provides longer



lasting specific protection. However, in some cases direct neutralization by antibodies is sufficient to confer protection such as the case with the clearance of some viruses [33]. In either case, understanding the vital role antibodies play in clearing infection allows for new strategies to be developed for creating better therapeutics.

In some cases, multivalent antigens allow many antibodies to bind simultaneously and form immune complexes (ICs) in a process known as opsonization. The close aggregation of a large number of Fc domains allows for the recruitment of immune cell subsets through interaction with surface bound Fc receptors [34].

Table 1.2: The Distribution and Affinity of the Human FcγRs for IgG.



Class	FcγRI	FcγRII			FcγRIII	
Subclass	FcγRI	FcγRIIa	FcγRIIb	FcγRIIc	FcγRIIIa	FcγRIIIb
Expression	Macrophages Monocytes Dendritic cells Eosinophils Neutrophils	Macrophages Monocytes Dendritic cells Platelets Neutrophils	Macrophages Monocytes Dendritic cells Eosinophils Neutrophils Mast cells B lymphocytes	NK cells	Macrophages Monocytes Dendritic cells Mast cells NK cells	Eosinophils Neutrophils Mast cells
IgG1 affinity	1.67 nM	980 nM	2.5 μM		1.8 μM	

A subtle balance of FcR affinity, quantity of membrane bound FcR molecules and the nature of the transduced signal ultimately determine the outcome of the cellular immune response. The most widely studied receptors are those that bind IgG or FcγRs. In humans, three main classes of IgG activating receptors are expressed (FcγRI, FcγRIIa, FcγRIIIa) while only a sole inhibitory receptor exists (FcγRIIb) (Table 1.2) [35]. The activating receptors trigger inflammatory signals via an immune-tyrosine activating motif (ITAM)

either as an intracellular tail of the receptor protein or through non-covalent association with a common gamma chain. A signaling cascade follows, beginning with SYK kinase and resulting in ERK, p38 and JNK signaling up-regulation to promote ADCC, ADCP, cytokine release and oxidative burst depending on the cell type activated [36] (Figure 1.2). Inhibitory signals are induced in a similar manner by FcγRIIb which contains an intercellular immunotyrosine inhibitory motif (ITIM). Phosphorylation of the ITIM by LYN results in the recruitment of SHIP phosphatase and the blocking of signaling pathways that would otherwise activate the cell.

Of the activating receptors FcγRI is best defined by an unusually high affinity due to the presence of a third extracellular domain. The exact role of this receptor in immune responses is not clear but several reports have demonstrated a strong ability to cross-present antigenic peptides in MHC complexes on professional APCs such as dendritic cells [37]. Cross presentation leads to the induction of strong cytotoxic T cell responses and is very important in the clearance of pathogens. FcγRI expression is also reported on several other cell types at varying levels; however the inflammatory state of the surrounding environment can have profound impact on receptor levels on cell surfaces. For example, the expression of FcγRI on neutrophils is increased significantly upon treatment with G-CSF [38].

FcγRIIa is the most widespread activating receptor with expression on most myeloid cells excepting lymphocytes and natural killer (NK) cells. Both high and low responding allelic variants are found in the population (H131 and R131 respectively) and the high affinity polymorphism is thought to have improved response to therapeutic antibodies and an improved clearance rate of immune complexes [39-41]. Unlike FcγRI and FcγRIIIa this receptor has the ITAM domain as a part of its intracellular tail rather than requiring the common gamma chain.

FcγRIIIa is perhaps the best understood Fc receptor and is expressed on professional APCs (macrophages, dendritic cells) as well as mast cells, NK cells and monocytes (Table 1.2). Importantly, FcγRIIIa strongly activates NK cell mediated ADCC, a mechanism that is shown to contribute strongly to the therapeutic effect of several clinical antibodies [42, 43]. Much of the evidence supporting this finding is due to the poorer therapeutic response for some cancers in donors homozygous for the lower affinity F158 polymorphism rather than the high affinity V158 polymorphism [44]. FcγRIIIa also has an unusual receptor homologue, FcγRIIIb, with a nearly identical extracellular domain but lacking any intracellular signaling domain. Strangely, this receptor does not recruit the common gamma chain for signaling and thus little is known about its function, except that it possibly associates with FcγRIIa in some cases [44].

The extracellular domain of the sole IgG inhibitory receptor FcγRIIb shares 93% sequence identity with FcγRIIa and down-regulates or often overrides the inflammatory response generated by activating FcγRs. Notably, FcγRIIb plays a critical role in preventing the development of autoimmunity by regulating B-cell responses at multiple stages of development [45, 46]. The loss of this essential receptor function in FcγRIIb knockout mice leads to development of autoantibodies [47]. In the context of therapeutic antibodies, FcγRIIb is important in defining the activating-to-inhibitory ratio (A/I) as determined by the affinity of the Fc domain for certain activating FcγRs (FcγRI, FcγRIIa, FcγRIIIa) divided by the Fc affinity for FcγRIIb. The A/I ratio has been used to evaluate the likelihood of clinical success of various antibody isotypes and engineered Fc variants; higher ratios typically correlate with activation of a more potent ADCC response [48, 49]. This was convincingly demonstrated in a seminal paper by Clynes and Ravetch in which FcγRIIb knockout xenograph mice ( $A/I > \infty$ ) showed greatly reduced tumor burden when treated with clinical grade Herceptin [50]. However, more recent studies

have revealed counter intuitive functions of Fc $\gamma$ RIIb suggesting the interplay between activation and inhibition is much more complex. For example, Fc $\gamma$ RIIb appears to be required for immunostimulatory activity in the function of agonistic anti-CD40 antibodies [51].

The exceptional half-life of IgG is mediated by FcRn a heterodimeric receptor that binds to the Fc domain at the CH2/CH3 interface. The FcRn name is derived from the essential function it performs in neonates whereupon maternal IgG is transcytosed across the placenta to provide protection against pathogens until the adaptive immune system can be trained in the first few weeks of life. At physiological pH in serum, IgG binds to FcRn with very poor affinity. However, random pinocytosis of humoral fluids by epithelial cells serves to sequester antibodies in acidified endosomes. The shift to a lower pH markedly improves IgG affinity for FcRn thus allowing transport across the cell layer. In adult life this pH dependency means IgG is bound to FcRn at the endosomal membrane and sorted for return to the cell surface rather than being targeted for degradation [52]. Surprisingly, this receptor has been found to play a key role in the cross presentation of antigen by certain dendritic cell subsets which is important for the induction of cytotoxic T cell responses [53].

### **Fc $\alpha$ RI Receptor Mediated Function**

While the Fc $\gamma$ Rs have been intensively studied in order to elucidate the mechanism of action of therapeutic IgG antibodies, the receptors of other antibody isotypes can have surprisingly potent action. The Fc domain of IgA associates with several receptor classes including Fc $\alpha$ R1, pIgR (transcytosis of IgA), and Fc $\alpha$ / $\mu$ R (receptor internalization and endocytosis) [54]. The best characterized of these receptors is Fc $\alpha$ R1 or CD89, a close homologue of the leukocyte Ig-like receptors [55]. Fc $\alpha$ R1 is

constitutively expressed on many cells of the myeloid lineage such as neutrophils, macrophages, Kupffer cells and eosinophils but not on lymphocytes, mast cells and basophils [56]. In contrast to IgG binding to Fc $\gamma$ R receptors, glycosylation of the Fc domain is not essential for binding to the Fc $\alpha$ R1 and aglycosylated Fc domains bind with similar affinity [57]. This receptor can both activate and inhibit potent inflammatory responses depending on the level of receptor aggregation triggered by IgA crosslinking via the bivalent binding of antigens [58]. In effect, non-specific inflammatory responses would be reduced in the periphery while targeted inflammatory responses strongly activated at required sites. When activation does occur, recruitment of the common gamma chain bearing an ITAM motif to Fc $\alpha$ RI triggers phagocytosis, respiratory burst and cytokine release [59]. On neutrophils, the interaction of IgA with Fc $\alpha$ R1 is far more effective at tumor cell killing than any other class of Fc receptor and was the motivation for the work presented in Chapter 1 [60].

### **Fc Mediated Activation of the Classical Complement System**

As well as leveraging powerful killing effects by cellular recruitment, IgG isotype antibodies can also recruit proteins from the classical complement pathway to directly lyse target cells or mark them for clearance (Figure 1.2). Initially, the C1 complex binds to the antibody Fc domain thus triggering conformational changes that result in proteolytic cleavage of C3 to deposit C3b fragments on the target surface. Once again the glycan appended to N297 in the Fc domain is critical in facilitating the C1q subunit interaction. C3b can mark the pathogen for complement receptor mediated phagocytosis or go on to recruit other complement proteins to form a membrane attack complex that

lyses the cell. Complement action is suspected to be particularly important in the clearance of some lymphoma cancers [61].

## **MONOCLONAL ANTIBODIES IN THE CLINIC**

A combination of superb specificity and the exceptional ability of antibodies to activate both the adaptive and innate arms of the immune system have largely contributed to their clinical and commercial success. The exploitation of monoclonal antibodies as therapeutics was facilitated greatly by Milstein and Kohler in 1975 who developed hybridoma technology for which they received a share of a Nobel prize in 1984 [62]. Hybridomas are generated by the fusion of a murine myeloma cell line and a B cell producing a single antibody clone to create an immortalized cell line. Problems with the severe immunogenicity of murine antibodies, whereupon adaptive immune responses are induced against non ‘self’ proteins, have limited their introduction to the clinic and the first approved monoclonal Muromomab showed limited efficacy after the first few doses. It was not until 1984 when Morrison *et al* described chimerization [63]. In this approach, VH domains from murine antibodies are grafted onto human constant domains to reduce the number of epitopes recognized as foreign. The process was further refined by humanizing antibodies where instead of the entire VH only the complementary determining regions (CDRs) are grafted into a human antibody framework [64] (Figure 1.3).

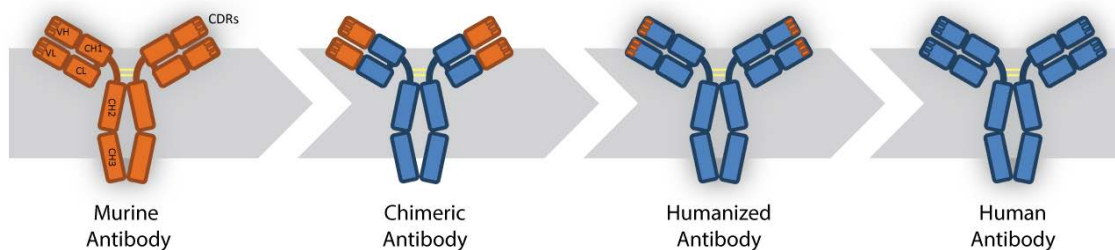


Figure 1.3: The Path to Developing Fully Human Antibodies.

Antibody technology has progressed since the discovery that murine antibodies could be generated from hybridomas to the point where fully human antibodies are entering the clinic.

Only a few years later phage display was discovered enabling the production of fully human synthetic libraries of antibodies to be screened. Despite the immense promise of this technology only one antibody generated by this method for the treatment of arthritis has been approved by the FDA, a testament to the power of the adaptive immune system in generating high affinity antibodies [65]. In the last few years the advent of revolutionary new genomic editing technology has enabled the proliferation of a large number of humanized mice where the VH genes from humans are introduced to the germline in place of murine versions. Several competing humanized transgenic mice including the Xenomouse, VelocImmune mouse and HuMab mouse are being used by the pharmaceutical industry. With the wide availability of technology to generate fully human antibodies, new methods to improve antibody efficacy are critically required for the clinic. Even with blockbuster antibody drugs only moderate improvements in life expectancy are often seen. For example, in clinical trials with the anti-CD20 antibody Rituxumab, only 48 % of the patients treated showed either complete or partial responses after a 12 month period [66]. Even more striking, a phase III clinical trial with Herceptin (anti-Her2/neu for metastatic breast cancer) provided only a 5 month average survival extension over standard chemotherapy treatment [67]. When coupled with the high cost

of antibody therapy due to the requirement for strictly controlled mammalian expression under sterile conditions, improved survival times are essential for future antibody treatments.

## **NEXT GENERATION THERAPEUTICS BY ANTIBODY ENGINEERING**

Several strategies have been developed to enhance antibody potency *in vivo* including; higher variable domain affinity for a target, targeting towards specific epitopes to have greater therapeutic effect, improved effector function by Fc modification and enhancement of pharmacokinetic and pharmacodynamics properties of antibodies [68, 69]. However, there is a limit to the effectiveness of variable domain affinity maturation. At a certain point the off rate of the antibody becomes so slow that only minute gains in performance are achieved. On the other hand, modification of the Fc domain to modulate the balance of binding affinities for the FcγRs, or even to use as a scaffold on which a payload may be attached, have shown considerable promise (Figure 1.4). Of note is the recent FDA approval of the antibody drug conjugate Trastuzumab-DM1 [70]. However, many other sequence or glycan engineered variants are now reaching late stage clinical trials as discussed in the following section.



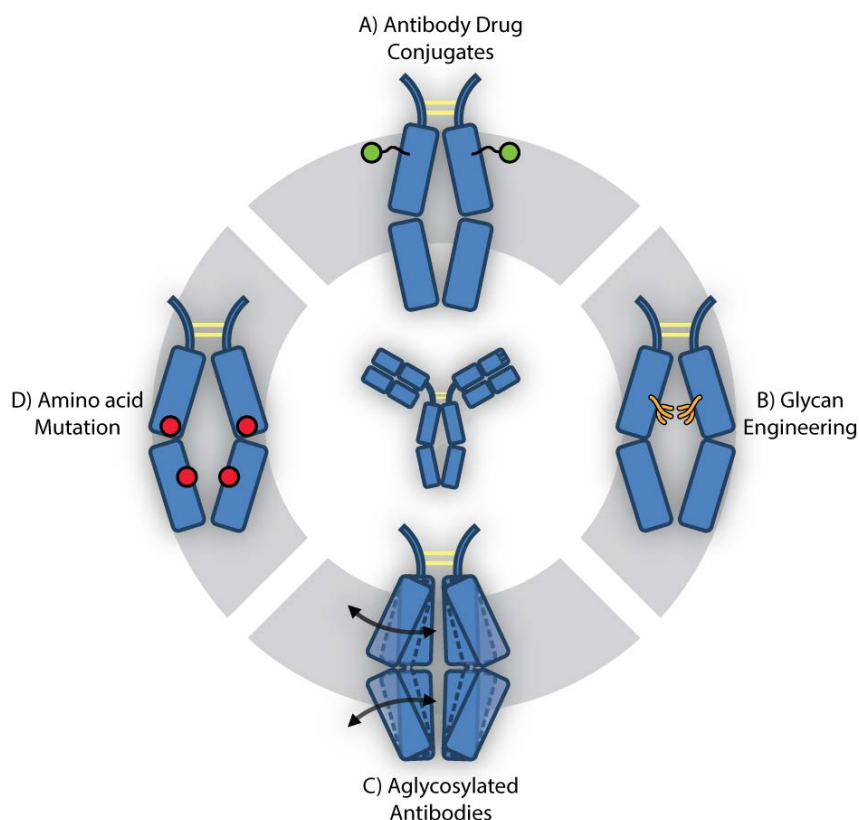


Figure 1.4: Strategies for Improving Antibodies by Engineering the Fc Domain.

A) Antibody drug conjugates use the Fc domain as a carrier to attach a payload of cytotoxic drugs B) engineering the glycan moieties can influence binding to the FcγRs to either increase or reduce inflammatory function C) making antibodies aglycosylated renders the Fc immune silent but it is possible to fix certain conformations by D) amino acid mutation to improve or reduce contacts with cognate Fc receptors.

### Amino Acid Modification in Glycosylated Antibodies

Modification of the Fc domain was first achieved in glycosylated antibodies by mutation of the polypeptide structure. In a landmark paper by Shields et al., high resolution alanine scanning of the Fc domain identified a large number of residues that either enhanced and reduced binding to FcγRI, FcγRIIa, FcγRIIb, FcγRIIIa and FcRn [71]. As part of this work several mutations were reported to enhance binding to

activating receptors over FcγRIIb thus providing the framework for a proliferation of engineered variants. Initial engineering efforts focused heavily on improving binding to FcγRIIIa. Unlike macrophages or neutrophils, NK cells express predominantly the activating FcγRIIIa receptor and not the inhibitory receptor FcγRIIb. Evidence suggested that these cells were largely responsible for the killing action of some clinical antibodies, such as trastuzumab [43]. However, the absence of a homeostatic mechanism for the down regulation of NK cells that have been activated by immune complexes has led to some controversy as to the significance of NK cells in antibody mediated tumor clearance [36].

Xencor used saturation mutagenesis and screening to guide the design of several variants to find, among others, the triple mutation S239D/I332E/A330L that exhibits over 100 fold improvement in affinity for FcγRIIIa while maintaining an enhanced A/I ratio [72]. The improved affinity translated *in vitro* to significant improvements in NK mediated cell killing of Her2+ tumor cell lines and several clinical trials are in progress to test S239D/I332E variants of this engineered Fc domain (XmAb5574) [73, 74]. Xencor has also reported variants with enhanced binding to FcγRIIa in order to improve macrophage mediated phagocytosis. In total more than 900 variants were constructed and screened against the whole FcγR panel. Surprisingly, the single mutation G238A was able to confer an impressive 70 fold increase in affinity for FcγRIIa while simultaneously improving the A/I ratio by 15 fold [75].

To improve the throughput of engineered and glycosylated Fc discovery several groups have used yeast screening technologies to express large libraries of variants. In the yeast system, proteins may be expressed as a fusion to Aga2 protein which forms a disulfide linked complex with Aga1 on the cell surface [76, 77]. Using this technology, MacroGenics screened more than  $1 \times 10^7$  mutations for variants with enhanced A/I ratios.

A group of 5 mutations was found to improve specific cell lysis of HT29 tumor cells the most (F243L, R292P, Y300L, V305I, P396L) and this translated to enhanced survival of mice when injected with ovarian cancer or B cell malignancies [78].

More recently, several variants with extremely low A/I ratios (High FcγRIIb binding and low FcγRIIa or FcγRIIIa binding) have been published. In some cases high binding to FcγRIIb is desirable, particularly for autoimmune diseases and allergic responses where attenuation of misdirected immune responses is essential for treatment. Xencor found the mutations S267E and L328F could confer an impressive 430 fold increased affinity for FcγRIIb but also retained considerable affinity for FcγRIIa<sub>R131</sub> [79]. When these mutations were added to an anti-CD19 antibody, significant suppression of humoral immunity was observed in mice grafted with B cells taken from sufferers of systemic lupus erythematosus and challenged with tetanus toxoid antigen. The recruitment of inhibitory FcγRIIb to the BCR signaling complex greatly increases the threshold required for activation of B cells. This engineered variant is now in phase I clinical trials to determine safety profiles and dosage regimes. The same engineered Fc domain has also been fused to an IgE Fc domain to create a tandem Fc structure. Crosslinking the inhibitory FcγRIIb receptor with the high affinity receptor for IgE, prevents mast cell degranulation, a key contributing mechanism to allergy and inflammation [80].

An Fc domain with even greater selectivity for FcγRIIb than the S267E/L328F variant was made with the goal of reducing residual affinity for FcγRIIa<sub>R131</sub>. Using high resolution mutagenesis, guided by a crystal structure of the mutant Fc in complex with FcγRIIb, residues in the Fc structure were identified with selective binding to FcγRIIb [81]. Six residues E233D, G237D, H268D, P271G, Y296D and A330R when combined

provide 217 fold improved binding to Fc $\gamma$ RIIb while maintaining binding to the activating receptors at close to or below wild type levels.

### **Glycan Modification for Enhanced Therapeutic Effect**

Other than mutation of the Fc amino acid sequence, significant effort has been directed at tailoring the composition of the N297 glycan in antibodies by developing highly sophisticated mammalian or non-mammalian expression systems [82-84]. Changes to glycan composition can have a large influence on the affinity of Fc $\gamma$ R binding and on the heterogeneity of glycosylation introduced by cell expression systems has been a long standing problem. One key example of such efforts is glyco-engineered *Pichia pastoris*, which expresses antibodies with human N-glycan structures, a technology developed by GlycoFi and acquired by Merck for \$400 million in 2006 [85]. Over 95% of antibodies produced in Chinese hamster ovary (CHO) cells, and 70% of those produced in mouse myeloma cells, are fucosylated [86]. However, the non-fucosylated fraction of serum IgG shows markedly enhanced Fc $\gamma$ RIIIa binding [26], which results in the induction of potent ADCC responses by NK cells *in vitro*. Hence, the expression of non-fucosylated antibodies has attracted significant commercial interest. Production can be accomplished using *FUT8* ( $\alpha$ -1,6 fucosyltransferase; intrinsic fucosylating enzyme) knockout cell lines [87].

Anti-inflammatory responses might also be mediated by antibodies if the glycan terminus is sialylated to promote interaction with the DC-SIGN receptor. The DC-SIGN receptor is a C-type lectin receptor expressed on macrophages and dendritic cells which typically recognizes mannose carbohydrates [88]. Nevertheless, some studies have shown DC-SIGN interaction with  $\alpha$ 2,6-sialylated structures, such as those in the Fc domain, and could provide a mechanism behind the success of intravenous Ig (IVIG) treatment for

autoimmune diseases [89, 90]. Measurement of circular dichroism spectra of sialylated Fc domains revealed that a closed conformation (distance between CH2 domains small) is adopted relative to the wild type form [91]. This evidence has led to the hypothesis that closed conformations trigger anti-inflammatory properties whereas open structures are more activating through binding to the FcγRs. However, this hypothesis remains contentious in literature especially since the recent publication of a sialylated Fc crystal structure failed to demonstrate a ‘closed’ CH2 domain conformation relative to wild type Fc domains [92, 93].

The impact of these new glycan engineered mutants in the clinic is yet to be seen and more data is required especially in comparison with wild type antibodies to truly measure their effect [94]. In the meantime, new strategies should be investigated as we hypothesize that high affinity for an activating receptor is possibly not as important as extreme receptor specificity.

### **Aglycosylated Antibodies as Novel Therapeutics**

The use of aglycosylated full length antibodies for therapy offers two important advantages: First, recent studies have shown that aglycosylated antibodies can be engineered to bind to FcγRs and thus elicit potent ADCC responses [95, 96]. Of particular significance is the high degree of Fc polypeptide flexibility conferred by the lack of glycosylation that can be exploited to elicit unique FcγR selectivity, in turn opening the way for new mechanisms of immunotherapy [97]. Second, bypassing glycosylation greatly simplifies bioprocessing both because control of glycan isoforms ceases to be a problem and because aglycosylated antibodies can be produced in prokaryotic or lower eukaryotic hosts, leading to much faster development timelines. To date, aglycosylated antibodies in clinical trials have been expressed in *E. coli*, yeast and

CHO cells. In addition, the production of full length, aglycosylated antibodies in algae has been described although no clinical trials with antibodies produced in this system have been reported [98].

The idea of using aglycosylated antibodies in the clinic was initially met with skepticism because of concerns with immunogenicity of the aglycosylated form, the possibility for altered pharmacokinetics *in vivo* and antibody stability during formulation and storage [99]. These concerns have since been largely dismissed opening the way for the clinical development of a number of aglycosylated IgG antibodies (Table 1.3).

Table 1.3: Aglycosylated Antibodies in Current or Past Clinical Trials.

Antibody	Target antigen	Origin	Company	Clinical trial phase
TRX518	GITRa	Humanized (Mouse)	GITR, MA, USA / Tolerx, MA, USA	I (Ongoing)
MTRX1011A	CD4	Humanized (Rat)	Genentech, CA,USA / Tolerx, MA, USA	I (Failed to meet pharmacodynamic targets)
TRX4 (Otelixizumab)	CD3	Humanized (Rat)	Tolerx, MA, USA	III (Failed to meet endpoint)
OA-5D5 (MetMAb)	HGFb	Humanized (Mouse)	Genentech, CA,USA	III (Ongoing)
ALD518 (BMS-945429)	IL-6	Humanized	Alder Biopharmaceuticals, WA, USA	II (Completed)

The first aglycosylated antibody to enter clinical trials was ChAglyCD3 (otelixizumab, Tolerx), a humanized version of a rat derived IgG1 directed against the CD3 T cell marker [10]. The aglycosylated form of the antibody was shown to be well tolerated in patients despite concerns of an initial cytokine burst release. However,

despite promising results in early phase clinical trials, orelizumab did not meet its phase III endpoint and development was halted [100-102] [97]. Despite the closure of Tolerx, two additional aglycosylated antibodies continued to clinical trials with sponsorship from other corporations. The first, TRX518, is a fully humanized IgG1 that binds to the glucocorticoid-induced tumor necrosis factor receptor (GITR) on CD3+ T cells, which stimulates the activation of tumor-antigen-specific T effector cells and simultaneously abrogates the suppression by T regulatory cells [103]. Second, MTRX1011A was a humanized rat IgG1 anti-CD4 mAb which was designed to suppress CD4 T cells that contribute to the pathogenesis of rheumatoid arthritis but failed Phase I as the pharmacodynamic activity did not meet the requirement for disease reduction [104].

Alder Biopharmaceuticals (WA, USA) completed a successful phase II clinical trial for an aglycosylated, humanized anti-interleukin-6 antibody (ALD518) [74]. The yeast-expressed ALD518 contains a mutation at N297 that abolishes glycosylation. Pharmacokinetic studies revealed that ALD518 has a serum half-life of 25 days, which is comparable to the typical half-life of glycosylated antibodies in humans [105]. Genentech (CA, USA) developed a novel “one-arm” (monovalent) anti-cMet antibody (MetMAb, OA-5D5) that acts exclusively as an antagonist to compete with the natural cMet ligand, hepatocyte growth factor (HGF), in the treatment of glioblastoma [106, 107]. Notably, the “one-arm” antibody is produced in *E. coli* by expressing a bi-specific Fc that capitalizes on the “knobs-in holes” approach for IgH (IgG heavy chain) heterodimerization with only one of the two IgH chains containing a Fab domain. The use of the monovalent OA-5D5 was necessitated by the finding that a conventional IgG with the same antigen specificity activates cMet by receptor crosslinking. The aglycosylated version of MetMAb was selected for clinical development in order to reduce agonistic activity through receptor engagement by the Fc domain. Initial

preclinical data suggested the clearance rate of the antibody would be faster than its bivalent counterpart but phase I clinical data subsequently revealed a promising pharmacokinetic profile [108]. Phase II trials successfully demonstrated improved survival time in some patients and phase III studies are now underway to determine which subset of patients would benefit most from MetMAb treatment [109].

Importantly, MetMAb is the first therapeutic full-length antibody that is manufactured in *E. coli*. This is significant on three accounts: First, it indicates that earlier concerns regarding the efficiency IgH : IgL (IgG light chain) pairing and possible product heterogeneity due to aberrant disulfide bond formation in bacteria can be successfully addressed at an industrial scale. Second, it demonstrates the use of bacteria for preparative IgG expression now opens the way for capitalizing on the numerous tools available for achieving very high yields of secreted proteins in bacteria [110]. Third, since *E. coli* does not have any protein glycosylation machinery it enables the production of fully aglycosylated antibodies without any N- or O- linked glycans while leaving residue N297 unmodified.

The engineering of aglycosylated antibodies, while not at the clinical trial level has also proved successful in creating promising new variants. Sazinsky *et al.* created small saturation libraries (amino acid residues at 296-299, 297-299, and 297-300) targeting the C'E loop of CH2 region that has been known to be critical for FcγR interaction [111]. By using yeast surface display and flow cytometric screening, they isolated Fc variants exhibiting high binding affinity to FcγRIIa. Despite the use of eukaryotic yeast for surface display of IgG molecules, variants containing mutations at the canonical N-linked glycosylation sequence (Asn-X-Ser/Thr) generated aglycosylated IgG instead of mannosylated IgGs. A S298G/T299A double mutant was shown to be aglycosylated when expressed in HEK293 cells but displayed FcγRIIa and FcγRIIb



affinities comparable to those of glycosylated, wild-type IgG. In a human FcγRIIa transgenic mouse model, an anti-platelet antibody containing the S298G/T299A mutations was shown to mediate platelet reduction suggesting that the engagement of FcγRIIa by the engineered antibody results in a physiologically relevant effect.

Jung *et al.* developed a robust system for the display of combinatorial libraries of aglycosylated Fc domains in *E. coli* and the isolation of variants that bind to desired fluorescently labeled FcγRs using flow cytometry [95]. Screening of very large libraries ( $\sim 10^9$  transformants) led to the isolation of a mutant containing two amino acid substitutions, E382V/M428I within the CH3 region that conferred binding to FcγRI with an affinity nearly identical to that of glycosylated IgG1 antibodies. Quite remarkably, this Fc mutant showed no binding to any other FcγRs (FcγRIIa, FcγRIIIa or, most importantly FcγRIIb). The E382V/M428I amino acid substitutions were introduced into the anti-Her2 antibody trastuzumab (trastuzumab-Fc5), which was preparatively expressed in *E. coli* by high cell density fermentation. Trastuzumab-Fc5 elicited dendritic cell-mediated ADCC in sharp contrast to the clinical grade glycosylated trastuzumab which lacked the ability to activate dendritic cells. Interestingly, when trastuzumab-Fc5 was expressed in glycosylated form in HEK293 cells it lost its selectivity for FcγRI and displayed binding to FcγRIIb (as well as FcγRIIa and FcγRIIIa) which in turn suppressed its ability to potentiate target tumor cell clearance with dendritic cells as effectors. The finding that glycosylation suppresses the FcγRI selectivity of trastuzumab-Fc5 and the location of the E382V/M428I mutations in the CH3 far away from the FcγR binding interface supported the hypothesis that these mutations may act by stabilizing a particular aglycosylated Fc conformer.

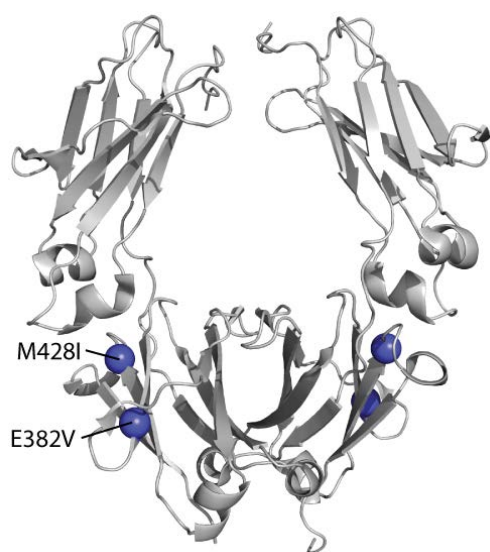


Figure 1.5: The Aglycosylated Fc5 Mutant.

An Aglycosylated Fc domain crystal structure (PDB: 3S7G) overlaid with the E382V and M428I mutations from Fc5 which confer highly selective binding to Fc $\gamma$ RI.

Small angle X-ray (SAXS) scattering experiments revealed that radius of gyration for the Fc5 variant is greater than a glycosylated IgG Fc but less than a wild type aglycosylated IgG Fc [112]. Because SAXS involves measurement of proteins in solution, many crystal packing artifacts can be avoided that may occur in crystallization methods. The result suggests a structural change is induced by the additional mutation in Fc5 which appears to limit the ‘openness’ of the structure in a manner that promotes binding to Fc $\gamma$ RI.

Long term, aglycosylated antibodies engineered for Fc $\gamma$ R binding specificity and activation may bypass the necessity for mammalian cell expression/glycoengineering and, importantly, establish novel mechanisms of antibody function. Chapters 3 and 4 of this work focus on the discovery and characterization of a new aglycosylated Fc domain engineered for enhanced binding specifically to Fc $\gamma$ RIIa over Fc $\gamma$ RIIb that displays greatly enhanced macrophage recruitment over wild type IgG.

## **Looking Beyond the IgG1 Isotype**

In order to further expand the function of Fc domains, the therapeutic action of antibody isotypes other than IgG should be considered to further enhance antibody effector function or, in the case of anti-inflammatory antibodies, make the Fc domain more immune silent. Typically, the IgG1 antibody subclass has been used to form the backbone of FDA approved therapeutics because of strong activation of ADCC and CDC. However, some of the more recent approvals have been of the IgG2 (panitumumab) or IgG4 (natalizumab, gemtuzumab ozogamicin) subclasses, which both exhibit greatly reduced Fc function [113]. These classes have also been hybridized in the Fc domain of eculizumab to further reduce inflammatory effector function [114].

Conversely, Fc domains with strong ADCC and CDC activation have been created by shuffling the constant domains of IgG1 and IgG3. When grafted to anti-CD20 variable domains this new Fc was able to significantly reduce B cell levels in the blood of cynomolgus monkeys as compared to a wild type IgG1 control suggesting the utility of domain shuffling as a method for enhancing antibody function [115]. Despite the promise of this method shuffling between completely separate antibody isotypes such as IgG and IgA to potentially combine the best features of both has not been attempted. As such, this area remains open for exploration as described in Chapter 1 of this work.

## **Chapter 2: Engineering of an IgG/IgA Chimeric Fc Domain with Fc $\alpha$ RI and Fc $\gamma$ R Receptor Binding**

### **INTRODUCTION**

A key part of antibody function is the recruitment of immune cells that can mediate potent antibody dependent cell cytotoxicity (ADCC) responses against target antigens (or cells) [44]. Initiation of the ADCC response depends on the interaction of the Fc region of antibodies with cell surface receptors (FcRs) located on immune effector cells [36, 48]. To provide modulation of the inflammatory response, several antibody isotypes have evolved (IgG, IgA, IgE, IgM or IgD) with unique binding profiles for both activating and inhibitory FcRs [116-118]. Currently, all FDA approved antibody therapeutics are of the IgG subclass that interact with Fc $\gamma$ Rs on effector cell subsets [2]. In particular, NK cells expressing high levels of Fc $\gamma$ RIIIa have been implicated as the primary effector cells in the anti-tumor activity of some clinical antibodies [43, 119]. Yet evidence is emerging that other cell subsets, such as neutrophils, might also significantly contribute to tumor clearance in the clinic [120]. In line with this finding, recent murine xenograft studies have shown that neutrophils are directly linked to the reduction in tumor burden by alemtuzumab and trastuzumab IgG antibodies [121, 122]. However, in addition to the Fc $\gamma$ Rs engaged by IgG, neutrophils also express high levels of Fc $\alpha$ RI receptors which can induce potent inflammatory action when cross-linked by IgA immune complexes [44, 123]. Both ADCC (oxidative burst, degranulation) and ADCP responses have been observed upon Fc $\alpha$ RI activation [124-128]. In fact, IgA can bind Fc $\alpha$ RI to activate neutrophils more potently than IgG antibodies can via the Fc $\gamma$ Rs [129, 130]. Hence, the efficacy of ADCC might be improved by enabling the engagement of neutrophil and other effector cell populations that are not normally activated as potently or not at all by IgG class antibodies.

The ability to strongly recruit neutrophils for cancer therapy is an attractive avenue of exploration since the neutrophil population comprises the greatest fraction of innate effector cells

found in circulation. It is also possible to rapidly expand neutrophils *in vivo* for therapy by injection of GM-CSF cytokine [123]. As mentioned above, immune complexes formed by IgA isotype antibodies can activate neutrophils to display potent cytotoxic effects towards target cells. However, despite the potential promise for using the IgA isotype to exploit the potent inflammatory effects of Fc $\alpha$ RI function for neutrophil mediated therapy, its therapeutic use has been disfavored due to its low expression yields [131]. Part of the problem with IgA expression is the heavily glycosylated hinge region of the antibody that includes up to six O-linked glycosylation sites [132]. Glycosylation not only impacts protein expression level but also introduces the potential for heterogeneity during production which can affect the immunogenicity and stability of protein therapeutics [133, 134].

We hypothesized that engineering Fc $\alpha$ RI binding into an IgG molecule could alleviate these concerns. Furthermore, IgA antibodies cannot bind Fc $\gamma$ Rs and hence cannot elicit the same kind of ADCC, ADCP and CDC reactions that IgG molecules are capable of. To do so would require combination therapy with IgA and IgG therapeutic antibodies which would be both clinically complicated and costly. Instead, engineering a chimeric IgG Fc domain that engages both Fc $\alpha$  and Fc $\gamma$  receptor classes synergistically could address these issues [135]. In this work we report the generation of a new class of engineered Fc domains that are able to bind both Fc $\alpha$  and Fc $\gamma$  receptors. Specifically, an IgG1 antibody Fc domain was engineered to introduce *de novo* binding to the IgA Fc $\alpha$ RI receptor while retaining near to wild type affinity for several Fc $\gamma$ Rs. This new chimeric Fc domain and its derivatives, when incorporated into full length antibodies, offer a broader range of effector function relative to either IgG or IgA alone. We show that such chimeric antibodies elicit potent ADCC with neutrophils as effector cells mediating the killing of Her2+ breast cancer cells *in vitro*.

## MATERIALS AND METHODS

### Alanine Mutagenesis

Alanine scanning mutagenesis on IgA was performed to help identify residues important for binding to Fc $\alpha$ RI. Based on crystal structure and Rosetta modeling, 11 sites in the IgA Fc domain were selected for alanine scanning mutagenesis (Figure 2.1). The following IgA mutants containing L257A (constructed using primers TKA4, TKA5), L258A (constructed using primers TKA6, TKA7), E313A (constructed using primers TKA8, TKA9), N316A (constructed using primers TKB1, TKB2), H317A (constructed using primers TKB3, TKB4), R382A (constructed using primers TKB7, TKB8), E389A (constructed using primers TKC1, TKC2), M433A (constructed using primers TKC5, TKC6), E437A (constructed using primers TKD1, TKD2), L441A (constructed using primers TKD5, TKD6), and F443A (constructed using primers TKE1, TKE2) were generated using Quikchange PCR with pTrc-DsbA IgA CH2 CH3 as the DNA template. Cloning into the mammalian expression vector pMaz-IgH was achieved by Gibson assembly [136] after amplification of the individual Fc domains (Primers WK346 and WK347) and amplification of the pMaz-IgH-Fc $\gamma$ RI-His backbone (Primers WK212 and WK314). Following transformation into *E. coli* JUDE-1 cells, the mutant genes were sequenced and DNA was prepared for transient transfection in HEK293F cells (Invitrogen). The IgA mutants were purified by Ni-NTA chromatography. PBS (25x) was added to a final concentration of 1x in addition to 10 mM imidazole, and the solution was passed through Ni-NTA affinity columns for IMAC chromatographic isolation of the Fc proteins. Bound protein was washed with PBS containing 20 mM imidazole and eluted in PBS with 250 mM imidazole directly into Amicon 10 kDa spin columns for buffer exchange and concentration. ELISA analysis was used to evaluate binding to Fc $\alpha$ RI. Briefly, each IgA variant was coated at 4  $\mu$ g/mL onto Ni-NTA ELISA plates (Qiagen), then Fc $\alpha$ RI-GST at 10  $\mu$ g/mL was added to the first well and serially diluted before

detection with goat anti-GST HRP (GE Healthcare). TMB substrate was added and the reaction quenched with 1 M H<sub>2</sub>SO<sub>4</sub> before the absorbance was measured at 450 nm.

### **Construction and Expression of Fc Domain IgA/G Chimeras**

All plasmids and primers are described in Tables A.1 and A.2. DNA sequences for mutants B-D were assembled by PCR using oligonucleotide primers synthesized in house shown in Table A.3 (Mutant B - WK188, 190, 194, 196, 198, 200, 202, 204, 206, 207; Mutant C - WK188, 191, 194, 196, 198, 200, 202, 204, 206, 207; Mutant D - WK188, 192, 194, 196, 198, 200, 202, 204, 206, 207). Each of the IgG mutants were then cloned into pMaz-Fc $\gamma$ RI-His by Overlap Extension PCR [137]. Double stranded megaprimers for mutant B (pMaz-IgH MutB) were generated with primers WK366 and WK209 and for both mutants C (pMaz-IgH MutC) and D (pMaz-IgH MutD) using primers WK370 and WK209. Exchange of the CH2 loop of MutD with that from IgA was performed similarly by OLE PCR. A megaprimer was generated using pMaz-IgH-MutD as a template with the primers WK385 and WK386 for cloning back into pMaz-IgH-MutD. Following DpnI digestion of all PCR reactions and transformation into JUDE-1 cells, plasmid DNA was prepared (Qiagen, HiSpeed Plasmid Midi Kit) for transfection. 293Fectin Transfection Reagent (Invitrogen) was used to transfect HEK293F (Invitrogen) cells cultured in GIBCO FreeStyle™ 293 Expression Medium (Invitrogen) in accordance with the manufacturer's instructions. Five to six days after transfection, the cell suspension was centrifuged at 2,000 rpm for 10 min to recover the supernatant fraction. Ni-NTA was used to purify the IgA/G chimeras as described in the previous method section.

### **Mammalian Expression of Fc receptors**

Fc $\alpha$ RI-GST, Fc $\gamma$ RI-GST, Fc $\gamma$ RIIa-R131-GST, Fc $\gamma$ RIIb-GST, and Fc $\gamma$ RIIIa-F158-GST were produced by transient transfection of HEK293F cells (Invitrogen) using the pMaz-IgH

(U.S. Patent No. 8,043,621) derived expression vectors described in Table A.1. Glutathione Sepharose (GE Healthcare) affinity chromatography was used according to the manufacturer's instructions to purify each variant to >95 % purity as assessed by SDS-PAGE. PBS at 25x concentration was added to the filtered supernatants six days after transfection to make a final PBS concentration of 1x, and the mixture was passed twice over the column. The column was washed with 100 mL of 1x PBS to remove nonspecifically bound protein. 4 mL of 1x PBS containing 10 mM reduced glutathione was used for elution into 10 kDa filter columns.

### **Fc Receptor Binding ELISAs**

ELISA plates (Qiagen) were coated with 4 µg/mL of each of the mutant Fc domains in 1x PBS (pH 7.4) overnight at 4 °C. The next day the plates were blocked for 2 h at room temperature with 2 % milk in 1x PBS containing 0.05 % Tween (PBST) and washed 3 times in PBST at pH 7.4. To the first well, 66 µL of 20 µg/mL of either FcαRI-GST, FcγRI-GST, FcγRIIa-R131-GST, FcγRIIb-GST, or FcγRIIIa-F158-GST dissolved in PBS with 2 % milk (PBSM) was added followed by 1:4 serial dilution. After 1 hour of incubation at room temperature, the plates were washed and 50 µL PBSM was added containing 1:5000 goat anti-GST HRP (GE Healthcare) for 1 hour. To develop the plates, the wells were washed 3x with PBST, 50 µL TMB substrate was added per well (Thermo Scientific), 50 µL of 1 M H<sub>2</sub>SO<sub>4</sub> was added to neutralize, and the absorbance at 450 nm was recorded.

### **Construction and Expression of Full Length IgA/G Chimeras and Control Antibodies**

All plasmids and primers are described in Tables A.1 and A.2. Plasmids for expression of wild type trastuzumab IgG heavy chain (pMaz-IgH-trastuzumab), trastuzumab kappa light chain (pMaz-IgL-trastuzumab) and trastuzumab IgG N297D heavy chain (pMaz-IgH-N297D-



trastuzumab) were constructed as described previously [96]. Inserts for trastuzumab IgA heavy chain (Primers WK353 and WK354) and trastuzumab MutD heavy chain (Primers WK364 and WK 356) were amplified for cloning into the pMaz-IgH (U.S. Patent No. 8,043,621) expression plasmid by OLE PCR. In each case plasmid pMaz-IgH-trastuzumab was used as the DNA template. After transformation into *E. coli* JUDE-1 cells, colonies were isolated for sequencing and DNA was prepared for each heavy chain and combined with an equal mass of light chain plasmid for transient transfection in HEK293F cells (Invitrogen). Five to six days after transfection, the cell suspension was centrifuged at 2000 rpm for 10 min to recover the supernatant fraction. Trastuzumab IgG and trastuzumab IgG N297D were purified over protein A affinity columns whereas trastuzumab IgA and trastuzumab MutD were purified over protein L affinity columns. Briefly, the supernatants were passed through 0.22  $\mu$ m filters before addition to polypropylene columns packed with either Protein A high capacity agarose resin (Thermo Scientific) or Protein L agarose resin (Invivogen). The resulting flow-through was collected and passed twice more through the column before any unbound protein was washed away with >10 CV (Column Volume) of 1x PBS. All antibodies were eluted with 3 mL of 100 mM citrate buffer (pH 3.0) and immediately neutralized with 1 mL of 1 M Tris (pH 8.0). Samples were buffer-exchanged into 1x PBS using Amicon Ultra-4 (Millipore) spin columns with a 10 kDa cutoff and the purity of purified samples was assessed by 4-20 % gradient SDS-PAGE gel (NuSep).

### **Mammalian Expression of Monomeric Fc $\gamma$ RIIa, Fc $\gamma$ RIIb and Fc $\alpha$ RI Receptors**

The genes encoding monomeric low affinity Fc receptors (Fc $\gamma$ RIIa and Fc $\gamma$ RIIb) and Fc $\alpha$ RI were generated by Gibson assembly as follows: The backbone of the pcDNA3.4 vector (Invitrogen) was amplified in two segments; a 2.5 kb fragment (using primers WK426 and WK463) and a 3.5 kb fragment (using primers WK425 and WK464). The insert for Fc $\gamma$ RIIa-R131 was created using primers WK448 and WK461 with plasmid pMaz-IgH-Fc $\gamma$ RIIa<sub>R131</sub>-His

as a template. Similarly the insert for FcγRIIb was generated using primers WK450 and WK462 with pMaz-IgH-FcγRIIb-GST as a template. To clone monomeric FcαRI into pcDNA3.4, the receptor insert was amplified from pMaz-IgH-FcαRI-GST using the primers WK459 and WK460. Each insert was combined with the two backbone segments for 60 min at 50 °C in a Gibson master mix [136], to create the plasmids pcDNA3.4-FcγRIIb-His and pcDNA3.4-FcγRIIaR131-His, before transformation into *E. coli*. The respective plasmids for FcγRIIa-R131, FcγRIIb and FcαRI expression were transfected for five to six days using Expi293F cells (Invitrogen). Purification was performed by Ni-NTA affinity chromatography as described previously and expression confirmed by 4-20 % SDS page gel.

### **SPR Affinity Measurements**

A Biacore 3000 instrument (GE Healthcare) was used to determine equilibrium KD values for MutD binding to FcγRIIa-R131, FcγRIIb and FcαRI. In all cases amine coupled BSA reference channels were used to subtract nonspecific binding signal. For evaluation of FcαRI binding to trastuzumab MutD and trastuzumab IgA, CM5 chips were immobilized with each of the antibodies (1820 RU and 1500 RU respectively) by amine coupling at pH 5.0 in 50 mM Sodium Acetate buffer. Concentrations ranging from 6 μM to 0 nM of soluble monomeric FcαRI were flowed in duplicate across the chip at 30 μL/min for 240 μL. A single step regeneration was used after each binding event; 5 min of 150 mM formic acid pH 5.0. A 1:1 Langmuir isotherm model ( $A + B \rightleftharpoons AB$ ) was fit to the equilibrium data to obtain apparent KD values for each of the interactions.

For affinity determination of FcγRIIb and FcγRIIa-R131 binding to trastuzumab MutD and trastuzumab IgG, antibodies were immobilized by amine coupling to CM5 chips (4310 RU and 4030 RU respectively) at pH 5.0 in 50 mM Sodium Acetate buffer. Concentrations ranging

from 10  $\mu$ M to 0  $\mu$ M of monomeric Fc $\gamma$ RIIb and Fc $\gamma$ RIIa-R131 were flowed in duplicate across the chip at 20  $\mu$ L/min until an equilibrium state was achieved. Dissociation was performed using an 8 min step in the HBS-EP running buffer (GE Healthcare). A 1:1 Langmuir isotherm model was fit to the equilibrium data to obtain KD values for each of the interactions.

To determine antibody affinity for Fc $\gamma$ RI, CM5 chips (GE Healthcare) were covalently immobilized with trastuzumab MutD (1140 RU) or trastuzumab IgG (820RU) by amine coupling in 50 mM pH 5.0 Sodium Acetate buffer. Duplicate concentrations ranging from 37.5 nM to 0 nM of soluble Fc $\gamma$ RI (R&D systems) were flowed in random order across the chip at 30  $\mu$ L/min. The chip was regenerated after each binding event by contact with 100 mM Sodium Citrate pH 4.5 for 30 s. The resulting binding profiles were fit to a 1:1 Langmuir isotherm model using Biaevaluation 3.0 software.

## **ADCC Assays**

Human neutrophils were isolated from Heparin-treated fresh human blood gathered from anonymous donors (IRB protocol 2012-08-0031) on the day prior to the ADCC assay. 10 mL of blood was diluted 1:1 with PBS (Mediatech) and layered over 13 mL of room temperature Histopaque 1077 (Invitrogen) in 50 mL conical tubes. The mixture was centrifuged at 2500 rpm for 30 min at 25 °C with no brake during the deceleration phase. Serum, Histopaque and mononuclear cells were discarded. The pellet was resuspended in 4 °C cold shock buffer (155 mM Ammonium Chloride, 10 mM Potassium Bicarbonate and 0.1 mM EDTA) and incubated on ice for 10 min to lyse the red blood cells. The neutrophil fraction was isolated by centrifuging at 1300 rpm for 7 min and washing twice with 50 mL PBS. After the final wash, the neutrophils were resuspended in RPMI media containing 10 % FBS as well as 50 ng/mL IFN- $\gamma$  (Peprotech). The cells were cultured overnight at a concentration of  $5 \times 10^6$  cells/mL in a 24 well plate under a humidified atmosphere of 5 % CO<sub>2</sub>. The following day expression of Fc $\gamma$ RI and Fc $\alpha$ RI was

determined by fluorescence activated cell sorting (FACS) to confirm activation. Meanwhile, SkBR-3 tumor cells (ATCC) were cultured in McCoy's 5a media containing 10 % FBS (Invitrogen) and Penicillin-Streptomycin (Invitrogen). On the day of the assay the tumor cells were recovered by trypsinization and labeled for 90 min with Cr51 (Perkin Elmer) in a 1mL volume at a density of  $1 \times 10^6$  cells/mL. The tumor cells were washed 3 times in RPMI containing 10 % FBS and seeded in 96 well V bottom plates at 5000 cells/well. Antibody variants at various concentrations were added to opsonize the tumor cells for 30 min at 37 °C. Neutrophils were then added at a 80 : 1 effector : tumor (E:T) cell ratio and the plates incubated at 37 °C with 5 % CO<sub>2</sub> for 4 h. Supernatants were recovered and 50 µl was added to Uncoated Scintiplate-96 plates (PerkinElmer). After overnight drying the plates were read in a MicroBeta scintillation counter (PerkinElmer).

### **Mammalian Expression of FcRn Peptide Fusion to MutD**

In order to reintroduce FcRn Binding to the MutD framework a C-terminal fusions with either a linear (QRFVTGHFGGLYPANG) or a cyclic binding peptide (QRFCTGHFGGLHPCNG) were generated by Gibson assembly [138]. The linear peptide insert was created using primers JL-GS-L-Rn 1 and JL-GS-L-Rn 2 and the cyclic peptide insert was generated with JL-GS-C-Rn 1 and JL-GS-L-Rn 2 primers. The vector backbone was created by amplifying a 6.5 kb fragment from pcDNA3.4-IgH-Trastuzumab-MutD using primers JL-Gibson R and JL-Gibson F. Following transformation into *E. coli* and sequencing to verify cloning success the linear and cyclic variants were transfected into Expi293 cells as above. After 5 days of culture the proteins were isolated by Protein L chromatography as described above and eluted in 100 mM pH 2.7 glycine HCl.

### **FcRn Binding ELISA Assay**

ELISA plates were coated with 4 µg/mL FcRn in PBS overnight. The following day wells were blocked with PBST containing a 2 % milk solution for 2 h at room temperature and washed 3x with PBST at pH 7.4. To the first well antibody variant was added at 140 µg/mL in either pH 7.4 PBS or pH 5.8 PBS with 40 mM MES and serially diluted by a factor of 4. After 1 hour at room temperature the plates were washed 3x with either pH 7.4 PBS or pH 5.8 PBS with 40 mM MES respectively depending on the pH at which the antibody was bound. The presence of antibody was detected by 1 hour incubation with a 1:5000 dilution of goat anti-human Cκ HRP in PBST with 2 % milk, washing with pH 7.4 PBS or pH 5.8 PBS with 40 mM MES buffer and development with 50 µL TMB substrate. The reaction as quenched with 50 µL 1M H<sub>2</sub>SO<sub>4</sub> was added to neutralize, and the absorbance at 450 nm was recorded.

## RESULTS

### Characterization of IgA interaction with the Fc $\alpha$ RI receptor

Before the publication of a co-crystal structure that established the IgA CH2/CH3 domain interface as the binding site for Fc $\alpha$ RI, mutagenesis studies had identified several key residues in the IgA structure that are critical for this interaction [139]. The substitutions L257R, P440A, A442R and F443R into the Fc domain of IgA showed ablation of Fc $\alpha$ RI binding and the mutation P440R resulted in a significant reduction in binding to Fc $\alpha$ RI. Notably, the mutation of residues distal to the CH2/CH3 hinge region of the IgA Fc (G259R) showed no impact on this interaction. Moreover, it was observed that despite a large disparity in sequence identity between bovine IgA and human IgA, the high conservation of residues in the CH2/CH3 binding pocket allows bovine IgA to bind human Fc $\alpha$ RI [139]. This evidence suggested that chimeras between IgA and IgG antibodies may be functional in receptor binding assuming certain core residues are left unchanged. Guided by the crystal structure of IgA in complex with Fc $\alpha$ RI [140], we first sought to identify the influence of additional residues to those previously published, particularly in the  $\alpha$ 2 loop of the IgA CH2 (Figure 2.1A and B). A panel of human IgA Fc domain mutants was constructed by Quikchange mutation to introduce alanine residues in place of the wild type residues at 11 sites (Figure 2.1A and B). IgA residues were selected for mutation based on their proximity to Fc $\alpha$ RI in the co-crystal structure and residues 257 and 433 were included for comparison with previously published results [139].

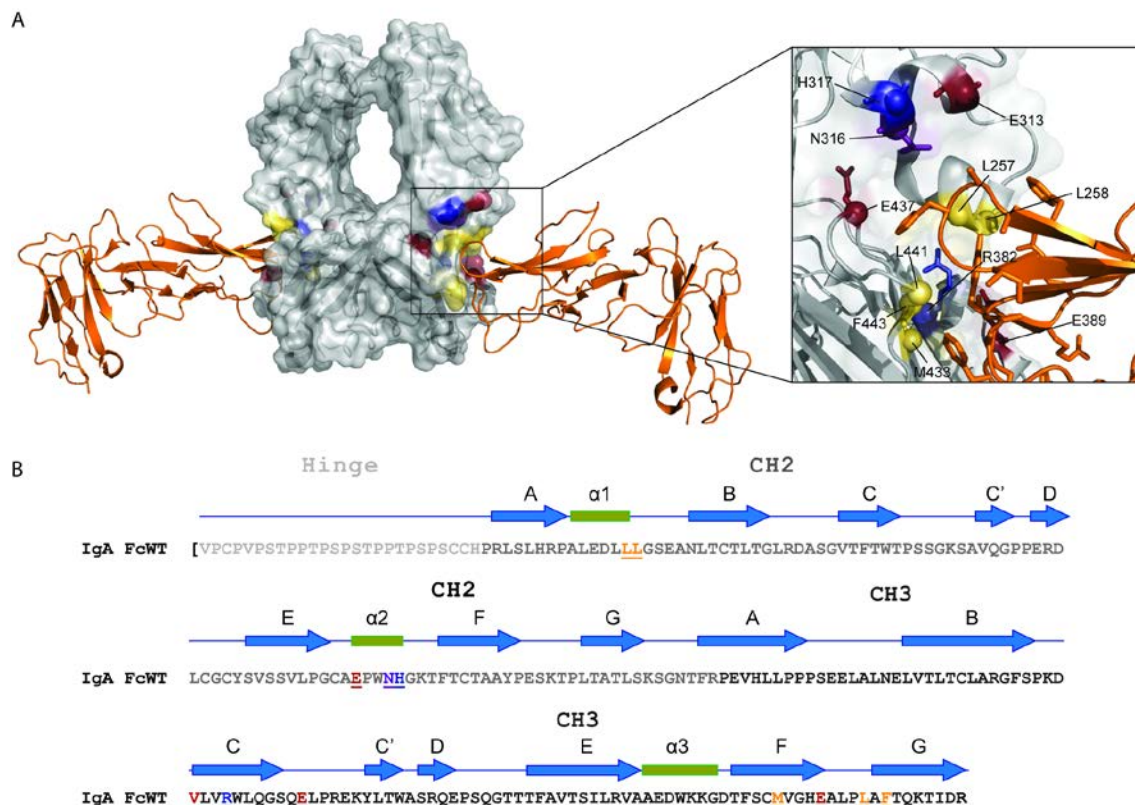


Figure 2.1: Residues Selected for Alanine Scanning in the Human IgA Fc Domain. The Fc domain was expressed with the hinge region and the tailpiece was truncated to remove the C-terminal cysteine responsible for dimerization.

To improve the affinity of Fc $\alpha$ RI for the IgA alanine mutants, the receptor was cloned with a C-terminal GST fusion, a dimeric protein, to promote dimerization of the Fc $\alpha$ RI exodomain in solution. Dimerization of the receptor greatly improves the chances of Fc $\alpha$ RI binding to IgA though avidity effects and reduces the apparent rate of dissociation. ELISA analysis revealed that mutation of position L257 in the  $\alpha$ 1 loop had little effect on binding affinity to Fc $\alpha$ RI, consistent with previous reports [139] (Figure 2.2). However, a significant ablation in affinity for Fc $\alpha$ RI was observed when residue L258 was altered. Previously, mutation of this residue to arginine had showed a similar reduction in binding [141], yet further investigation by non-reducing SDS-PAGE gel analysis showed poor assembly of this particular construct (Figure A.1). Disruption of the secondary structure of the protein can cause misfolding

or changes to the tertiary structure to prevent proper formation of the interchain disulfide bonds in the hinge region.

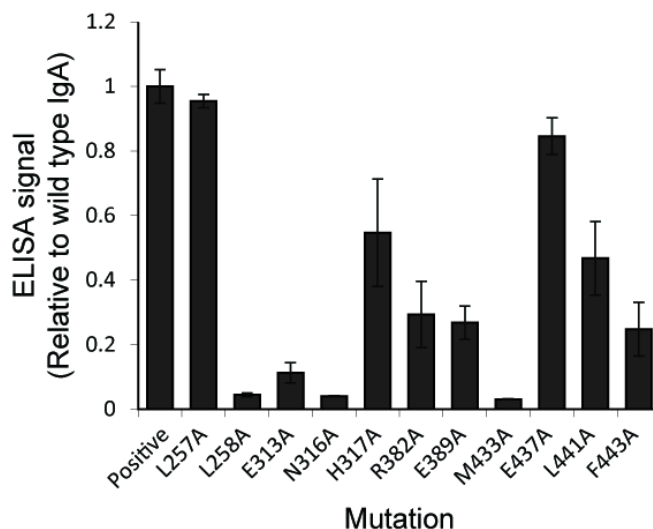


Figure 2.2: ELISA Analysis of Binding between IgA Variants with Alanine Point Mutations.

Interestingly, mutations to the IgA CH2  $\alpha$ 2 loop all had a large impact on binding to Fc $\alpha$ RI with the exception of the Histidine at position 317. This region was poorly resolved in the crystal structure but our result indicates the possibility of hydrogen bond interaction between E313, or N316, with Y86 in the Fc $\alpha$ RI structure. In the IgA CH3 domain, charged residues in the C beta sheet (R382 and E389) were moderately important for binding. Towards the C-terminus of the IgA Fc, M433 was critical for binding as a key part of the hydrophobic binding pocket. Likewise, while mutation of the charged residue E437 did not influence binding, alanine substitution of the proximal hydrophobic residues L441 and F443 had a moderate contribution to the binding affinity.

IgA has two N-linked glycan sites in the Fc domain at positions 263 and 459 and heavy O-linked glycosylation in the hinge at positions 225, 236, 228, 230 and 232 [57]. Studies removing glycans by enzymatic digestion [142], or by mutation of the single glycan site N263



[57] showed little glycan influence on Fc $\alpha$ RI affinity, yet in each case the removal of glycans is incomplete or the structure has been mutated from wild type. To mitigate these concerns we expressed an aglycosylated wild type IgA1 truncated to remove the tailpiece in bacteria that lack all glycosylation transferase machinery. Binding to dimeric Fc $\alpha$ RI was determined by ELISA and showed only a slight reduction as compared to full length human IgA, possibly due to poor assembly of the bacterial construct (Figure A.2A and B).

### **Construction and Receptor Binding Properties of Hybrid IgA/IgG Mutants**

Antibodies of all isotypes are comprised of domains belonging to the immunoglobulin superfamily and share an exceptional level of structural homology even if there is low amino acid sequence identity [143]. Swapping of entire Ig domains, such as the VH, is regularly performed to create chimeric antibodies [63]. Likewise, in the case of the VH domain, CDR3 loops within the Ig domain may be vastly altered to change the specificity of binding [64]. Therefore, we reasoned the tolerability of the VH domain to large scale sequence swaps might be extended to the Fc region (CH2 and CH3 domains) of immunoglobulins. Based on the information obtained from the alanine scanning, several Fc domain-swap variants were made in order to recapitulate binding affinity for Fc $\alpha$ RI in an IgG1 scaffold (Figure A.3). Residues in the IgG1 CH2 and CH3 domains were replaced with corresponding IgA1 sequences. Mutant B replaces IgG1 residues 336-443 (KGQPR....LSPGK, Kabat numbering [144]) with IgA1 residues 335-444 (SGNTF...KTIDR). This mutant was generated as a negative control for ELISA assays and was previously been shown not to have affinity for the Fc $\alpha$ RI receptor [139]. Mutant C replaces IgG1 residues 336-443 (KGQPR....LSPGK) and 242-254 (PKPKDTLMISRTPE) with IgA1 residues 336-443 (SGNTF...KTIDR) and 245-257 (PALEDLLLGSEAN), respectively. In the IgA:Fc $\alpha$ RI crystal structure the  $\alpha$ 1 IgA CH2 domain loop (PALEDLLLGSEAN) makes extensive contacts with the Fc $\alpha$ RI receptor [140]. Therefore

the entire  $\alpha 1$  loop (PALEDLLLGSEAN) from IgA was substituted into IgG in order to preserve native contacts. Mutant D replaces IgG1 residues 336-443 (KGQPR...LSPGK) and 242-254 (PKPKDTLMISRTPE) with IgA1 residues 336-443 (SGNTF...KTIDR) and 245-257 (PALEDLLLGSEAN), respectively, but also contains an additional glycine following IgA1 residue 257. The glycine residue was added to ensure that the length of the modified IgG CH2 polypeptide is consistent with that of wild type IgG, thus preserving secondary structure contacts. Furthermore, the addition of glycine to the C-terminal end, rather than the N-terminal end of the  $\alpha 1$  loop, was found to be critical for assembly of the hybrid Fc domain (data not shown). ELISA analysis of variant binding to dimeric Fc $\alpha$ RI showed complete loss of binding for MutB whereas both MutC and MutD displayed comparable binding (Figure A.4A). However, SDS-PAGE analysis showed that the MutD Fc assembled into the dimeric form much more efficiently than either MutB or MutC highlighting the importance of the introduced glycine residue to the structure (Figure A.4B).

Surprisingly, exchange of the  $\alpha 2$  loop in the CH2 domain of MutD (residues 307-315 TVLHQDWLN) with IgA residues 307-315 (PGCAEPWNH), identified via alanine scanning, did not confer improved binding to Fc $\alpha$ RI as compared to the unmodified MutD construct. In an attempt to minimize the potential diversity of residues exchanged, Rosetta protein modeling software was used to computationally design several additional variants with substitutions to the IgG  $\alpha 2$  loop. Again, while similar binding affinity to MutD was observed, no significant improvements in binding to Fc $\alpha$ RI were seen by ELISA analysis (data not shown). Hence, MutD was selected for further characterization.

### **Evaluation of Full Length IgA/G Hybrid Binding to Fc Receptors and Complement Factors**

In order to fully recapitulate possible steric and conformation effects generated by the presence of the Fab when Fc receptors are engaged, MutD was expressed in HEK293 cells as a

full length antibody. Control isotype IgG and IgA antibodies were also expressed in the same system to minimize glycan heterogeneity introduced by different expression hosts. When compared by SDS-PAGE to full length IgA, MutD showed a higher percentage of fully assembled protein indicating a greater propensity for correct hinge region disulfide bond formation (Figure 2.3). Circumventing troublesome IgA expression is key to harnessing its therapeutic power and we have consistently noted higher MutD expression levels in HEK293F cell culture than IgA.

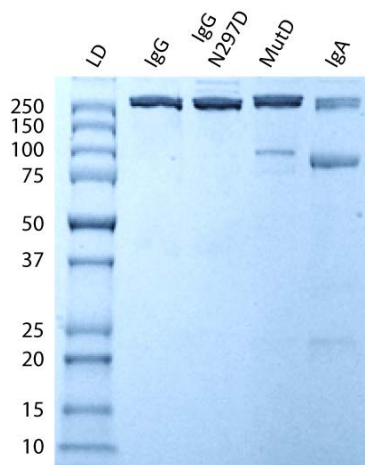


Figure 2.3: 4-20 % SDS-PAGE Analysis of Full Length Expression of Trastuzumab Antibodies.

The dissociation constants ( $K_D$ ) of MutD, IgA and IgG for  $FC\alpha RI$  and the various  $FC\gamma$  receptors were determined by surface plasmon resonance (SPR) (Table 2.1). For evaluation of  $K_D$  values to the low affinity receptors  $FC\gamma RIa$ ,  $FC\gamma RIb$  and  $FC\alpha RI$  interactions, equilibrium binding studies were performed by immobilization of the antibody to the chip surface and the injection of soluble monomeric receptors [145, 146]. Kinetic analysis was used to determine binding affinity, including on and off rates, for immobilized antibody interaction with soluble high affinity  $FC\gamma RI$  receptors.

Table 2.1: SPR Data for MutD Binding to Fc Receptors.

Full length IgG, IgA or MutD antibodies were amine coupled to a CM5 chip surface in 10 mM pH 5.0 Sodium Acetate buffer. Equilibrium binding was established for the low/moderate affinity FcγRIIa, FcγRIIb and FcαRI by flowing monomeric receptor analyte at 30 μL/min. Receptors were left to dissociate in running buffer with the exception of FcαRI which was regenerated with 5 min of contact with 150 mM pH 5.0 formic acid. Kinetic assays were performed on the high affinity FcγRI receptor interactions and the chip was regenerated in 100 mM pH 4.5 citrate buffer. N.D indicates binding not detected.

Variant	$K_D$ (nM)					
	FcγRI	FcγRIIa	FcγRIIb	FcγRIIIa	FcRn	FcαRI
IgG	$0.36 \pm 0.06$	$1140 \pm 50$	$2550 \pm 140$	N.D	N.D	-
IgA	-	-	-	-	-	$233 \pm 11$
MutD	$0.83 \pm 0.16$	$2020 \pm 110$	$4330 \pm 240$	-	-	$502 \pm 41$

The FcαRI:IgA complex naturally forms with 2:1 stoichiometry but apparent affinities can be determined using a simplified 1:1 Langmuir binding model at equilibrium. The mutations made to form MutD introduce *de novo* binding to FcαRI with an apparent affinity of 502 nM, only slightly reduced from the  $K_D$  value of 233 nM determined for wild type IgA. Surprisingly we found that MutD also retains binding for select FcγRs despite the introduction of large structural changes to the CH3 and CH2 domains. FcγRI was shown to bind with a  $K_D$  of 0.83 nM essentially identical to the  $K_D$  of 0.36 nM displayed by wild type IgG. For each of the FcγRIIa and FcγRIIb receptors which have a high degree of sequence identity, the binding affinity for MutD (2.02 μM and 4.33 μM respectively) was reduced by 50% as compared to that of wild type IgG (1.14 μM and 2.55 μM respectively). However, binding affinity for FcγRIIIa was completely lost. Because the mutations to MutD structure lie outside the putative FcγRIIIa binding site it is likely conformational shifts within the CH2 domain altered the Fc structure in a manner detrimental to binding to FcγRIIIa. To investigate the loss of FcγRIIIa binding further, an IgG variant was generated with only residues 245-257 from the α1 swapped with those from IgA (PKPKDTLMISRTPE > PALEDLLLGSEAN). This new variant displayed limited binding to

Fc $\gamma$ RIIIa by ELISA, suggesting the both the CH2 and CH3 domains of IgG play an essential role in binding to this receptor (Figure 2.4).

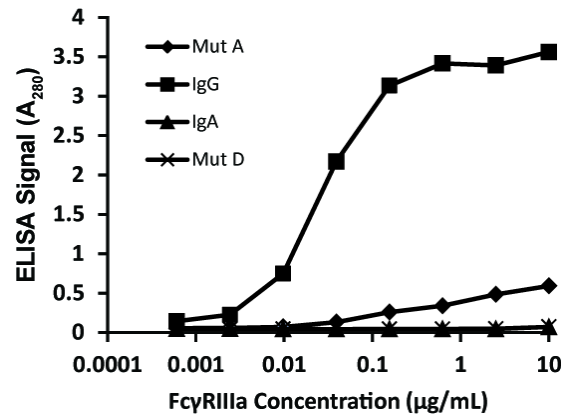


Figure 2.4: ELISA Analysis of Variant Binding to Fc $\gamma$ RIIIa. Hydrophobic ELISA plates were coated with 4  $\mu$ g/mL of each antibody variant and Fc $\gamma$ RIIIa-GST was serially diluted. Bound receptor was detected by goat anti-GST HRP.

Fc $\alpha$ RI binds to IgA antibodies at the CH2/CH3 interface in the Fc domain whereas the Fc $\gamma$ Rs bind near the hinge region and the upper CH2 domain. The overlapping nature of the binding sites for Fc $\gamma$ RI, Fc $\gamma$ RIIa/b and Fc $\gamma$ RIIIa requires engagement of these receptors to be mutually exclusive. By introducing Fc $\alpha$ RI binding to MutD while retaining binding to Fc $\gamma$ Rs we inferred that simultaneous binding of multiple receptors might now be possible. As a positive control, a tandem Fc antibody was constructed containing an IgA Fc domain as a C-terminal fusion to a full length antibody. Simultaneous binding of Fc $\alpha$ RI and His-tagged Fc $\gamma$ RI receptor was detected by sandwich ELISA using an anti-His HRP secondary antibody as described in Figure 2.5A. The data in Figure 2.5B revealed that Fc $\alpha$ RI and Fc $\gamma$ RI bind concurrently to MutD. Since Fc $\alpha$ RI and also Fc $\gamma$ RI share the common gamma chain to transduce activation signals, this

finding might imply this variant could trigger strong cellular responses by bringing surface bound activating receptors into closer proximity than a typical Fc domain.

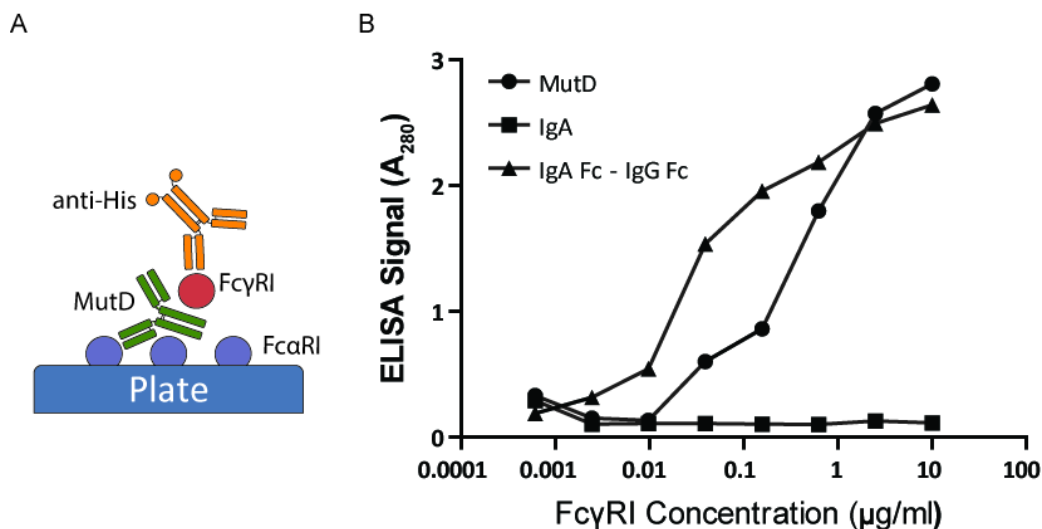


Figure 2.5: ELISA Analysis Shows MutD can Simultaneously Bind to both FcαRI and FcγRI.

A) Sandwich ELISA design. The ELISA plate was coated with 4 μg/mL of dimeric FcαRI followed by 4 μg/mL of each antibody variant. Monomeric His tagged FcγRI was serially diluted and detected with anti-His HRP. B) Concurrent MutD binding to FcγRI and FcαRI. A full length IgA variant was constructed with a C-terminal IgG Fc fusion for use as a positive control (IgA Fc – IgG Fc).

As the FcγRs share a common binding site with C1q, the first molecule in the classical complement pathway, we suspected C1q affinity might be retained in the MutD variant. IgG binding to the complement protein C1q triggers a cascade that is essential in the clearance of bacteria and has been implicated in the clinical mechanism of Rituximab (anti-CD20) for the treatment of lymphoma [61]. ELISA analysis revealed MutD has approximately 10 fold lower affinity for C1q compared to wild type IgG whereas IgA did not bind over the range of concentrations tested as expected (Figure 2.6). IgA is reported

to activate complement by an alternative C1q-independent pathway and was therefore included as a negative control [147].

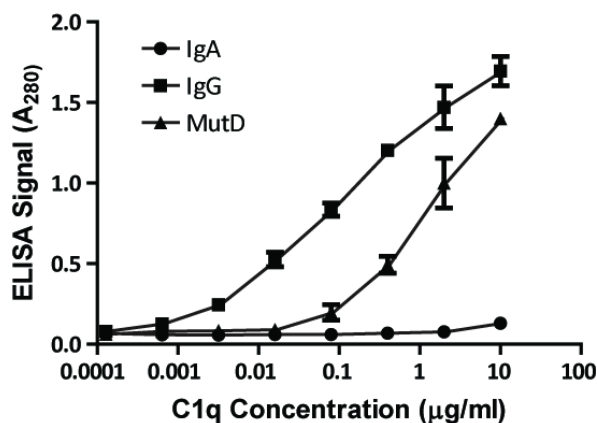


Figure 2.6: MutD Binds C1q from the Classical Complement Pathway. Variants were coated at 4ug/mL on hydrophobic plates and C1q was serially diluted. Detection of bound C1q was performed using a sheep anti-C1q HRP polyclonal secondary.

### ***In vitro* Recruitment of Effector Cells by IgA/G Hybrid Antibodies for Tumor Cell Killing**

*In vitro* cell based ADCC assays provide an important method by which to evaluate immune activation by antibody variants. Importantly, these assays are designed to mimic the *in vivo* formation of immune complexes upon antigen-antibody interaction, which generates high Fc domain avidity for the FcRs. In addition, as the FcRs are bound to cell surfaces, steric effects are accounted for that are not included when evaluating the binding interaction of soluble FcRs with antibodies by SPR or ELISA. The gold standard for evaluating antibody performance in the killing of tumor cells by ADCC is the Cr51 release assay. Tumor cells are loaded with radioactive Cr51 which is released to solution for detection by a scintillation counter upon cell lysis. A higher radioactive count per minute (cpm) indicates better tumor cell lysis efficiency and the percentage of lysis is

calculated as  $100 \times (\text{cpm sample} - \text{cpm background}) / (\text{cpm max lysis} - \text{cpm background})$ . Maximum lysis is determined by incubating tumor cells in a complete lysis buffer to release all intracellular Cr51.

In order to test our MutD variant, neutrophils were chosen as effector cells as they express high levels of both Fc $\alpha$ RI and Fc $\gamma$ Rs and have been shown to mediate potent cytotoxic responses when activated [125] (Figure A.7). Neutrophils were isolated from fresh anti-coagulated human blood obtained from healthy donors in accordance with IRB protocol #2012-08-0031. Following red blood cell lysis, the cells were cultured overnight with IFN- $\gamma$  to mimic the inflammatory environment associated with infection or the presence of a tumor. IFN- $\gamma$  has been reported to upregulate the expression of Fc $\gamma$ RI on neutrophils [148] and this was confirmed by FACS using anti-Fc $\gamma$ RI fluorescent antibodies for each donor (Figure 2.7). After overnight culture, the neutrophil fraction was mixed with Cr51 loaded Her2+ SkBr-3 tumor cells opsonized with anti-Her2 trastuzumab antibody variants. As a negative control an aglycosylated trastuzumab IgG was included that contains the glycan eliminating N297D mutation. Removal of the antibody Fc glycan greatly reduces antibody affinity for the Fc $\gamma$ Rs. All of the antibodies used in the ADCC assay were analyzed for lipopolysaccharide (LPS) levels prior to use to ensure <1 EU/mg was present. LPS can cause antibody independent activation of neutrophil samples that might introduce bias to the ADCC results [149].



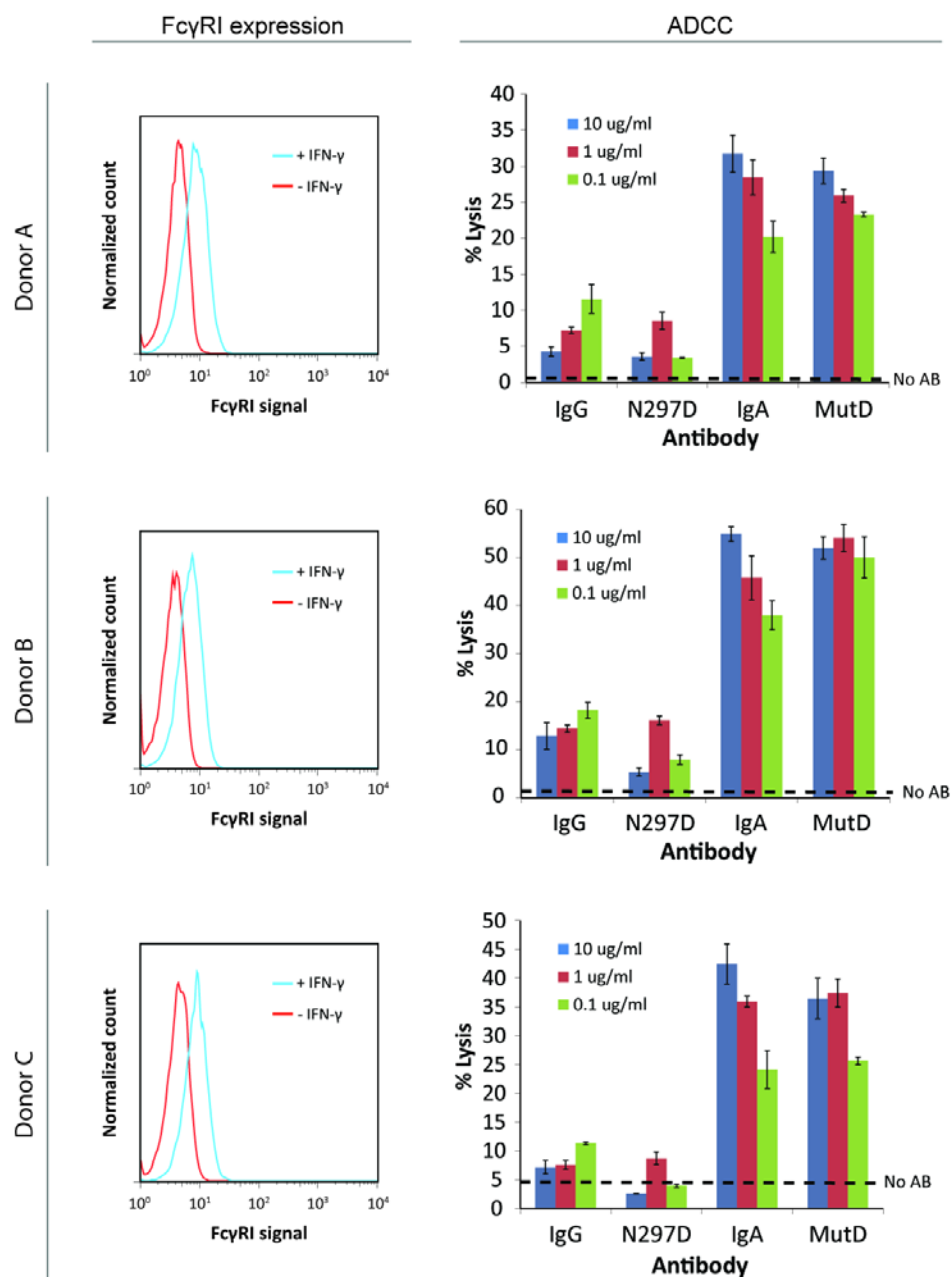


Figure 2.7: MutD Mediated Killing of Her2+ SkBR-3 Cells by ADCC. Neutrophils were purified from fresh blood and cultured overnight in the presence of 50 ng/mL IFN- $\gamma$ . The levels of Fc $\gamma$ RI on the neutrophils were measured before combination with MutD, aglycosylated N297D, IgA or IgG trastuzumab variants at concentrations between 10 and 0.1  $\mu$ g/mL. Tumor cell lysis was determined by release of Cr51 isotope for a 80:1 E:T ratio.

Overnight culture of neutrophils from each donor with IFN- $\gamma$  induced only a moderate two fold increase in Fc $\gamma$ RI expression (Figure 2.7). However, culture with the cytokine did help to maintain neutrophil viability in excess of 95 % for all donors as determined by trypan blue staining. We observed trastuzumab MutD induced high levels of neutrophil mediated ADCC at antibody concentrations as low as 0.1  $\mu$ g/mL. Despite the reduced affinity of MutD for Fc $\alpha$ RI as compared to IgA, the percentage lysis was comparable to trastuzumab IgA. This observation suggests some Fc $\gamma$ R activity might be contributing to MutD mediated neutrophil activation. The contribution of Fc $\gamma$ R activation to tumor cell lysis is likely small as exemplified by the low percentage killing by wild type IgG (3-4 fold less tumor lysis than than IgA). Surprisingly, aglycosylated antibodies containing the N297D mutation also showed some small level of tumor cell killing in excess of the no antibody negative control levels. Recent work has shown that while binding to the Fc $\gamma$ Rs is greatly reduced in aglycosylated antibodies, residual affinity for high affinity Fc $\gamma$ RI be amplified by avidity effects when in immune complex form to activate immune cells [150].

### **Approaches for Half-life Extension of MutD Hybrid IgA/G antibodies**

The serum half-life of IgG antibodies is greatly enhanced by binding to FcRn [52]. Under acidic conditions (pH < 6.5) FcRn binds tightly to IgG sequestered within early stage endosomes formed following the pinocytosis of fluid from circulation. Upon return to the cell surface, the slight alkalinity of the serum (pH 7.4) triggers release back into circulation. Unfortunately, the amino acid substitutions made at the CH2/CH3 hinge region to generate MutD have abolished affinity for FcRn and binding to this receptor was not detected (Table 2.1). The loss of FcRn binding is likely to reduce the serum half-

life of MutD, although Fc $\alpha$ RI binding has been shown to have a moderate contribution in the recycling of IgA antibodies [151]. However, both linear (QRFVTGHFGGLYPANG) and cyclic peptides (QRFCTGHFGGLHPCNG) have been recently discovered which bind to FcRn in a pH dependent manner; low binding is observed at pH 7.4 and high binding at acidic pH 5.8 [138]. We thought to evaluate FcRn binding to C-terminal fusions of each of the peptides with full length trastuzumab MutD.

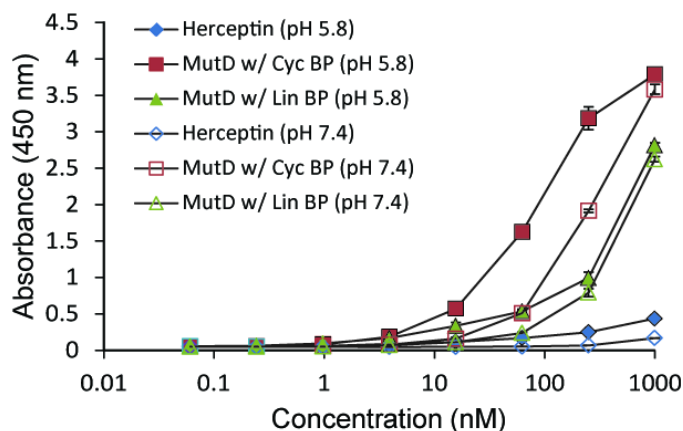


Figure 2.8: Characterization of MutD with C-terminal Peptide Fusion Binding to FcRn at pH 5.8 and 7.4. FcRn was bound to the plate surface and antibodies at 1  $\mu$ M were added before detection with anti-Human heavy and light chain HRP secondary antibody at a 1:5000 dilution.

When analyzed by ELISA, fusion of the cyclic FcRn binding peptide to MutD had the highest binding to FcRn at both pH 5.8 and substantial but reduced binding at pH 7.4 (Figure 2.8). By contrast, fusion of linear peptide fusion did not show significant difference in binding between pH 5.8 and 7.4. The inefficient release of antibody at physiological pH can have the unintended consequence of reducing the serum half-life of therapeutic antibodies [152]. The binding of clinical grade IgG Herceptin without any

peptide fusion to FcRn was barely detectable by ELISA suggesting the peptide fusions have affinity for FcRn far in excess of wild type levels. Because the Fc domain is homodimeric, avidity effects created by the close proximity of two copies of the fusion peptides at the antibody C-terminus likely account for this increase in observed affinity. Both MutD fusions will require *in vivo* testing to truly evaluate the effect on half-life of these peptides.

## DISCUSSION

The challenges associated with IgA expression and purification have limited the use of this isotype as a therapeutic despite the wide range of inflammatory function that can be mediated by the Fc $\alpha$ RI receptor. By engineering Fc $\alpha$ RI binding into an IgG Fc scaffold to form MutD, we have introduced potent new function in the recruitment of neutrophils for ADCC while retaining close to wild type binding for most of the Fc $\gamma$ Rs. The MutD variant is particularly significant in that it is the first Fc domain engineered to have binding for receptors of multiple antibody isotypes. Deconvolution of the exact contribution towards inflammatory function mediated by each of the receptor classes (Fc $\alpha$ RI and the Fc $\gamma$ Rs), as well as C1q from the complement cascade, is now required to better understand MutD function and guide the design of future variants. This undertaking is somewhat complicated by the widespread expression of both the Fc $\gamma$ Rs and Fc $\alpha$ RI on human myeloid lineages [44, 153]. However, Fc $\alpha$ RI is not expressed in mice owing to an ancient genomic translocation event that deleted the receptor gene [154]. Mice might therefore provide a model system to evaluate the Fc $\gamma$ R function mediated by MutD.

Peculiarly, while binding to Fc $\gamma$ RIIa and Fc $\gamma$ RI is maintained, MutD does not bind Fc $\gamma$ RIIIa even though the Fc $\gamma$ R family shares a common binding site in the antibody hinge region. Analysis of the afucosylated IgG1 crystal structure complexed with Fc $\gamma$ RIIIa, as shown in Figure 2.9, indicates that none of the Fc domain amino acids providing contacts with Fc $\gamma$ RIIIa are in close proximity to the MutD mutations. Though it is plausible the MutD structure assumes a CH2 domain conformation which selectively excludes Fc $\gamma$ RIIIa binding, there are also possible contacts between the glycans appended to N297 and the  $\alpha$ 1 loop in the CH2 domain of the Fc (dashed circle in Figure 2.9). The disruptions caused by exchange of this loop might have altered the glycan conformation

or even prevented glycan attachment thus eliminating binding to FcγRIIIa. Information provided by solving of the MutD crystal structure will be invaluable for guiding the design of next generation variants of MutD with restored FcγRIIIa binding.

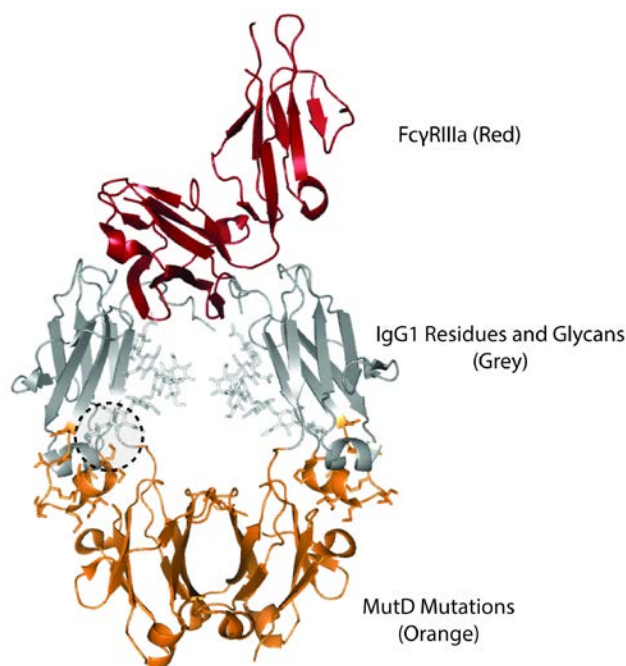


Figure 2.9: Afucosylated IgG1 Fc Domain in Complex with FcγRIIIa (PDB: 3ay4). Residues mutated in MutD are highlighted orange and the dashed circle shows the location of possible glycan contacts with the  $\alpha 1$  loop of the IgA structure.

Despite the loss of FcγRIIIa binding, MutD recruits IFN- $\gamma$  activated neutrophils for the killing of Her2+ SkBr-3 cells with similar efficiency to IgA and shows significantly better killing than wild type IgG. The robust killing of tumor cells mediated by MutD recruitment of neutrophils could be very important for the treatment of *in vivo* cancers. The sheer abundance of the neutrophil population in circulation is a distinct advantage, especially since expansion can be rapidly accomplished via injection of G-CSF [123]. As well as directing cytotoxic responses, neutrophils secrete a variety of

cytokines and chemokines to recruit additional immune cell subsets for inflammatory action [155]. For example, depletion of neutrophils from murine tumor models reduced cytotoxic T lymphocyte activation suggesting neutrophils play a vital role in modulating inflammatory adaptive immune responses [156]. The discovery of MutD provides access to the wide array of function mediated by Fc $\alpha$ RI without any of the current regulatory and expression concerns surrounding the use of IgA or IgA antibodies in conjunction with IgG. The development of tumor models using Fc $\alpha$ RI transgenic mice [56, 157] will be essential for evaluating therapeutic potential of MutD and future hybrid IgG/A variants.

### **Chapter 3: Effective Phagocytosis of Low Her2 Tumor Cell Lines with Engineered, Aglycosylated IgG Displaying High FcγRIIa Affinity and Selectivity**

#### **INTRODUCTION**

Antibodies trigger a wide array of responses in leukocytes by linking antigenic targets on pathogens with FcγRs expressed on the surface of macrophages, granulocytes, dendritic cells, natural killer (NK) cells and B cells. Evidence suggests that the ratio of binding affinities of IgG1 in solution for the activating FcγRs and inhibitory FcγRIIb (A/I ratio) guides the extent of effector functions displayed by immune cells [48, 72, 158]. However, since signaling by FcγRs requires multivalent interaction with ICs, other parameters such as avidity of the ICs, FcγR expression level and cell surface distribution of the FcγRs on effector cells likely influence the nature of the response in addition to the A/I ratio. Although significant effort has been expended engineering Fcs for enhanced binding to FcγRIIIa to promote better NK cell killing, other cell subsets, including macrophages, can be strongly activated by FcγRIIa [75].

There are two common polymorphisms within the FcγRIIa subclass which affect the binding affinity to IgG1 antibodies [116]. Individuals expressing the high affinity FcγRIIa-H131 allele are correlated in some studies with improved clinical response when treated with trastuzumab, rituximab or cetuximab [39-41]. Conversely, those homozygous for FcγRIIa-R131 have an increased risk of bacterial infection and autoimmunity due to the low affinity interaction with IgGs impairing immune complex clearance [159-162]. Because the low affinity FcγRIIa-R131 allele arises at a frequency between 0.47 - 0.57 in African Americans, 0.45 - 0.53 in Caucasians and 0.19 - 0.45 in Asians, the engineering of antibody Fc domains that can enhance responses in patients bearing the FcγRIIa-R131 allele is of significant mechanistic and clinical interest [162-



164]. Particularly, the engagement of FcγRIIa is strongly implicated in the phagocytosis of tumor cells by macrophages, which were shown to comprise nearly 20% of infiltrating leukocytes in breast cancer biopsies [165].

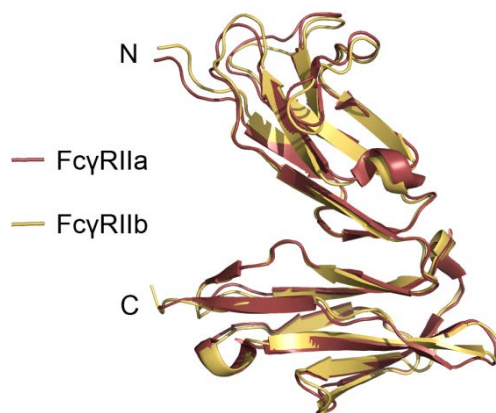


Figure 3.1: Overlaid FcγRIIa (PDB: 1H9V) and FcγRIIb (PDB: 2FCB) have High Structural Homology and Sequence Identity.

Attempts to engineer IgG1 antibodies with enhanced FcγRIIa selectivity have either led to comparatively modest improvements in the A/I ratio (less than 6 fold change compared to wild-type) and/or increased affinity for both FcγRIIa and FcγRIIb [71, 75, 166]. Two predominant issues complicate the engineering of antibodies that display optimal FcγRIIa/FcγRIIb selectivity and FcγRIIa affinity for enhanced phagocytic potential: First, FcγRIIa shares 96% amino acid identity with FcγRIIb and therefore the generation of Fc ligands with discriminating power between the two is challenging (Figure 3.1) [167]. Second, because of the avidity effects involved when antibody-decorated tumors interact with effector cells it is not easy to determine *a priori* whether high affinity to FcγRIIa, or a higher A/I ratio, or both are needed to enhance phagocytosis. Using aglycosylated antibodies as scaffolds for the reintroduction of FcγR

function presents a new approach to tackle these problems. The high flexibility of the CH2 domain in aglycosylated Fcs might allow for the identification of amino acid substitutions that stabilize certain conformers not accessible to glycosylated antibodies. We hypothesized that such substitutions might confer unusually high FcγRIIa affinity and selectivity with respect to binding to the highly homologous but inhibitory FcγRIIb for improved phagocytic potentiation. Accordingly, we report here that using a new library screening system we successfully isolated an engineered trastuzumab variant displaying >160 fold increased affinity for the FcγRIIa-R131 allele and a >25 increase in A/I ratio compared to clinical grade glycosylated trastuzumab (Herceptin). The Fc engineered trastuzumab was shown to elicit a striking increase in ADCP when using human macrophages as effector cells relative to Herceptin for both +3 (SKOV-3) and +2 (MDA-MB-453) Her2 expressing cell lines [168]. To provide design criteria for further improving the efficacy of Fc variants a mathematical model was developed to establish the relationship between IgG binding to FcγRIIa/FcγRIIb and the activation of phagocytosis.

## **MATERIALS AND METHODS**

### **Library Construction**

An error prone PCR library using the trastuzumab-CH2-CH3 region of Fc5-2a as a template was created using standard techniques [169] and the two primers STJ#485 and STJ#67. VH-CH1 was then PCR amplified using the primers STJ#474 and STJ#486 from the template (pSTJ4-AglycoT). The two fragments, hinge-CH2-CH3 regions and VH-CH1 regions, were assembled by gene assembly PCR using the primers STJ#474 and STJ#67 to generate the trastuzumab heavy chain (VH-CH1-Hinge-CH2-CH3) library. The amplified heavy chain library genes were ligated into SfiI-digested pPelBFLAG. The resulting plasmids were transformed into *E. coli* Jude-1 harboring the light chain plasmid (pBAD-AglycoT(L)-His).

### **Culture and Spheroplasting of *E. coli* for Library Screening**

For screening, *E. coli* Jude-1 cells containing the heavy chain plasmid (pPelB-VH-CH1-Hinge-CH2-CH3) and the light chain plasmid (pBAD-AglycoT(L)-His) were cultured overnight at 37 °C with 250 rpm shaking in TB supplemented with 2% (w/v) glucose and appropriate antibiotics (40 µg/mL of chloramphenicol and 50 µg/mL of kanamycin). The overnight cultured cells were diluted 1:100 in 110 mL of fresh TB. After incubation at 37 °C for 2 h and cooling at 25 °C with 250 rpm shaking for 20 min, protein expression was induced with 1 mM of isopropyl-1-thio-D-galactopyranoside (IPTG). Following protein expression for 20 h, spheroplasts were prepared from 36 mL of culture broth for library screening.

## Library Screening

Glycosylated FcγRIIa-R131-GST [170] was labeled with Alexa488 using an Alexa488 labeling kit (Invitrogen). A competitive screen was used to isolate clones with high binding affinity for FcγRIIa over FcγRIIb in which spheroplasts were incubated with fluorescent FcγRIIa-R131-GST-Alexa488 with excess amounts of non-fluorescent FcγRIIb-GST present (concentration of FcγRIIa-R131-GST-Alexa488: concentration of non-fluorescent FcγRIIb-GST = 30 nM: 100 nM for the 1st round, 10 nM: 100 nM for the 2nd round, 10 nM : 100 nM for the 3rd round, 5 nM : 100 nM for the 4th round, and 5 nM : 200 nM for the 5th round of sorting). More than  $4 \times 10^8$  spheroplasts were sorted in the first round of screening on a MoFlo flow cytometer (Dako Cytomation) equipped with a 488 nm argon laser for excitation. In each round, the top 3% of the population showing the highest fluorescence was isolated and resorted immediately after the initial sorting. The heavy chain genes (VH-CH1-CH2-CH3) in the spheroplasts were amplified from the collected spheroplasts by PCR with two specific primers STJ#474 and STJ#67, ligated into *Sfi*I restriction enzyme digested pPelBFLAG-Fc, and transformed in electrocompetent *E. coli* Jude-1 cells. The resulting transformants were grown on chloramphenicol containing LB agar plates and prepared again as spheroplasts for the next round of sorting.

## SPR Analysis

Surface plasmon resonance (SPR) was performed using a BIAcore 3000 instrument (GE Healthcare). Herceptin, AglycoT-Fc5-2a, AglycoT-Fc1001, AglycoT-Fc1002, AglycoT-Fc1003, and AglycoT-Fc1004 were individually immobilized on CM5 sensor chips by amine coupling as recommended by the manufacturer. Binding

experiments were performed in HBS-EP buffer (10 mM HEPES pH 7.4, 150 mM NaCl, 3.4 mM EDTA, and 0.005% P20 surfactant)(GE Healthcare). Dimeric FcγRIIa-131R-GST, FcγRIIa-H131-GST, and FcγRIIb-GST receptors were injected in duplicate at a flow rate of 30 µl/min for 60 s with a dissociation time of 5 min. The chip was regenerated after each run by sequential injection of 50 mM glycine, pH 4.0, 50 mM glycine, pH 9.5, and 3 M NaCl for 2 min each. For each run, a bovine serum albumin-coupled (BSA) surface was used to subtract non-specific receptor binding. Equilibrium dissociation constants (KD) for monovalent receptor binding were determined by fitting a 2:1 bivalent analyte model ( $A + 2B \rightleftharpoons AB + B \rightleftharpoons AB_2$ ) to the data using BIAevaluation 3.2 software (GE Healthcare) in accordance with earlier analyses [171]. To determine binding to FcγRI, purified IgGs were immobilized on activated amine CM5 Biacore chips in 10 mM sodium acetate buffer (pH 5.0) and BSA in 10 mM sodium acetate (pH 5.0) was immobilized to a control lane on each chip for background receptor binding subtraction. 30 µl samples of purified FcγRI (R&D Systems) in HBS-EP running buffer were injected in duplicate and dissociation was monitored over a 5 min period. 10 mM glycine at pH 3.0 was used for chip regeneration between samples. The data were fit to a 1:1 Langmuir binding model as described earlier to obtain kinetic constants [172].

## ELISAs

ELISA plates (Corning) were coated with 4 µg/mL of Her2 protein (Sino Biological) in 0.05M Na<sub>2</sub>CO<sub>3</sub> (pH 9.5) overnight at 4 °C. The next day the plates were blocked at room temperature for 2 h with 2% milk in PBS containing 0.05% Tween (PBST) and washed four times in PBST at pH 7.4 before the addition of 4 µg/mL of antibody dissolved in PBS with 2% milk (PBSM). After 1 h of incubation, the plates were washed with PBST 4x and then 66 µl of FcγRIIIa-GST at 20 µg/mL added to the

first well followed by 1:4 serial dilution. The plates were incubated at room temperature for 1 h, washed with PBS 4x and 50  $\mu$ l PBSM was added containing goat anti-GST HRP (GE Healthcare) 1:5000 for 1 h. To develop the plates, the wells were washed 4x with PBST and 50  $\mu$ l TMB substrate was added per well (Thermo Scientific). 50  $\mu$ l of 1 M  $\text{H}_2\text{SO}_4$  was used for neutralization and the final  $\text{Abs}_{450}$  was recorded.

### **HER2 Cell Surface Density**

To qualitatively evaluate the density of HER2 receptors on the surface of SKBR-3 (ATCC), SKOV-3 (ATCC), and MDA-MB-453 (ATCC) cells, 10  $\mu\text{g}/\text{mL}$  of Herceptin or IgG1 pooled from human serum (Sigma-Aldrich) as a control were incubated with 106 cells for 45 min on ice in 1 mL of Stain buffer (BD Biosciences). Subsequently, the Herceptin or IgG1 bound cells were washed with 1 mL of Stain buffer by centrifugation at 400 x g for 5 min, and labeled with 1:50 diluted donkey anti-human IgG (H+L) FITC-conjugate Fab (Jackson ImmunoResearch Laboratories) on ice for 45 min. The cells were washed twice more with 1 mL of Stain buffer following the centrifugation procedure above and cell fluorescence was analyzed by flow cytometry (BD FACSCalibur).

### **Preparation of Human Monocyte-derived Macrophages**

PBMCs were isolated from fresh human pooled blood samples (Gulf Coast Regional Blood Center) by Histopaque (Sigma-Aldrich) gradient centrifugation. Briefly, 20 mL Histopaque was added to 50 mL conical tubes followed by 30 mL of blood gradually. The mixture was centrifuged for 15 min in a swinging bucket rotor without

braking at 800 x g. PBMCs were aspirated from the sample and transferred to a fresh tube. The sample was washed twice with 50 mL PBS containing 2% FBS (Mediatech) and 1 mM EDTA by centrifuging without braking at 120 x g for 10 min to remove platelets from the sample. CD14<sup>+</sup> monocytes were isolated by magnetic bead separation (Stemcell Technologies) according to the manufacturer's instructions. Cells were resuspended in RPMI (Invitrogen) containing 15% FBS and seeded at  $1.5 \times 10^6$  cell per well in 96 well plates containing 3 mL of the same media supplemented with 50 ng/mL GM-CSF (R&D systems). The cells were grown at 37 °C in 5% CO<sub>2</sub> and at days 2 and 5 of culture and an additional 1 mL of media with fresh cytokine was added to each well. After 7 days, non-adherent cells were aspirated and the plate was washed with Dulbecco's PBS (Mediatech). 1 mL HyQTase (Thermo Scientific) solution was added for 15 min at 37 °C for the detachment of macrophages from the plate surface. Recovered cells were washed with 50 mL RPMI media and resuspended in RPMI containing 10% Human AB serum (Mediatech). Macrophage differentiation was confirmed by staining with 10 µg/mL anti-CD14-APC (Clone M5E2, Biolegend) and 10 µg/mL anti-CD11b-APC (Clone ICRF44, Biolegend).

### **Quantification of FcγRs on Macrophages**

The anti-FcγRIIb antibody, 2B6-N297D [22] was transiently expressed and FITC labeled alongside an aglycosylated human IgG1 isotype control using a FITC conjugation kit (Invitrogen). Monocyte-derived macrophages were cultured as above and labeled separately with 20 µg/mL anti-FcγRI-FITC (Clone 10.1, Genetex), 10 µg/mL anti-FcγRIIa-FITC (Clone IV.3, Stemcell Technologies), 20 µg/mL anti-FcγRIII-FITC (Clone 3G8, Abcam), 1 µg/mL 2B6-N297D-FITC, 1 µg/mL human aglycosylated IgG1-FITC

isotype control as well as FITC conjugated murine isotype control antibodies for IgG1 (20 µg/mL Clone 15H6, Biolegend) and IgG2b (10 µg/mL Clone MG2b-57, Biolegend). Receptor counts were determined in a FACS assay by comparing the fluorescent values of antibody labeled macrophages to standard curves generated by bead standards that capture precisely known numbers of each of the labeling antibodies (Quantum Simply Cellular anti-mouse and anti-human, Bangs Laboratories).

### **ADCP Assays**

Tumor cells were recovered from culture flasks by trypsinization, labeled with PKH67 (Sigma-Aldrich) according to the manufacturer's instructions and resuspended in RPMI with 10% human AB serum. These cells were seeded at  $2 \times 10^4$  per well in 96 well V-bottom plates (Corning) followed by addition of macrophages at the appropriate effector: tumor cell ratio (1:5 MDA-MB-453, 1:10 SKOV-3) and antibodies, to a final concentration of 0.5 µg/mL. The plate was briefly spun at 2,000 rpm for 1 min and incubated at 37 °C with 5% CO<sub>2</sub> for 2 h (MDA-MB-453) or 4 h (SKOV-3). Cells were detached from the plate by HyQTase treatment for 15 min and stained with 10 µg/mL anti-CD11b-APC and 10 µg/mL anti-CD14-APC on ice for 1 h. Phagocytosis was evaluated by FACS on an LSRFortessa (BD Bioscience), and reported as the fraction of double positive cells over the total number of tumor cells in the sample (see Figure 3.5 for process overview). Fluorescent microscopy was performed on an Axiovert 200M (Carl Zeiss MicroImaging GmbH).



## RESULTS

### Development and Characterization of a Full Length Antibody Display System in Bacteria

Previous work showed that *E. coli* spheroplasts (bacteria lacking the outer membrane after chemical treatment to render periplasmic and inner membrane proteins accessible to exogenously added ligands), expressing engineered human Fc domains with the hinge region, bound FcγRI with affinity comparable to those determined *in vitro* using SPR analysis of binding kinetics [172]. However, we found that the binding of the aglycosylated Fc2a mutant, which had been engineered to bind FcγRIIa/FcγRIIb [166], was impaired when displayed in the homodimeric Fc display system [172]. Therefore, a full length IgG1 display system was developed by Dr Sang Taek Jung to accurately capture the conformational and steric effects present when antibodies interact with Fc binding ligands (Figure 3.2).

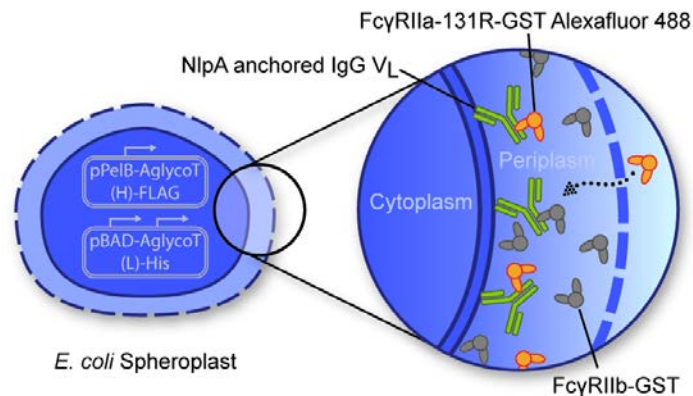


Figure 3.2: Full Length Display of IgG Antibodies in Bacteria. NlpA anchors light chains to the inner membrane surface in the periplasm for assembly with soluble heavy chains and soluble light chains expressed concurrently. Spheroplasting disrupts the outer membrane to provide access for exogenous FcγRs that, if fluorephore labeled, indicate binding when interrogated by flow cytometry.

For this purpose, the light chain (L chain) was fused at the N-terminal with the PelB leader peptide and the first 6 amino acids of the *E. coli* inner membrane lipoprotein NlpA which anchor it to the periplasmic side of the bacterial inner membrane [173]. To avoid steric constraints that might arise if both L chains of an IgG molecule are membrane-anchored, we constructed the dicistronic pBAD-AglycoT(L)-His plasmid which expresses NlpA anchored L chain ( $V_L$ -C $_{\kappa}$ ) as well as unanchored L chain from the same promoter (Figure B.1A). Heavy chain polypeptides expressed by pPelB-AglycoT(H)-FLAG and secreted into the periplasm assemble either with: (i) two unanchored L chains, (ii) a membrane-anchored and an unanchored L chain, or (iii) two membrane-anchored L chains. The unanchored IgG in the periplasm is preferentially released from the bacteria following spheroplasting, whereas anchored IgG comprising one membrane-anchored and one unanchored L chain (or two membrane-anchored L chains) is retained on the surface of the spheroplasts. The Fc domain in the membrane-anchored IgG is free to interact with exogenously added, fluorescently labeled Fc $\gamma$ Rs for fluorescence activated cell sorting analysis (FACS) and library screening. To validate the IgG display strategy, the H and L chains of AglycoT-Fc5 (aglycosylated trastuzumab with E382V/M428I [172]) and AglycoT-Fc2a (aglycosylated trastuzumab with S298G/T299A [166]) were cloned separately into pPelB-AglycoT(H)-FLAG vector and expressed in *E. coli*. Under optimized culture conditions, AglycoT-Fc5 expressing spheroplasts displayed high fluorescence following labeling with Fc $\gamma$ RI-FITC (Figure B.1B) whereas spheroplasts expressing AglycoT-Fc2a could be labeled selectively with Fc $\gamma$ RIIa-GST/anti-GST-FITC (Figure B.1C). In both instances, a large increase in fluorescent signal was observed relative to the negative control, indicating that inner membrane-anchored IgG display is well suited for the engineering of aglycosylated

antibody Fc variants that bind to other Fc receptors (FcγRI, FcγRIIa, FcγRIIb, FcγRIIIa/b, or FcRn).

### **Isolation and Characterization of Aglycosylated IgG Fc Variants Displaying High Affinity and Binding Selectivity towards the FcγRIIa-R131 Allele**

An IgG that combined mutations from both Fc5 and Fc2a (E382V/M428I/S298G/T299A) was constructed and shown to display binding affinity to both FcγRI and FcγRIIa/FcγRIIb comparable to that of Fc5 and Fc2a respectively when expressed as individual variants (Figure B.1D). SPR analysis of the purified AglycoT-Fc5-2a conducted by Tae Hyun Kang revealed that binding to FcγRI was significantly reduced relative to Herceptin (11 fold decrease or a 3-fold decrease relative to AglycoT-Fc5). Interestingly, this antibody showed a small (40 %) but reproducible increase in the selectivity for FcγRIIa-R131 allele relative to FcγRIIb (AIIa-R131/I ratio) when compared to Herceptin and an even more significant increase in AIIa-R131/I relative to AglycoT-Fc2a (Table 3.1:). Therefore, AglycoT-Fc5-2a was used as a template for random mutagenesis and the isolation of variants that exhibit improved binding to the low affinity FcγRIIa-R131 allele and simultaneously increased AIIa-R131/I ratios. A library of random mutations in the Fc domain of AglycoT-Fc5-2a was created by error prone PCR to yield  $4.8 \times 10^9$  transformants. Cells were incubated with a progressively increasing excess of unlabeled FcγRIIb-GST (extracellular domain of FcγRIIb fused with glutathione-S-transferase (GST) from *Schistosoma japonicum*), over highly homologous fluorescent FcγRIIa-GST-Alexa488 conjugate to help enrich variants displaying improved FcγRIIa/FcγRIIb selectivity. After five rounds of sorting, four individual clones showing markedly improved fluorescence upon incubation with 20 nM FcγRIIa-GST–

Alexa-488 and 100 nM of FcγRIIb-GST relative to spheroplasted cells expressing AglycoT-Fc5-2a were isolated (Figure B.2 and B.3A). Cells expressing the clone termed AglycoT-Fc1001 (S298G, T299A, H268P, E294K, N361S and E382V, M428L (Figure 3.4A)) exhibited the highest fluorescence under these conditions. Interestingly, the best performing variant in ADCP assays, AglycoT-Fc1004 (S298G, T299A, N390D, E382V, M428L (Figure 3.4B)) showed the lowest fluorescent signal.

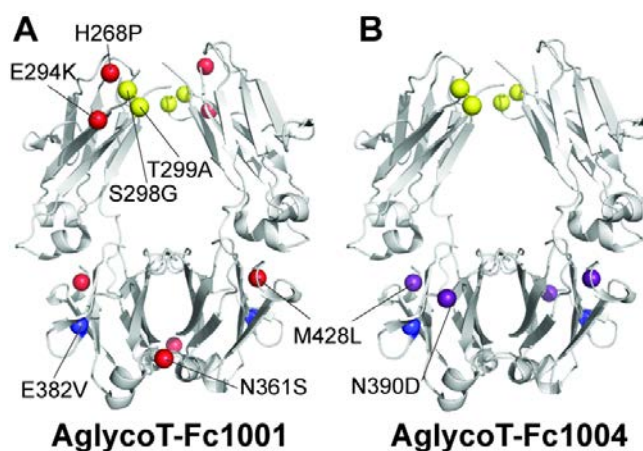


Figure 3.3: Mutations Isolated in AglycoT-Fc1001 (A) and AglycoT-Fc1004 (B) are Shown on the 3D Structure of an Aglycosylated IgG1 Fc (PDB: 3S7G). Yellow = AglycoT-Fc2a base mutations, Blue = AglycoT-Fc5 base mutations, Red = AglycoT-Fc1001 mutations, and Purple = AglycoT-Fc1004.

Expression differences between the Fc1001 and Fc1004 variants are likely to be responsible for the qualitative difference between FACS signal and FcγRIIa binding; this can be addressed by two color sorting that also monitors antibody expression. Note that in AglycoT-Fc5-2a, residue M428 had been mutated to Ile, which was further changed to an Leu in AglycoT-Fc1004 and the three other selected clones pointing to the functional significance of this residue for effector FcγR binding (Figure B.2).

The four IgG variants corresponding to the sequences encoded by the highest fluorescence clones isolated by FACS were expressed in HEK293F cells to limit endotoxin contamination and purified (Figure B.3B). All IgGs contained the S298G/T299A mutations which block glycosylation at N297 and thus do not bind Concanavalin A. Binding of dimeric purified GST fusions of FcγRIIa-H131, FcγRIIa-R131 and FcγRIIb to each IgG variant was determined by SPR analysis (Table 3.1). A bivalent binding model was used to fit the sensorgram curves and obtain monomeric binding constants in accordance with earlier studies (Figure B.4) [171]. This methodology resulted in equilibrium dissociation values,  $k_{on}$  and  $k_{off}$  rate constants for the binding of Herceptin and the various mutant Fcs to FcγRs that were in excellent agreement with the recent comprehensive binding data of all human IgG subclasses to effector FcγRs [116]. For easy comparison in Table 3.1, the binding data is reported as  $K_{D, \text{mutant}} / K_{D, \text{Herceptin}}$  ratios and also as  $(A/I)_{\text{mutant}} / (A/I)_{\text{Herceptin}}$  values. AglycoT-Fc1004 IgG displayed the highest affinity for both FcγRIIa polymorphisms: a remarkable 163 fold improvement in  $K_D$  for the low affinity FcγRIIa-R131 relative to Herceptin and a more modest 5.7 fold affinity improvement for the high affinity FcγRIIa-H131 allele. The large increase in affinity towards FcγRIIa-R131 is consistent with the use of this receptor polymorphism for FACS screening. While AglycoT-Fc1004 showed somewhat higher affinity towards the inhibitory FcγRIIb, the much greater increase in FcγRIIa-R131 affinity resulted in 25 fold improvement in  $A_{\text{IIa-R131}}/I$  selectivity compared to Herceptin and a 16 fold increase in selectivity relative to its parental variant, AglycoT-Fc5-2a. AglycoT-Fc1001 displayed 21 fold higher FcγRIIa-R131 affinity than Herceptin and an  $A_{\text{IIa-R131}}/I$  of 7.5 (5.3 fold increase relative to AglycoFc5-2a). The two other IgGs isolated from the screening displayed only marginal increases in FcγRIIa-R131 binding and lower affinity towards the FcγRIIa-H131 allele.

Table 3.1: SPR Analysis.

Showing the Ratio of Variant Affinity of Aglycosylated Trastuzumab Fc Variants to That of Glycosylated Herceptin for FcγRIIa-R131, FcγRIIa-H131 FcγRIIb, and FcγRI

Variant	Ratio of variant affinity relative to Herceptin				A/I ratio	
	FcγRI	FcγRIIa (H131)	FcγRIIa (R131)	FcγRIIb	H131	R131
Herceptin	1 <sup>#</sup>	1	1	1	1	1
AglycoT-Fc5-2a	0.096	0.32	1.1	0.81	0.40	1.4
AglycoT-Fc1001	0.020	0.60	21	2.8	0.22	7.5
AglycoT-Fc1002	N/A	0.63	1.4	0.68	0.92	2.1
AglycoT-Fc1003	N/A	0.67	2.6	1.3	0.51	2.0
AglycoT-Fc1004	0.024	5.7	163	6.5	0.88	25

The binding kinetics of the two highest affinity clones AglycoT-Fc1004 and AglycoT-Fc1001 and their parental AglycoT-Fc5-2a towards FcγRI were evaluated by SPR and the data were fit with a 1:1 Langmuir binding model [171]. AglycoT-Fc5-2a displayed a 10 fold decrease in FcγRI binding compared to Herceptin, which was further reduced in AglycoT-Fc1004 and AglycoT-Fc1001 to almost a 50 fold lower level. Evidently, the S298G/T299A mutations that conferred binding to FcγRIIa and FcγRIIb to aglycosylated IgGs suppressed the ability of the Fc5 amino acid substitutions to bind FcγRI. The fact that AglycoT-Fc1004 has only two amino acid substitutions in the CH3 domain (N390D, M428L), yet has 5 fold lower KD for FcγRI relative to its parental AglycoT-Fc5-2a template. Our data shows that the reason for the decreased FcγRI affinity of Fc1004 results from the N390D mutation and the subtle change I428L

(compared to I428M in the parental antibody Fc5-2a). Both of these mutations are in the CH3 domain which is distal to the FcγR binding epitope, underscoring the significance of conformational flexibility in these interactions. This finding is consistent with the recent structural data that indicates in the absence of glycosylation the Fc domain displays a high degree of conformational flexibility and our hypothesis that mutations within the CH3 domain can stabilize particular conformers with unusual FcγR binding properties [112]. In particular, M428L is located near the hinge region of the CH2 and CH3 domains where this mutation likely influences the local conformation and favorably impacts the binding of antibodies to FcRn [174].

The isolated IgGs displayed no binding to either of the two FcγRIIIa polymorphisms (F158 and V158) as determined by ELISA (Figure B.3C). Interestingly, both AglycoT-Fc1001 and AglycoT-Fc1004 showed higher binding to the neonatal Fc receptor, FcRn, at endosomal pH 6.0 but not at physiological pH (Figure B.3D). This was most likely the consequence of the M428L mutation, which had been shown earlier to improve binding affinity for FcRn at pH 6.0 by 11 fold and thus confer extended IgG serum persistence and pharmacokinetics in animal models [174].

### **Enhanced ADCP of Low and Medium Her2<sup>+</sup> Cell Lines**

Surface expression of Her2 on SKBR-3, SKOV-3 and MDA-MB-453 Her2<sup>+</sup> cells was evaluated by FACS following incubation with Herceptin and a fluorescently labeled secondary antibody. SKBR-3 cells showed a 2 fold higher FACS signal relative to SKOV-3 which in turn had a 2 fold greater Her2 binding signal than MDA-MB-453 cells

(Figure 3.4A). These results are consistent with the total Her2 expression in these cell lines as determined by Western blotting [175].

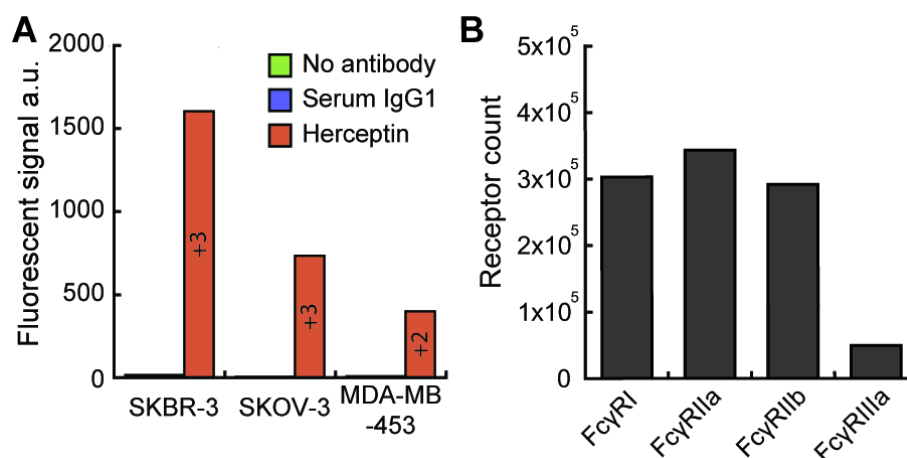


Figure 3.4: Expression Level of Her2 and FcγR on Tumor Cell Lines and Macrophages for ADCP Assay.

(A) Her2 expression level on tumor cell lines used for ADCP was confirmed by labeling with 10 μg/mL Herceptin or IgG1 pooled from human serum followed by fluorescent donkey anti-human IgG (H+L) FITC Fab at a 1:50 dilution. (B) FcγR counts on macrophages were determined using a fluorescent Quantum Simply Cellular bead assay. Macrophages were labeled with 20 μg/mL anti-FcγRI-FITC, 10 μg/mL anti-FcγRIIa-FITC, 1 μg/mL 2B6-N297D-FITC and 20 μg/mL anti-FcγRIII-FITC.

CD14<sup>+</sup> CD11b<sup>+</sup> macrophages were prepared from pooled PBMCs (Peripheral blood mononuclear cells) following cultivation with GM-CSF cytokine [75]. The surface densities of FcγRI, FcγRIIa, FcγRIIb and FcγRIII on macrophages were determined by FACS. We observed high FcγRI, FcγRIIa and FcγRIIb levels in macrophages prepared at different times and from different pooled PBMC fractions (Figure 3.4B). Notably, the



level of FcγRI (CD64) was comparable to that of FcγRIIa and FcγRIIb in contrast to an earlier report that showed low level FcγRI expression in human macrophages [75].

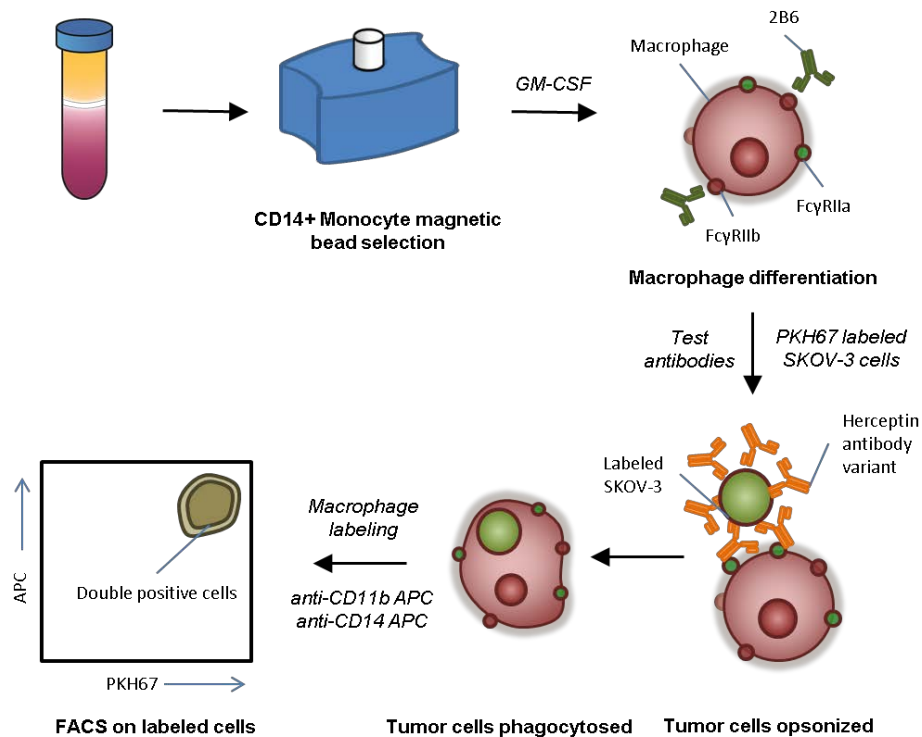


Figure 3.5: Schematic Diagram of ADCP Experimental Workflow.

ADCP was determined by incubating PKH67 labeled, IgG opsonized tumor cells with macrophages at a low (1:5 MDA-MB-453 or 1:10 SKOV-3) ratio of target to effector cells. The numbers of CD11b<sup>+</sup> CD14<sup>+</sup> macrophages that stained with PKH67 (arising from associated/ingested tumor cells) were determined by FACS [75] (Figure B.6) and fluorescence microscopy (Figure 3.6C - E). As a positive control we used glycosylated trastuzumab with the mutation G236A (GlycoT-G236A), which has been reported to confer the highest  $A_{IIa-R131/I}$  and  $A_{IIa-H131/I}$  ratios reported in the literature (5.5 and 5.7

respectively, relative to wild-type IgG) and to mediate increased macrophage mediated ADCP of EpCAM<sup>+</sup> LS180 cells [75]. We found that AglycoT-Fc1004 internalized approximately 75% more tumor cells ( $P<0.01$ ) relative to Herceptin and 40% more relative to its glycosylated, Fc engineered GlycoT-G236A variant (Figure 3.6A and B, Figure B.6). Equally importantly, AglycoT-Fc1004 displayed the same high level of ADCP with both the SKOV-3 and with the even lower Her2 expressing MDA-MB-453 cell line. These two cell lines correspond to approximately +3 and +2 Her2<sup>+</sup> tumor cells respectively which have been shown to be recalcitrant to Herceptin treatment [176, 177]. Consequently, AglycoT-Fc1004 may provide the opportunity to treat patients having tumors with Her2 moderate or low expression that do not respond well to Herceptin. We expect binding to the low affinity FcγRIIa-R131 polymorphism to be particularly desirable since therapeutic responses in patients that are homozygotic or heterozygotic for this allele show poorer responses to anti-neoplastic antibodies [39-41]. On the other hand, AglycoT-Fc1001 could not induce phagocytosis of tumor cells above background for either cell line. Likewise, the addition of 2B6, an antagonistic FcγRIIb antibody, had no significant effect on ADCP with any of the engineered antibodies tested or with Herceptin, suggesting that tumor cell surface-bound ICs likely displace 2B6 from FcγRIIb allowing ITIM mediated signaling to occur.

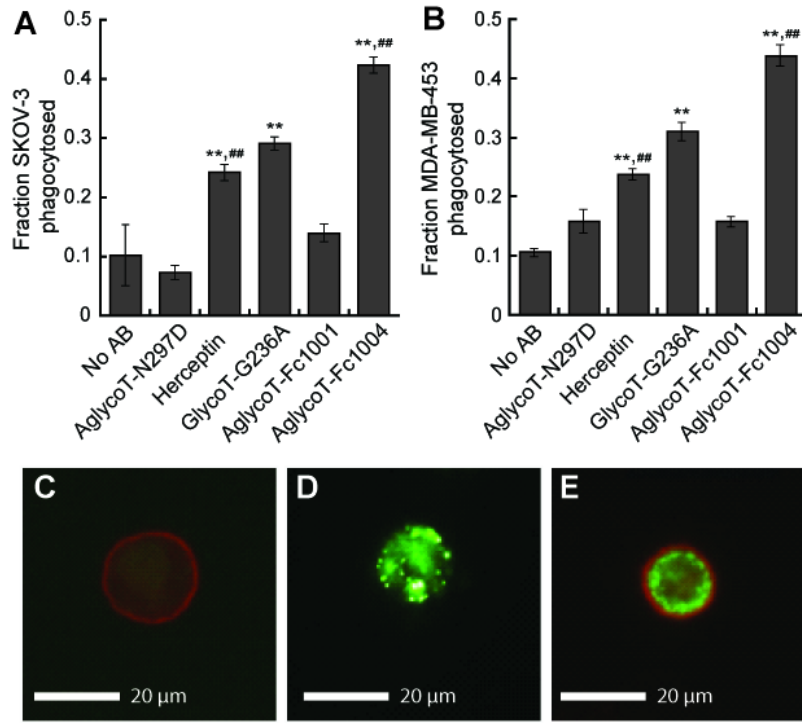
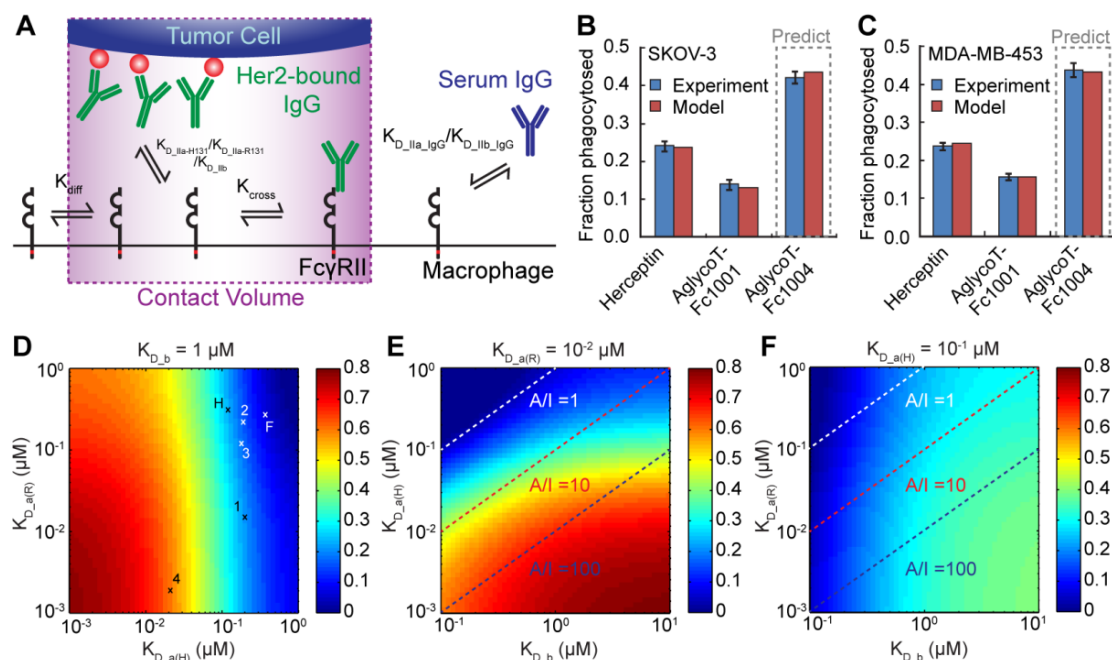


Figure 3.6: ADCP Mediated by Human Monocyte Derived Macrophages. Experiments were performed using AglycoT-Fc1001 and AglycoT-Fc1004 with +3 Her2<sup>+</sup> SKOV-3 ovarian cancer (A) and +2 Her2<sup>+</sup> MDA-MB-453 breast cancer (B) tumor cell lines as target cells. \*\* Welch's t test  $P < 0.01$  for samples compared to No Ab negative control, ## Welch's t test  $P < 0.01$  for samples relative to G236A positive control. (C - E) Fluorescent microscopy images showing macrophages labeled with 10  $\mu$ g/mL anti-CD14-APC and 10  $\mu$ g/mL anti-CD11b-APC (C), PKH67 membrane labeled MDA-MB-453 tumor cells (D), and phagocytosed tumor cells (E).

### Mathematical Modeling of ADCP

To gain insights on the puzzling lack of phagocytosis of Her2 expressing tumor cells opsonized with the AglycoT-Fc1001 antibody, a quantitative model to relate the formation IgG:Fc $\gamma$ RIIa and IgG:Fc $\gamma$ RIIb ICs to phagocytosis was developed by the Sarkar lab from the University of Pennsylvania (see Figure 3.7A).



**Figure 3.7:** Mathematical Modeling Provides Insights into Design Rules Governing Phagocytic Potency of Fc Variants. (A) Schematic depicting the binding reactions considered in the mathematical model. (B and C) Validation of the mathematical model (red bars) with ADCP data (blue bars). ADCP data for trastuzumab and AglycoT-Fc1001 were used to fit intrinsic signaling potencies of the receptor subunits (Table B.5). This model was then directly used to predict ADCP responses for AglycoT-Fc1004 with both SKOV-3 cells (B) and MDA-MB-453 cells (C). (D) Predicted fraction of SKOV-3 cells phagocytosed for a range of  $K_{D\_IIa-H131}$ ,  $K_{D\_IIa-R131}$ , and  $K_{D\_IIb}$  values.  $K_{D\_IIb}$  was held constant at 1  $\mu\text{M}$  and  $K_{D\_IIa-H131}$  and  $K_{D\_IIa-R131}$  values were varied. Phagocytic responses for Herceptin (H), AglycoT-Fc5-2a (F), AglycoT-Fc1001 (1), AglycoT-Fc1002 (2), AglycoT-Fc1003 (3) and AglycoT-Fc1004 (4) were predicted based on their experimentally determined equilibrium binding constants to FcγRIIa-H131 and FcγRIIa-R131 (see Table 1). (E)  $K_{D\_IIa-R131}$  was held constant at 0.01  $\mu\text{M}$  and  $K_{D\_IIb}$  and  $K_{D\_IIa-H131}$  values were varied: fixed  $K_{D\_IIb}/K_{D\_IIa-H131}$  ratios of 1 (white dash), 10 (red dash), and 100 (blue dash) are shown. (F)  $K_{D\_IIa-H131}$  was held constant at 0.1  $\mu\text{M}$  and  $K_{D\_IIb}$  and  $K_{D\_IIa-R131}$  values were varied. The same ratios of A(R)/I affinity as in (E) are shown.

Our simulations suggest that antigen-bound IgG, but not monomeric IgG, can elicit a significant phagocytic response because the clustered presentation of antigen-

bound IgGs in the contact region results in an increased local concentration of Fc domains that leads to the displacement of monomeric IgG and promotes a sufficiently high level of FcγR crosslinks to elicit effector responses. This result is in complete agreement with *in vivo* observations that serum IgG alone, in the absence of ICs, cannot elicit FcγR signaling [34].

To link biomolecular interactions at the cell surface to ADCP efficacy, we assigned an “intrinsic signaling potency” parameter to each receptor subunit and assumed that the signaling potency of each dimeric IgG:FcγR (used as a proxy for higher-order IgG:FcγR clusters) was equal to the sum of its constituents. The net signal generated by all FcγR complexes on the macrophage surface constituted the level of ADCP response (3). With the exception of the intrinsic signaling potencies for FcγRIIa-H131 and FcγRIIa-R131 (relative to FcγRIIb), all other parameters were obtained from experimental data, literature values or simulations (Table B.4). To parameterize the two relative signaling potencies for FcγRIIa-H131 and FcγRIIa-R131, the model was fit only to ADCP data for Herceptin and AglycoT-Fc1001 and then used to predict the expected ADCP response of AglycoT-Fc1004 (Figure 3.8B and C). Similarly, parameterization of the model using the data for any two antibodies within the Herceptin, AglycoT-Fc1001, and AglycoT-Fc1004 set accurately predicted the ADCP response for the third antibody (Figure B.7A - E). The model provides a framework for understanding the molecular basis for enhanced ADCP response. Figure 3.7D-F show heat maps of the predicted phagocytic responses for different  $K_{D\_IIa-H131}$ ,  $K_{D\_IIa-R131}$ , and  $K_{D\_IIb}$  values. The IgG variants examined in this work were overlaid on Figure 3.7D based on their  $K_{D\_IIa-H131}$  and  $K_{D\_IIa-R131}$  values to show their approximate expected ADCP responses (see Figure B.7E for actual predictions). The simulations show that enhanced ADCP most

dominantly correlates with increased affinity to FcγRIIa-H131, which is predicted to have a greater intrinsic signaling potency than FcγRIIa-R131 (Table B.5). This prediction is also consistent with clinical observations that FcγRIIa-R131 homozygous individuals are more susceptible to bacterial infections and autoimmune diseases [159-161], perhaps due to inefficient generation of activation signals in the absence of FcγRIIa-H131 subunits.

It has been suggested that effector response can be predicted by the A/I ratio, defined as the ratio of IgG Fc affinity for FcγRIIa to that for FcγRIIb (6). To investigate the utility of A/I ratio in predicting phagocytosis, lines of constant  $A_{IIa-H131}/I$  or  $A_{IIa-R131}/I$  were plotted for fixed  $K_{D_{IIa-R131}}$  and  $K_{D_{IIa-H131}}$ , respectively in Figure 4D (i.e.,  $K_{D_{IIb}}/K_{D_{IIa-H131}}$  in Figure 4E and  $K_{D_{IIb}}/K_{D_{IIa-R131}}$  in Figure 4F). Even though a higher A/I ratio tends to elicit a higher effector response phagocytic activity can vary significantly even for a fixed A/I ratio, indicating that absolute receptor affinities also play a significant, if not dominant, role in shaping cellular response. Interestingly, for a fixed A/I ratio, increasing FcγRIIa-H131 affinity generally leads to increased phagocytosis (Figure 3.7E), while increasing FcγRIIa-R131 affinity leads to decreased phagocytosis (Figure 3.7F). This can be explained by the relative intrinsic signaling potencies of the receptor subunits (Table B.5). At a fixed  $A_{IIa-H131}/I$ , increasing the affinity for FcγRIIa-H131 (potency > 1) would also increase the affinity for FcγRIIb (potency = -1), but the net effect would be increased activation due to the differential potencies. By contrast, at a fixed  $A_{IIa-R131}/I$ , increasing affinities for both subunits would reduce ADCP response because FcγRIIb is more potent at signaling than FcγRIIa-R131 (potency < 1). Our findings agree with recent crystal structure data that suggests the FcγRIIa-R131 polymorphism adopts a conformation that maybe less favorable for multimerization than FcγRIIa-H131, therefore limiting the proximity of ITAM domains

required to transduce activation signals [178]. The model suggests that efforts to improve the design of IgG Fc variants for enhanced ADCP should first focus on increasing affinity for FcγRIIa-H131 (Figure 3.7D and E) and, if not possible or insufficient, then on decreasing affinity for FcγRIIb (Figure 3.7E). If binding to the low affinity FcγRIIa-R131 allele is required then both improved R131 affinity and A/I ratio are necessary for more potent ADCP (Figure 3.7F). While FcγRIIa and IId have been established to be by far the most important receptors for phagocytosis by tumor cells [75, 179], the inclusion of FcγRI and FcγRIIIa in the model could be used to determine design criteria for glycosylated antibodies or future aglycosylated variants with more complex FcγR mediated effector function.

## DISCUSSION

So far, aglycosylated antibodies have been used for applications where inflammatory engagement of FcγRs or C1q complement proteins is undesirable [180]. Yet the generation of aglycosylated antibodies with unique affinities and selectivities may open the possibility for a new class of therapeutics with intriguing biological properties. To discover new aglycosylated Fc mutants, a bacterial display system has been developed in which full length IgG1 antibodies are tethered to the inner membrane of *E. coli*, leaving the Fc domain free to interact with fluorescently labeled FcγRs. By screening very large libraries ( $>10^8$  variants) of IgGs containing randomly mutated Fc domains we isolated an aglycosylated antibody, AglycoT-Fc1004, that displays remarkably high affinity towards FcγRIIa-R131 as well as selectivity over FcγRIIb binding. To the best of our knowledge, this is the first report of an aglycosylated antibody that binds to FcγRs with affinity and selectivity which far exceed those of clinically used glycosylated antibodies, or of any engineered glycosylated mutants reported thus far, engineered either through mutagenesis programs or via glycoengineering [71, 75, 181, 182].

The generation of highly FcγR selective Fc domains might allow for directed recruitment of certain immune effector cells, such as macrophages as shown here (because AglycoT-Fc1004 does not engage FcγRIIIa and has 50 fold lower affinity for FcγRI). So far, aglycosylated antibodies have been used for applications where inflammatory engagement of FcγRs or C1q complement proteins is undesirable [180]. The generation of aglycosylated antibodies with unique affinities and selectivities may open the possibility for a new class of therapeutics with intriguing biological properties. Fc engineered aglycosylated IgGs offer additional advantages by bypassing the need for N-linked glycosylation; eliminating glycan heterogeneity and broadening the range of



expression systems that can be used to produce large quantities of antibody. In several recent clinical trials, no evidence of aglycosylated antibody immunogenicity has been reported [180]. However, at this point it is unclear whether mutations to an aglycosylated structure will induce immunogenicity either through residue change or the generation of non-native conformational epitopes. The results from these studies will be reported in the future.

## **Chapter 4: An Engineered Aglycosylated Fc Variant with High FcγRIIIa-R131 Selectivity over FcγRIIb Shows NK Cell-Independent Killing of Her2+ Tumors *in vivo***

### **INTRODUCTION**

The use of antibodies as therapeutics has revolutionized the treatment of cancer, infection and autoimmunity in modern medicine. Engineering the antibody Fc domain to improve binding to activating Fc receptors on immune cells has the potential to further enhance inflammatory responses such as ADCC or ADCP. Recently, we isolated an aglycosylated variant with both high selectivity and affinity for FcγRIIIa over inhibitory FcγRIIb as described in detail in Chapter 3 [96]. In particular, the variant Fc1004 (S298G, T299A, E382V, N390D, M428L) exhibited selective binding to the low affinity polymorphic variant of FcγRIIIa (160 fold improvement over glycosylated trastuzumab) which contains an arginine at position 131 rather than a histidine that defines the high affinity allele. As well as individual receptor affinity for the Fc domain, the activating to inhibitory ratio, defined as the affinity for the activating receptors in relation to the inhibitory FcγRIIb receptor, is a key predictor for ADCC and ADCP performance [183]. Despite a lack of binding to FcγRIIIa, the A/I ratio of Fc1004 (FcγRIIIa-R131/FcγRIIb) was improved by more than 25 fold for which translated to significantly improved killing of Her2+ tumor cell lines by macrophages *in vitro*. While some clinical trials have demonstrated a correlation between the low affinity polymorphism of FcγRIIIa and poor prognosis in monoclonal antibody therapy for cancer [39-41], the significance of the R131 allele is not conclusively established [184]. However, it is recognized that FcγRIIIa-R131 homozygotes have impaired clearance of immune complexes which can contribute to autoimmunity and increased susceptibility to bacterial infection [185].

Because of the widespread expression of FcγRIIa on most myeloid cell lineages, we hypothesized our enhanced Fc1004 variant might recruit multiple cell populations for the killing of tumors *in vivo*. The mechanism of several clinical antibodies (trastuzumab, rituximab) is thought to rely on NK mediated killing through engagement of FcγRIIIa [43, 119]. Yet, knockout of inhibitory FcγRIIb in mice, a receptor not expressed on NK cells [36], leads to enhanced tumor killing suggesting other cell subsets have a significant influence on tumor clearance [50]. In fact, the tumor microenvironment contains large numbers of infiltrating myeloid leukocytes following chemotherapy treatment, of which macrophages comprise nearly 20 % [186]. Often, tumor associated macrophages (TAMs) are indicative of poor prognosis for patients with breast, lung and lymphoma cancers [187-189]. Several reports suggest TAMs can suppress the adaptive immune system, remodel the surrounding cellular matrix and promote angiogenesis or metastasis [188, 190]. Despite these pro-tumor effects, a recent study indicated TAMs retain their anti-tumor activity if sufficiently activated suggesting these cells might be repurposed during monoclonal antibody therapy [191]. Likewise, tumor associated neutrophils (TANs) are strongly correlated with poor prognosis and also comprise a large portion of tumor infiltrating cells [192, 193]. Similar to macrophages, neutrophil hyper-activation via therapeutic antibody Fc engagement or by cytokines such as TGF-β can promote anti-tumor effects [121, 156].

Taken together this evidence suggests antibodies engineered for high binding to FcγRIIa might be able to potentiate NK cell-independent killing of tumor cells *in vivo*. Consequently, we demonstrate here preliminary evidence for killing of Her2+ human SkBr-3 breast cancer cells by Fc1004 using human macrophages (generated by *in vitro* differentiation of blood monocytes) and also in a NOD/SCID xenograft mouse model reconstituted using leukocytes from human FcγRIIa-R131 homozygous donors. This

study provides a framework for further investigation into the mechanisms of tumor killing *in vivo* and suggests exciting new applications for the Fc1004 antibody.

## **MATERIALS AND METHODS**

### **Construction and Expression of Full Length trastuzumab Fc1004 and Control Antibodies**

Plasmids used or constructed in this project are described in Table C1 and C2. The plasmids for expression of wild type trastuzumab IgG heavy chain (pMaz-IgH-trastuzumab), trastuzumab kappa light chain (pMaz-IgL-trastuzumab) and trastuzumab IgG N297D heavy chain (pMaz-IgH-N297D-trastuzumab) were constructed as described previously [96]. DNA was prepared for each heavy chain and combined with an equal mass of light chain plasmid for transient transfection in HEK293F cells (Invitrogen). Five to six days after transfection, the cell suspension was centrifuged at 2000 rpm for 10 min to recover the supernatant fraction. Trastuzumab IgG and trastuzumab IgG N297D were purified over protein A affinity columns as follows. The supernatants were passed through 0.22  $\mu$ m filters before addition to polypropylene columns packed with Protein A high capacity agarose resin (Thermo Scientific). The resulting flow-through was collected and passed twice more through the column before any unbound protein was washed away with >10 CV (Column Volume) of 1x PBS. All antibodies were eluted with 3 mL of 100 mM citrate buffer (pH 3.0) and immediately neutralized with 1 mL of 1 M Tris (pH 8.0). Samples were buffer-exchanged into 1x PBS using Amicon Ultra-4 (Millipore) spin columns with a 10 kDa cutoff.

The polypeptide chain encoding the trastuzumab Fc1004 heavy and trastuzumab light chains were cloned into pcDNA3.4 plasmids for higher expression yields by Gibson cloning [136]. The plasmid backbone of pcDNA3.4 (Invitrogen) containing a wild type rabbit heavy chain was amplified using primers WK425 and WK 426. The trastuzumab Fc1004 heavy chain insert including the VH, CH1, CH2 and CH3 domains was amplified from pMaz-IgH-Fc1004-trastuzumab with primers WK429 and WK430. Likewise, the plasmid backbone for the light chain was prepared from pcDNA3.4 (Invitrogen)

containing a rabbit light chain by amplification with primers WK427 and WK428. The trastuzumab light chain (VL-C $\kappa$ ) was recovered from pMaz-IgL-trastuzumab using primers WK431 and WK432. After incubation of both insert and backbone fragments in Gibson master mix for 1 hour at 50 °C to create pcDNA3.4-IgH-Fc1004-trastuzumab and pcDNA3.4-IgL-trastuzumab, the products were desalted and transformed into electrocompetent JUDE-1 *E.coli* cells. Following sequencing of individual colonies, bulk DNA stocks were prepared by Maxiprep (Qiagen) for transient transfection of expi293F cells (Invitrogen) according to the manufacturer's instructions. Five to six days after transfection, supernatants were purified over protein A columns as above except an additional wash with 4 °C PBS containing 0.1 % triton X-114 was included to reduce endotoxin contamination of the purified antibodies. Antibody purity was assessed by SDS-PAGE gel and endotoxin levels were verified to be below 1 EU/mg using a chromogenic testing kit (Associates of Cape Cod).

### **Endpoint PCR Genotyping**

Genotyping of the Fc $\gamma$ RIIa allele was performed based on optimized conditions from literature [194]. Briefly, genomic DNA was isolated from blood draw from anonymous donors in accordance with IRB protocol # 2012-08-0031 (Titled: Isolation of whole peripheral blood from healthy donors for antibody immunodiscovery) using a DNeasy blood and tissue kit (Qiagen). 25  $\mu$ L PCR reactions were set up as described in Table 4.1. For detection of the Fc $\gamma$ RIIa-H131 allele the forward primer WK124 and the reverse primer WK126 were used to produce a product of 949 bp. Similarly, detection of Fc $\gamma$ RIIa-R131 used the forward primer WK125 and the reverse primer WK126 to make a fragment of the same size. Each genomic DNA sample was run with a set of control

primers; WK127 forward (No homology to either polymorphism) and WK126 reverse to ensure amplification of the allele was specific.

Table 4.1: PCR Reaction Conditions for Endpoint Genotyping.

Reagent	Volume/Amount (μL)
10x buffer (– MgCl <sub>2</sub> )	5
MgCl <sub>2</sub> (50 mM stock)	1.25
dNTPs (10 mM stock)	2
Genomic DNA (or control plasmid)	75-100 ng (1 ng plasmid)
Fwd primer	0.25 (8 ng)
Rev primer	0.25 (8 ng)
Taq polymerase	0.5 (1.5 U)
ddH <sub>2</sub> O	to 25

In addition, positive plasmid controls were included for each of the primer allele specific primer sets (pMaz-IgH-FcγRIIaH131-GST and pMaz-IgH-FcγRIIaR131-GST) which generate 179 bp fragments due to the lack of introns in the plasmid sequence encoding FcγRIIa. The PCR reactions were cycled as follows; 45 cycles with 98 °C denaturation for 45 s, 63 °C annealing for 30 s and 72 °C extension for 90 s before a 7 min final extension step. The resulting products were run on a 1% agarose gel containing ethidium bromide for visualization by UV light.

### Taqman Probe Genotyping

Genomic DNA was isolated from consenting donors as above for use in TaqMan Genotyping assays (Invitrogen, SNP ID: rs1801274) reconstituted in TaqMan Genotyping Master Mix to a final volume of 25 μL (1 – 10 ng DNA in each reaction). Samples were run for 40 cycles of 15 s denaturation at 95 °C and a 1 min

annealing/extension step at 60 °C on a LightCycler 96 real-time PCR system (Roche). All samples were independently run in triplicate to verify the genotype result.

### **Preparation of Human Monocyte-derived Macrophages.**

PBMCs were isolated from the fresh blood of genotyped homozygous FcγRIIa-R131 or FcγRIIa-H131 donors by Histopaque (Sigma-Aldrich) gradient centrifugation. In short, 15 mL Histopaque was added to 50 mL SepMate conical tubes (Stemcell Technologies) followed by 15 mL of blood diluted 1:1 with PBS. The mixture was centrifuged for 15 min in a swinging bucket rotor without braking at 800 x g. PBMCs were aspirated from the sample and washed twice with 50 mL PBS containing 2 % FBS (Mediatech) and 1 mM EDTA by centrifuging without braking at 120 x g for 10 min. CD14<sup>+</sup> monocytes were isolated by magnetic bead separation (Stemcell Technologies) according to the manufacturer's instructions. Cells were resuspended in RPMI (Invitrogen) containing 10 % FBS as well as Penicillin/Streptomycin and seeded at  $1.5 \times 10^6$  cell per well in 96 well plates containing 3 mL of the same media supplemented with 50 ng/mL GM-CSF (Peprotech). The cells were grown at 37 °C in 5 % CO<sub>2</sub> and, at days 2 and 5 of culture, an additional 1 mL of media with fresh cytokine was added to each well. After 7 days, non-adherent cells were aspirated and the plate was washed with Dulbecco's PBS (Mediatech). 1 mL HyQTase (Thermo Scientific) solution was added for 15 min at 37 °C for the detachment of macrophages from the plate surface. Recovered cells were washed with 50 mL RPMI media and resuspended in RPMI containing 10 % Human AB serum (Mediatech).



## **ADCP Assays**

MDA-MB-453 tumor cells were grown in DMEM containing 10 % FBS. Cells were recovered from culture flasks by trypsinization, labeled with PKH67 (Sigma-Aldrich) according to the manufacturer's instructions and resuspended in RPMI with 10% human AB serum. These cells were seeded at  $5 \times 10^3$  per well in 96 well V-bottom plates (Corning) followed by addition of macrophages at the appropriate effector: tumor cell ratio (1:5 MDA-MB-453) and antibodies, to a final concentration of 5, 0.5 or 0.05  $\mu\text{g/mL}$ . The plate was briefly spun at 2,000 rpm for 1 min and incubated at 37 °C with 5 %  $\text{CO}_2$  for 2 h (MDA-MB-453). Cells were stained with 10  $\mu\text{g/mL}$  anti-CD11b-APC (Clone ICRF44, Biolegend) and 10  $\mu\text{g/mL}$  anti-CD14-APC (Clone M5E2, Biolegend) on ice for 1 h. Phagocytosis was evaluated by FACS on an LSRFortessa (BD Bioscience), and reported as the fraction of double positive cells over the total number of tumor cells in the sample.

## **Pharmacokinetic Study of Aglycosylated Fc1004 in Mice**

C57BL/6 Fc $\gamma$ R null mice transgenic for human Fc $\gamma$ RIIa-R131 and Fc $\gamma$ RIIb were obtained from Rockefeller University. The Fc $\gamma$ R null background was generated by knockout of both the Fc $\gamma$ R $\alpha$  locus (Fc $\gamma$ RIIb, Fc $\gamma$ RIII and Fc $\gamma$ RIV negative) and the Fc $\gamma$ RI gene [195]. The mice were divided into two cohorts and injected intraperitoneally (IP) with 8 mg/kg of trastuzumab Fc1004 (n=5) or clinical grade Herceptin (n=5). At 1 week intervals blood samples were recovered from the tail vein for a total of 3 weeks. Blood samples were allowed to clot and serum was recovered by spinning at > 10,000 rpm in microcentrifuge tubes for 10 min. ELISA analysis was used to quantify the relative abundance of the therapeutic antibodies in each serum sample. ELISA plates (Qiagen) were coated with 1  $\mu\text{g/mL}$  of recombinant Her2 antigen (Sino Biological) in 1x PBS (pH

7.4) overnight at 4 °C. The next day the plates were blocked for 2 h at room temperature with 2 % milk in 1x PBS containing 0.05 % Tween (PBST) and washed three times in PBST at pH 7.4. To the first well, 66 µL of each serum sample was added followed by 1:4 serial dilution in PBS containing 2 % milk. After 1 h of incubation at room temperature, the plates were washed and 50 µL PBSM was added containing 1:5000 goat anti-Human Heavy and Light HRP (Jackson ImmunoResearch) for 1 hour. To develop the plates, the wells were washed 3x with PBST, 50 µL TMB substrate was added per well (Thermo Scientific), 50 µL of 1 M H<sub>2</sub>SO<sub>4</sub> was added to neutralize, and the absorbance at 450 nm was recorded.

### **SkBr-3 Tumor Xenograft Cancer Model**

NOD/SCID mice were injected subcutaneously with  $1 \times 10^6$  SkBr-3 Her2+ tumor cells and the tumors were grown until palpable. On day 0 of the experiment, the mice were split into three cohorts receiving either 12 mg/kg Fc1004 (n = 2), 12 mg/kg clinical grade Herceptin (n = 2) or PBS (n = 2) on day 0 via intraperitoneal injection. To provide functional immune cells, peripheral blood mononuclear cells (PBMCs) and peripheral blood cells (PBCs) from genotyped FcγRIIa-R131 donors were adoptively transferred on the same day. In brief, fresh 15 mL blood samples were mixed 1:1 with PBS and layered over Histopaque (Sigma-Aldrich) in 50 mL conical tubes. The tubes were spun at 800 g for 15 min with no brake. The PBMC fraction was recovered and the remaining pellet containing the PBC fraction was split between two 50 mL conical tubes. Red blood cells (RBCs) were lysed by a 10 min incubation step on ice with 45 mL cold shock buffer (155 mM NH<sub>4</sub>Cl, 10 mM KHCO<sub>3</sub>, 0.1 mM EDTA). Both PBMCs and PBCs were washed twice with PBS and reconstituted for intravenous injection.  $1 \times 10^7$  cells were delivered to each mouse at a PBC:PBMC ratio of 2:1. After 3 days, a maintenance dose

of 3 mg/kg of each antibody was injected IP along with PBS for the control cohort. Tumor progression was determined by sizing using Vernier calipers over the next 5 weeks.

## **RESULTS**

### **Genotyping of Donors for FcγRIIa Polymorphism**

First we examined the effect of FcγRIIa polymorphic status on the ability of human to eliminate cancer cells by ADCP. The FcγRIIa H131 and R131 alleles encoding genetic polymorphisms differ by a single nucleotide in the genome. PCR methods can be employed to determine the FcγRIIa polymorphism in blood samples from human donors. After isolation of genomic DNA, the sample is split between three PCR reactions each containing forward primers differing by a single 3' nucleotide and identical reverse primers [194]; two of the forward primers are specific for each of the polymorphic variants respectively while the third acts as a control primer with a 3' base mismatch to both polymorphisms (Figure 4.1A). Amplification should only occur if there is perfect homology between the forward primer and the DNA template resulting in a band at 949 bp when run on an agarose gel. The control primer, with no homology to either polymorphism, is used to confirm specificity of the method during each reaction. As an additional positive control, plasmids encoding both FcγRIIa-R131 and H131 are included in separate reactions in place of the genomic DNA template. Successful amplification from the plasmid template produces smaller bands of 179 bp because of the removal of genomic introns from the sequence. This method was used to genotype several healthy donors as shown in Figure 4.1B.

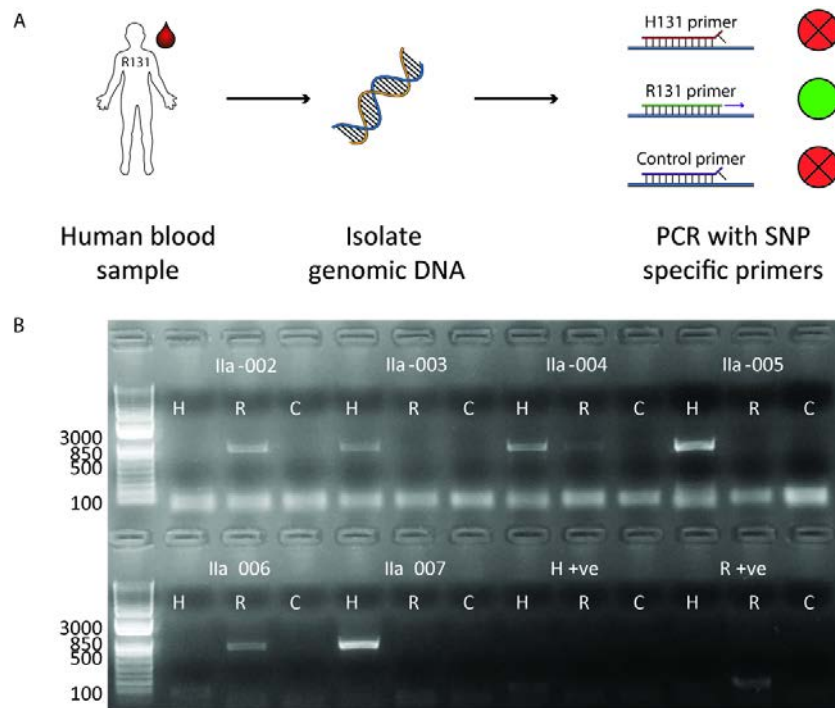


Figure 4.1: PCR Endpoint Genotyping of Anonymous Donor Pool.

A) Genomic DNA is isolated from small quantities of human blood for PCR. Amplification of the FcγRIIa gene occurs only if the primer has exact identity to the template DNA, single mismatches at the 3' end of the primer yield no product. B) Agarose gel bands at 949 bp indicate presence of the allele. Plasmids containing each of the FcγRIIa allelic variants were run as controls.

Despite the success of the endpoint genotype technique, a more accurate genotyping method was required as band intensity could differ significantly between donors (See donor 003 vs 005 in Figure 4.1B). Thus we elected to use real-time PCR analysis using TaqMan probes for each of the FcγRIIa polymorphisms for genotyping (Figure 4.2). Of the 18 donors genotyped, the homozygous alleles were seen at a frequency of 0.28 compared to a heterozygous donor frequency of 0.44 in line with the reported frequencies for this allele [162-164] (Table C.3).

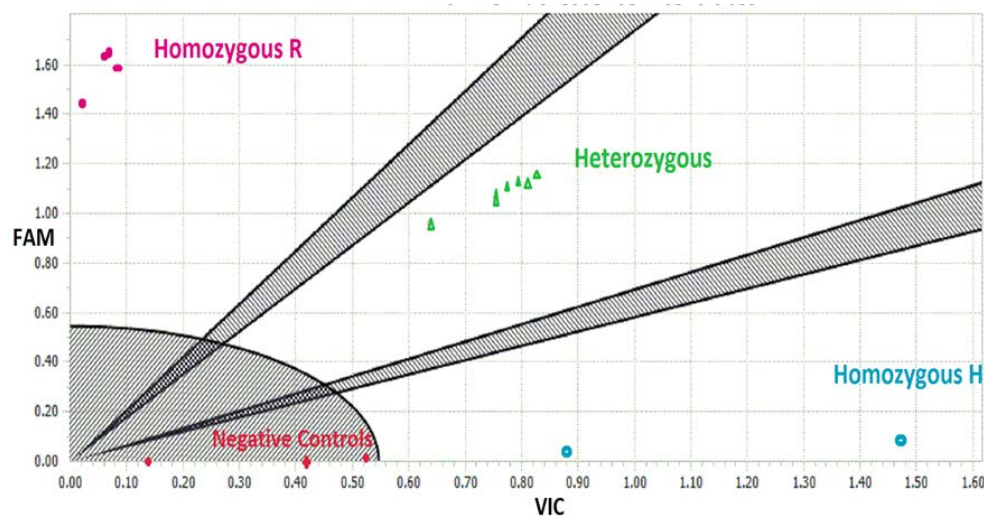


Figure 4.2: Genotyping Using Real-time PCR and Taqman Probes.  
The R131 probe was labeled with FAM fluorescent dye and the H131 probe was labeled with VIC dye.

#### Effect of FcγRIIa Polymorphism on Killing of Her2+ Tumor Cells by Fc1004

To evaluate the effect of FcγRIIa alleles on the potency of killing responses mediated by Fc1004, CD14<sup>+</sup> CD11b<sup>+</sup> macrophages were differentiated from monocytes isolated from the blood of genotyped donors for ADCP. Flow cytometry was used to determine the number of PKH67-labeled MDA-MB-453 tumor cells internalized by macrophages stained with anti-CD11b APC and anti-CD14 APC antibodies. The MDA-MB-453 tumor cell line is graded as +2 (moderate expression) for Her2 antigen surface expression by immunohistochemical staining on a scale that varies from 0 (no expression) to +3 (high expression) [168, 196]. Higher scores correlate with better clinical response to Herceptin therapy in patients bearing Her2+ tumors. This cell line was selected for comparison with previous ADCP assays described in Chapter 3. Clinical grade Herceptin was included as a positive control and antibodies containing the glycan deleting mutation N297D were included as a negative control. The removal of the glycan

at Asparagine 297 abrogates binding to the Fc $\gamma$ Rs, although some residual binding to Fc $\gamma$ RI might remain if sufficient avidity is generated during immune complex formation [197].

We found that at the highest antibody concentration of 5  $\mu$ g/mL, homozygous R131 macrophages were able to engulf up to 40 % of tumor cells using Fc1004 compared to 20 % engulfment by H131 macrophages (Figure 4.3A and B). The percentage of phagocytosis for the R131 macrophage sample was consistent with that observed using pooled donor blood in the ADCP assays performed in Chapter 3. At lower antibody concentrations, R131 macrophages were also more effective at phagocytosis than the H131 allele. Importantly, for macrophages isolated from the R131 donors, cell killing was significantly improved over clinical grade Herceptin with the exception of the lowest antibody concentration (0.05  $\mu$ g/mL). In all experiments the N297D variant showed significantly less killing than the other antibodies but was consistently above the no antibody controls.

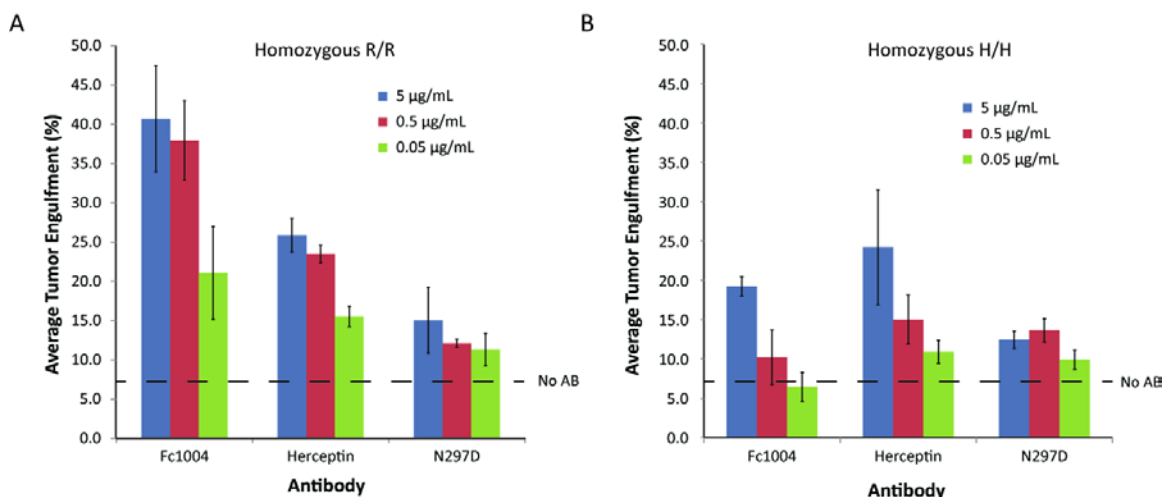


Figure 4.3: Representative ADCP Data for Genotyped Individuals in the Killing of Her2+ MDA-MB-453 Breast Cancer Cells. Antibodies at up to 5 µg/mL were incubated with tumor cells and mixed at a 1:5 ratio with monocyte derived macrophages from either homozygous R131 (A) or homozygous H131 donors (B).

### ***In vivo* Pharmacokinetics of Aglycosylated Fc1004**

Initially, uncertainly surrounded proposals to use aglycosylated antibodies for therapy because of potential immunogenicity, altered pharmacokinetic profiles and formulation instability [99]. Subsequent clinical trials with aglycosylated antibodies have allayed these concerns for the most part, as described in Chapter 1, but as yet no clinical trials have been undertaken with engineered aglycosylated antibodies. Hence, the pharmacokinetic behavior of engineered Fc1004 was investigated in mice. Fc1004 was expressed in HEK293F cells and purified by protein A affinity chromatography. Endotoxin levels were evaluated using a chromogenic Limulus Amebocyte Lysate assay and the protein preparations used were shown to have very low endotoxin levels. (< 1 EU/mg antibody). A low endotoxin level is necessary not only to prevent systemic



inflammation upon injection into mice but also to prevent activation of human immune cells used in the adoptive transfer tumor model described in the following section.

Transgenic mice expressing human Fc $\gamma$ RIIa and Fc $\gamma$ RIIb [195] were used in this study to account for the possibility that engagement of Fc1004 by human receptors in the mouse model might impact its biodistribution and half-life in the blood. Mice were injected with a single IP dose of either trastuzumab Fc1004 or clinical grade Herceptin at 8 mg/kg and blood samples were recovered from the tail vein. The concentration of Fc1004 antibody in serum samples was determined by ELISA using purified Her2 antigen as the capture reagent. While the average serum levels of Fc1004 and clinical grade Herceptin was comparable for the first two weeks but there was a statistically significant higher level of Fc1004 than Herceptin at the final timepoint after 3 weeks (Figure 4.4).

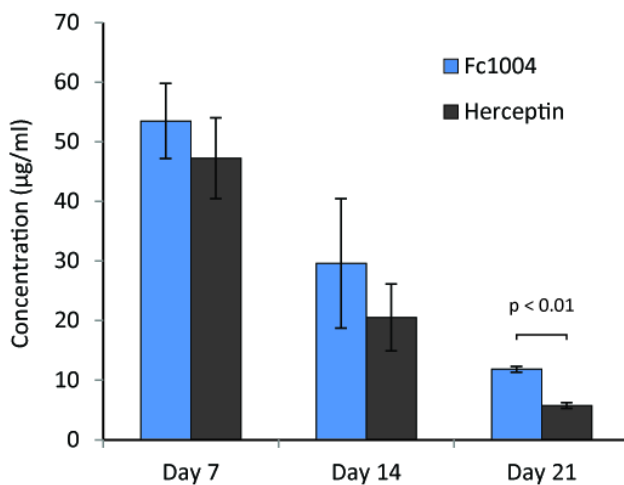


Figure 4.4: Pharmacokinetic Profile of Serum Persistence of Fc1004 as Compared to Clinical Grade Herceptin.

Mice were injected with 8 mg/kg of Herceptin (n=5) or Fc1004 (n=5) and tail vein bleeds were drawn at weekly intervals for 3 weeks. Antibody persisting in the serum was measured by ELISA with Her2 antigen capture.

All data points were fit to an exponential decay model in Matlab to give half-lives for each of the antibodies as presented in Table 4.2. There was no significant difference between either of the antibodies despite the divergence in serum concentrations at the final time point. The Fc1004 Fc domain contains the mutation M428L which was previously reported to confer 7 fold higher affinity for FcRn than wild type glycosylated antibodies [198]. When injected into rhesus monkeys, this improved affinity translated to a 1.8 fold improvement in half-life over the wild type version of the same antibody. The loss of glycosylation in the Fc domain is reported to have little effect on the affinity for FcRn and therefore we expect the M428L mutation in aglycosylated Fc1004 likely accounts for the difference in antibody concentration at the last time point [199, 200].

Table 4.2: Half-life of Fc1004 and Clinical Grade Herceptin Antibodies in Mouse Serum.  
Data points were fit using Matlab software to an exponential decay model.

Antibody	Half Life (Days)	95 % Confidence	
		Min	Max
Fc1004	7.3	5.2	11.8
Herceptin	5.3	4.0	7.7

#### **Enhanced Clearance of Her2+ Tumors in NOD/SCID Mice Reconstituted with Immune Cells from Human FcγRIIa-R131 Donors**

Immunodeficient mice bearing human Her2 expressing tumor xenografts have been used extensively for the evaluation and mechanism of action of trastuzumab (Herceptin) in the treatment of human cancer [201-204]. Herceptin works in part by interfering with the dimerization of Her2 on the tumor cell surface and inhibiting multiple intracellular signaling pathways resulting in cell cycle arrest and apoptosis [205, 206].

However, potent ADCC responses are also elicited through the recruitment of cell subsets with cytotoxic potential, such as NK cells, and thus immunodeficient mice cannot be used to evaluate killing by these mechanisms. Alternative immunocompetent mouse tumor models are available [207], but the testing of Fc engineered antibodies is particularly challenging due to several confounding factors. First, although mouse FcγRs do bind to human antibodies, both the FcγR classes and cellular expression patterns differ from humans [208]. Therefore, it is likely wild type mice do not suitably recapitulate the human immune system especially when considering the subtle balance of altered FcγR affinities in the engineered variants being tested. Second, to prevent rejection, syngeneic tumors compatible with the host mouse strain must be used with well characterized surface expression of a murine antigen against which a monoclonal antibody exists. However, the clinical antibodies often used as model drugs for evaluating new antibody therapeutics are against targets of human origin. Mouse tumor cell lines transgenic for surface bound human antigens might be used instead, although ensuring the long term stability of antigen expression levels in these cell lines is difficult *in vivo* in the absence of selection pressure provided *in vitro* by a selectable marker such as an antibiotic cassette.

To circumvent these problems we used a NOD/SCID xenograft model with immune function reconstituted by the adoptive transfer of human leukocytes prepared from the blood of FcγRIIa-R131 homozygote donors. This approach allows for the use of human tumor cell lines as well as human effector cells to test engineered Fc variants. In pilot experiments, mice injected only with R131 peripheral blood leukocytes revealed a rapid decline in all cell subsets by FACS, with the exception of lymphocytes, after one week (Data not shown). As a result, leukocyte fractions were prepared from whole blood by Histopaque gradient separations and recombined at a ratio of 2:1 polymorphonuclear

leukocytes (PMLs; including neutrophils, macrophages) to peripheral blood mononuclear cells (PBMCs; including lymphocytes, monocytes). Each mouse was injected subcutaneously with  $1 \times 10^6$  human SkBR-3 breast cancer tumor cells (Figure 4.5), clinically graded as +3 for Her2 expression. A high Her2 expressing cell line was used maximize the likelihood of antibody mediated tumor regression in this preliminary study.

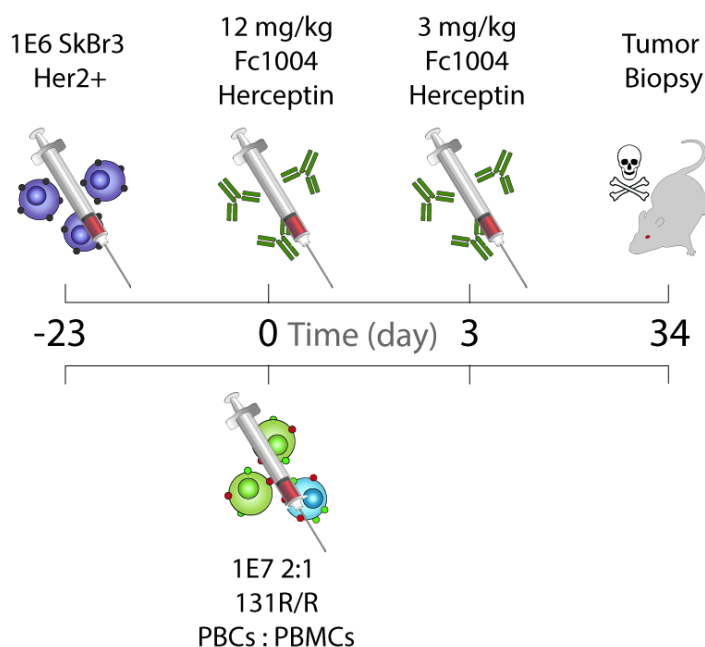


Figure 4.5: Experimental Design for Adoptive Transfer Tumor Xenograft Study. NOD/SCID mice were injected with  $1 \times 10^6$  human SkBR3 cells prior to the start of the experiment. Once palpable tumors form antibodies at 12 mg/kg are injected I.P along with  $1 \times 10^7$  PBCs and PBMCs reconstituted at a 2:1 ratio after isolation from human homozygous R131 donors. A maintenance dose of 3 mg/kg was injected I.P 3 days after the initial injection.

Once the SKBR-3 tumors had grown to a palpable size, a total of  $1 \times 10^7$  reconstituted PMLs and PBMCs were injected via the tail vein. Concurrently, the mice were dosed with 12 mg/kg of each antibody intraperitoneally in accordance the dosage rates reported for 4D5, the trastuzumab murine precursor, in previous xenograft studies [201]. Based on

the half-life of the Fc1004 antibody reported in Table 4.2, a maintenance dose of 3 mg/kg was injected intraperitoneally after 3 days. The size of tumors was followed until either complete remission was observed or the mice were sacrificed (Figure 4.6).

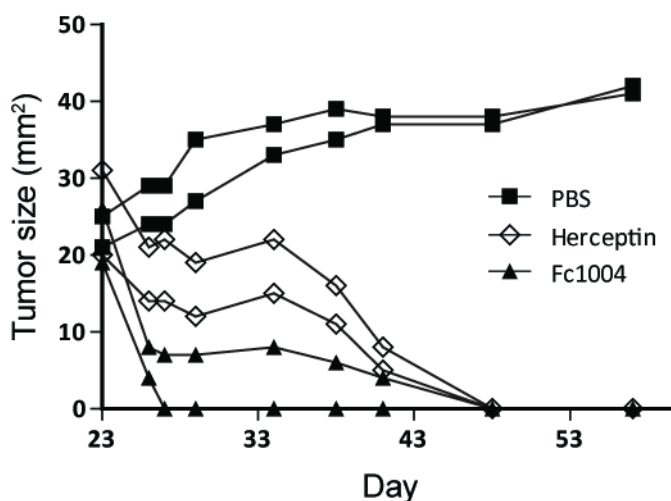


Figure 4.6: Adoptive Transfer Tumor Xenograft Study. NOD/SCID mice bearing SkBr3 Her2+ tumors were injected with Fc1004 (n=2), clinical grade Herceptin (n=2) or PBS (n=2). Tumor size was measured with Vernier calipers at regular intervals for 34 days.

An immediate reduction in tumor size was noted after a time of 3 days following the first antibody injection and the rate of decrease in tumor size was considerably faster in the mice treated with Fc1004 than Herceptin. As expected, the mice receiving a R131 donor leukocyte injection and PBS instead of antibody did not show any reduction in tumor size during the experiment. However, tumor growth was observed to plateau in this model, possibly due to antibody independent control of the tumor provided by the donor leukocytes injected. This finding suggests a more robust tumor model will be required in future studies with faster growing tumor cell lines. Despite concerns surrounding the slow growth of the SkBR-3 tumors, one of the mice injected with Fc1004 showed

complete remission following the antibody maintenance dose and all the remainder of the treated cohorts had tumors eliminated by day 47 (25 days after the start of treatment).

## DISCUSSION

The mechanism behind the clinical effect of many monoclonal antibodies, including trastuzumab and rituximab, has long been linked to NK effector cells. NK cells are powerful agents in the innate arm of immunity, particularly because they are one of the few cell types that lack expression of inhibitory FcγRIIb and therefore the cytotoxic responses they mediate are less regulated than other effector cells. Nevertheless, in accordance with recent studies that suggest other cell populations might contribute significantly to the clearance of tumors [121, 191], we report preliminary evidence of NK-cell independent killing of Her2+ tumors by an engineered aglycosylated antibody. As Fc1004 has no detectable binding to FcγRIIIa, the only FcγR expressed on NK cells, it is likely tumor killing is mediated by other cell subsets such as neutrophils and macrophages. Future studies are required to elucidate in detail the mechanism behind the potent action of Fc1004 *in vivo*. In addition, we have identified *in vitro* that Fc1004 selectively enhances the macrophage ADCP response of low affinity FcγRIIa-R131 homozygous donors who respond more poorly to antibody treatments in certain instances. The ADCP response of heterozygous donors to Fc1004 treatment is currently under evaluation. Previous studies have shown that heterozygotes expressing both FcγRIIa polymorphisms can use wild type antibodies to mediate *in vitro* ADCP with a phenotype similar to individuals homozygous for high affinity FcγRIIa-H131 [161]. Based on the dominance of the high affinity allele, we anticipate Fc1004 will show a similar but inverted trend because of exceptional affinity for the FcγRIIa-R131 polymorphism. Thus, the phagocytic killing of tumor cells by heterozygous donors is expected to parallel Fc1004 mediated ADCP using macrophages differentiated from FcγRIIa-R131 homozygotes. Successful demonstration of enhanced ADCP by heterozygous donors would greatly expand the potential therapeutic relevance of Fc1004.

While aglycosylated antibodies have been used *in vivo* for anti-inflammatory function, we believe this is the first report of an engineered aglycosylated antibody with enhanced *in vivo* inflammatory potency. This is significant for several key reasons and provides the rationale for further *in vivo* studies to test Fc1004 in more robust cancer models. Importantly, the pharmacokinetic data indicate that the serum persistence of the aglycosylated Fc1004 antibody is at least as long as its wild type glycosylated counterpart. Thus it is likely that there is no significant instability in serum introduced by the removal of glycans or the mutations introduced to the antibody structure. Furthermore, these changes have not significantly increased the immunogenicity of the antibody, which would result in the generation anti-Fc1004 antibodies and a more rapid clearance from serum. As well as the therapeutic activity offered by engineered aglycosylated antibodies, the discovery of additional variants with selective binding FcγRs might help in understanding antibody mechanism and the cell subsets that are most influential in the treatment of certain diseases.



## **Chapter 5: Future Directions and Perspectives**

### **ENGINEERING NEW Fc MUTANTS**

Millions of years of evolution have produced a finely balanced relationship between antibody subclass and the Fc receptors that can be engaged to potentiate immune function. Activating the immune system too strongly can result in systemic inflammation triggered by cytokine storms and even death. As a result the immune system has evolved inhibitory receptors to limit inflammation while still protecting the host from invading pathogens [209]. However, overriding these checkpoints through Fc engineering has emerged as a key strategy to treat diseases such as cancer where strong inflammatory function is desired. As a result, the pharmaceutical industry has invested heavily in the development of Fc domains with improved effector function. As these engineered Fc domains progress through to clinical trials, new strategies will be required to further improve the potency of antibodies and extend the range of applications for existing monoclonal antibodies. In this work two new engineered Fc domains have been described with interesting therapeutic potential. The generation of antibodies that bind receptors from multiple isotypes as exemplified by the discovery of MutD opens the possibility for combining functions from other antibody classes to create Fc domains for specific purposes. For example, it might be possible to harness the Fc $\epsilon$ RI receptor in combination with binding to the Fc $\gamma$ Rs in order to improve ADCC of tumor cells [210]. Further optimization of the MutD variant might also be possible through reintroduction of binding to Fc $\gamma$ RIIIa or enhanced binding to Fc $\gamma$ RIIa. Interaction with additional receptors could aid recruitment of additional immune cell subsets such as NK cells or enhance current interactions with the neutrophil subset. Likewise, engineered aglycosylated antibodies have demonstrated impressive discrimination in the receptors that can be bound, and in the case of Fc1004, even single amino acid polymorphic variations can be

distinguished (FcγRIIa-R131 vs FcγRIIa-H131). We have hypothesized the exceptional flexibility of aglycosylated antibodies allows the sampling of conformation space that cannot be accessed by glycosylated antibodies. By introducing point mutations to the structure certain conformations favorable for binding to select Fc receptors can be fixed. In future studies, the engineering of variants with high affinity and selectivity for FcγRIIb would be especially beneficial for applications where anti-inflammatory properties are desirable such as autoimmunity or anaphylaxis. Similarly, variants with selectively high binding to FcγRIIa-H131 might be found to complement the high FcγRIIa-R131 binding of Fc1004.

While Fc receptors are well established binding ligands for antibodies, a new class of Fc binding proteins, termed Fc receptor-like proteins (FcRL), has been recently described. Certain members of this class bind with affinity comparable to IgG interaction with FcγRs to mediate both inflammatory and anti-inflammatory activity [211]. As more becomes known about their function, these proteins may emerge as viable targets for Fc engineering efforts focused on creating better therapeutics.

## **INVESTIGATING THE MECHANISM AND POTENTIAL OF ENGINEERED FC VARIANTS**

To understand the therapeutic potential of newly discovered Fc variants the mechanisms of action must first be investigated. Along with the variants described in this work, the previously reported aglycosylated Fc5 variant discovered in the Georgiou lab might have applications in certain therapeutic niches [95]. The mutations in Fc5 confer selective binding to FcγRI with high affinity (~5 nM) and were demonstrated to recruit dendritic cells for ADCC, a function that glycosylated antibodies cannot perform. The ability to activate dendritic cells suggests utility of Fc5 for inducing adaptive immune responses. FcγRI on expressed on dendritic cells is shown to be unique in mediating

effective cross presentation of antigen to MHC class I molecules to activate CD8+ cytotoxic T lymphocytes as well as presentation on MHC II molecules for CD4+ T cell induction [212]. The degree of activation is heavily regulated by antibody affinity for the inhibitory FcγRIIb receptor [213]. Yet, despite FcγRIIb binding, clinical data indicates some monoclonal antibodies are able to induce both anti-tumor cytotoxic T cell activity and increase the serum titer of anti-tumor antibodies in patients [214]. As Fc5 lacks detectable binding to FcγRIIb, enhanced levels of antigen presentation would be expected to improve T cell activation over current therapeutic antibodies. Figure 5.1 outlines an experimental plan to measure and compare antibody mediated T cell activation *in vitro*. Dendritic cells are differentiated from blood derived monocytes and pulsed with dead tumor cells previously opsonized with antibody variants. Following dendritic cell co-culture with autologous T cells, the small fraction of tumor antigen specific T cells will be induced to proliferate and express large amounts of inflammatory IFN-γ cytokine that can be detected by intracellular FACS. More T cell proliferation and IFN-γ expression indicates the Fc variant is able to mediate better antigen presentation.

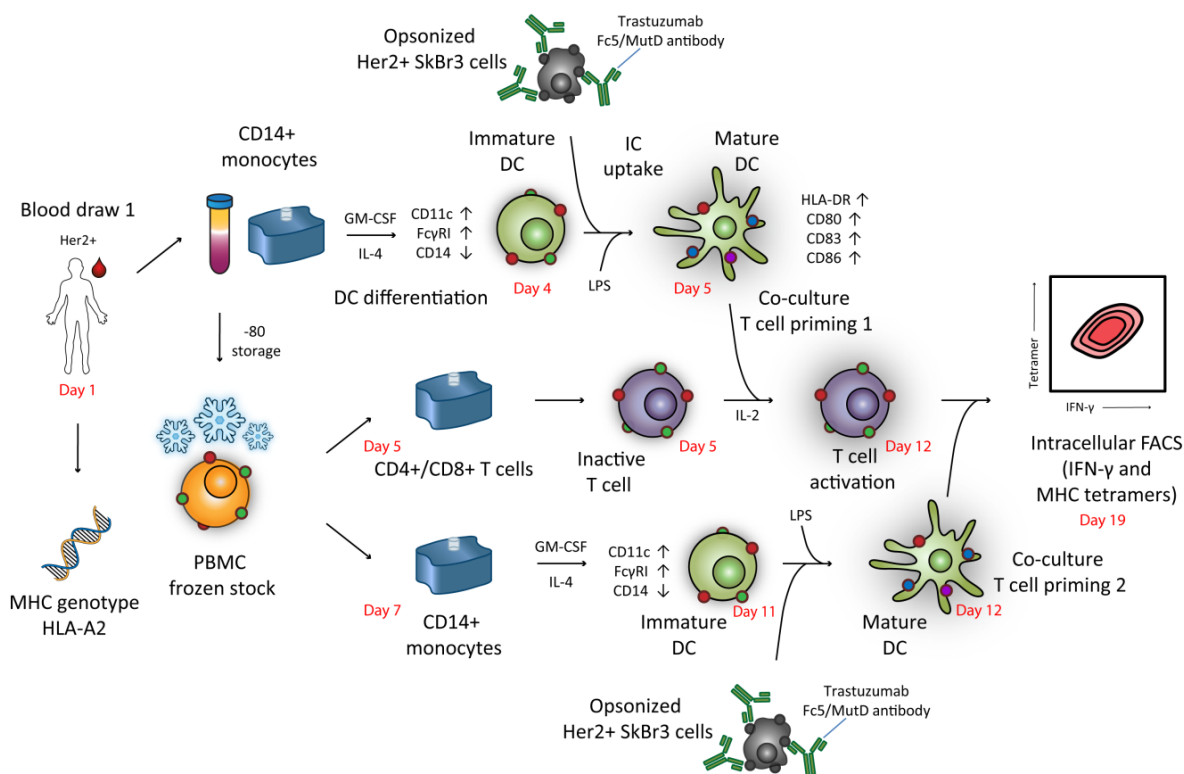


Figure 5.1: Experimental Design for the Evaluation of Engineered Fc Domain Mediated Antigen Presentation for Enhanced T Cell Activation. Blood is isolated from donors and PBMCs are collected. Dendritic cells are differentiated from monocytes and pulsed with antibody opsonized dead tumor cells before co-culture with autologous T cells. Activation of T cells is determined by quantification of intracellular IFN- $\gamma$  levels using FACS.

### Applications for Aglycosylated Fc1004

Other therapeutic applications might be found for Fc1004 antibodies, which have high binding to Fc $\gamma$ RIIa-R131, and can recruit macrophages for tumor cell ADCP *in vitro*. For example, recent investigations into the mechanisms of action of the anti-CTLA-4 antibody ipilimumab in mouse models have found the activation of tumor associated macrophages indirectly contributes to the clearance of melanoma lesions [215]. In part, ipilimumab acts as a CTLA-4 antagonist on cytotoxic T lymphocytes (CTLs) to prevent continual CD80/CD86 stimulation that can lead to T cell exhaustion reduced efficacy of

tumor clearance [216] (Figure 5.2). However, Treg cells within the tumor microenvironment also express high levels of CTLA-4 and serve to regulate CTL responses further. Tumor biopsies from mice revealed ipilimumab depletion of these Treg cells from the tumor microenvironment was dependent on infiltrating CD11b<sup>+</sup> macrophages. Thus, in the absence of inhibitory signals, tumor antigen specific CTLs can become hyper-activated to mediate potent anti-tumor ADCC.

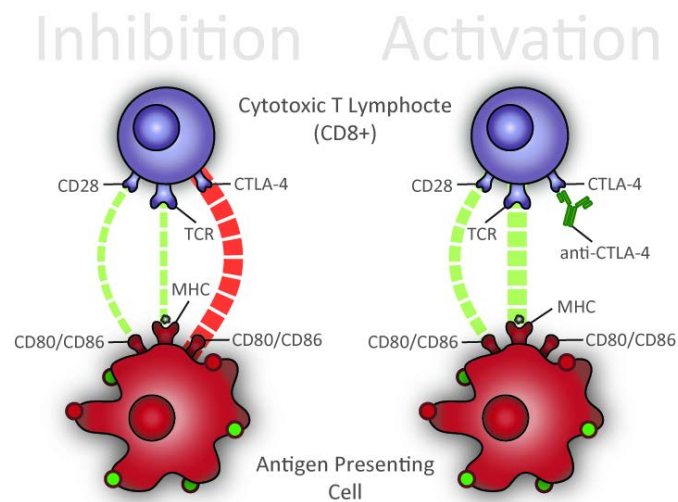


Figure 5.2: Partial Mechanism of Ipilimumab Action.

The blockage of anti-CTLA-4 on cytotoxic T lymphocytes prevents inhibitory signals by CD80 and CD86 ligands on antigen presenting cell surfaces.

Because Fc1004 enhances macrophage ADCP, we hypothesize ipilimumab containing the Fc1004 mutations would have improved *in vivo* efficacy in the removal of Treg cells over wild type ipilimumab and improved CTL action in reducing tumor burden. To test this hypothesis, the treatment of B16 tumors grown in transgenic mice expressing human FcγRIIa and FcγRIIb [195] might be explored using an anti-mouse CTLA-4 antibody (9D9, [217]). The use of transgenic mice bearing human FcγR genes is essential to

capture the refined binding specificity of Fc1004 especially since mouse FcγRs might have an altered affinity profile for human antibodies. As a preliminary step, an ADCP assay was performed to confirm the suitability and function of macrophages differentiated from the bone marrow of the FcγRIIa/FcγRIIb transgenic mice (Appendix D). As shown in Figure 5.3, trastuzumab Fc1004 is able to engulf Her2+ MDA-MB-453 tumor cells more effectively than either wild type IgG or the N297D aglycosylated negative control. Importantly, this preliminary data supports the testing of Fc1004 in an *in vivo* mouse model.

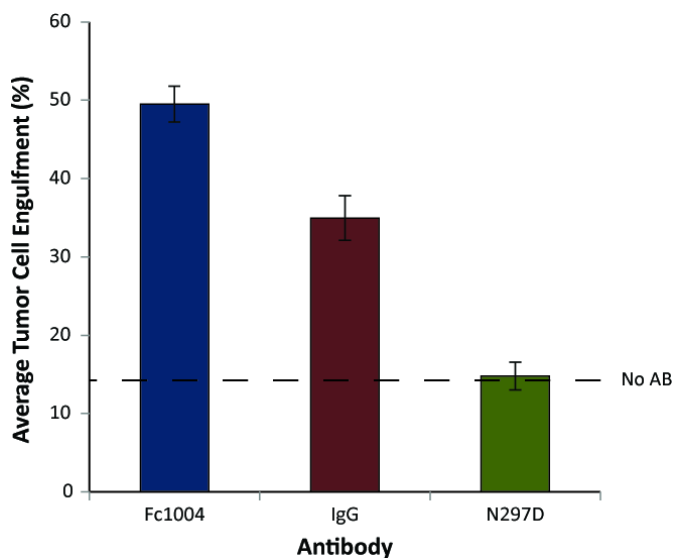


Figure 5.3: ADCP of Her2+ MDA-MB-453 Breast Cancer Cells by Transgenic FcγRIIa/b Mouse Macrophages. Trastuzumab antibodies were incubated at 5ug/mL with a ratio of 1:5 tumor cells to bone marrow monocyte derived macrophages.

The plasticity of the antibody structure allows for the facile interchange of Fc domains between monoclonal antibodies to create mutants with altered target specificity for new applications. The work in this dissertation has described two new engineered

variants, Fc1004 and MutD, with enhanced potency in the clearance of tumor cells and a multitude of possible applications. By engineering both aglycosylated and cross isotype hybrid Fc domains we have demonstrated new approaches that might be used to develop the next generation of antibody therapies.

## Appendix A

Table A.1: Plasmids Used in Chapter 2.

Plasmids	Relevant characteristics	Reference or Source
pTrc-DsbA IgA CH2 CH3	IgA Fc domain with truncated tailpiece (Residues 222-445) in bacterial expression vector	This study
pMaz-IgH-Fc $\alpha$ RI-GST	Fc $\alpha$ RI gene in pMaz-IgH for dimeric mammalian expression	This study
pMaz-IgH-Fc $\gamma$ RI-His	Fc $\gamma$ RI gene in pMaz-IgH for monomeric mammalian expression	This study
pMaz-IgH-Fc $\gamma$ RI-GST	Fc $\gamma$ RI gene in pMaz-IgH for dimeric mammalian expression	[96]
pMaz-IgH-Fc $\gamma$ RIIaR131-GST	Fc $\gamma$ RIIa gene in pMaz-IgH for dimeric mammalian expression	[96]
pMaz-IgH-Fc $\gamma$ RIIb-GST	Fc $\gamma$ RIIb gene in pMaz-IgH for dimeric mammalian expression	[96]
pMaz-IgH-Fc $\gamma$ RIIIa-GST	Fc $\gamma$ RIIIa gene in pMaz-IgH for dimeric mammalian expression	[96]
pMaz-IgH-MutB	Mutant B Fc domain only in dimeric mammalian expression vector	This study
pMaz-IgH-MutC	Mutant C Fc domain only in dimeric mammalian expression vector	This study
pMaz-IgH-MutD	Mutant D Fc domain only in dimeric mammalian expression vector	This study
pMaz-IgH-trastuzumab	Wild type IgG1 trastuzumab heavy chain mammalian expression vector	[96]
pMaz-IgL-trastuzumab	Wild type IgG1 trastuzumab kappa light chain mammalian expression vector	[96]
pMaz-IgH-IgA-trastuzumab	Wild type IgA1 trastuzumab mammalian expression vector	This study
pMaz-IgH-N297D-trastuzumab	IgG1 trastuzumab heavy chain mammalian expression vector with glycosylation knockout at N297	[96]
pMaz-IgH-MutD-trastuzumab	Mutant D trastuzumab in a mammalian expression vector	This study
pcDNA3.4-Fc $\gamma$ RIIb-His	Soluble His tagged monomeric Fc $\gamma$ RIIb mammalian expression vector	This study
pcDNA3.4-Fc $\gamma$ RIIaR131-His	Soluble His tagged monomeric Fc $\gamma$ RIIaR131 mammalian expression vector	This study

Table A.2: Primers Used in Chapter 2.



Primer Name	Primer nucleotide sequence (5' → 3')
JL-Gibson F	TGAGCGGCCGCTCGAGGC
JL-Gibson R	TTTGCCCGCCAGCCTGTCGATGGTCTTCTGGGTGAA
JL-GS-C-Rn-1	CGACAGGCTGGCGGGCAAAGGCGGCGGCGGCAGCCAGAGATTCTGCACCGGCCACTTCGGCG
JL-GS-C-Rn-2	GCCTCGAGCGGCCGCTCAGCCGTTGCAGGGGTGCAGGCCGCCGAAGTGGCCGGTGCA
JL-GS-L-Rn-1	CGACAGGCTGGCGGGCAAAGGCGGCGGCGGCAGCCAGAGATTCTGTACCGGCCACTTCGGCG
JL-GS-L-Rn-2	GCCTCGAGCGGCCGCTCAGCCGTTGGCGGGGTACAGGCCGCCGAAGTGGCCGGTCAC
TKA4	GCGTTGGAAGACCTTGCGCTTGGTAGCGAAGCG
TKA5	CGTTTCGCTACCAAGCGCAAGGTCTTCCAACGC
TKA6	CGTTGGAAGACCTTCTGGCGGGTAGCGAAGCGAATCTG
TKA7	CAGATTCGCTTCGCTACCCGCCAGAAGGTCTTCCAACG
TKA8	CTGTCGGGTTGCGCAGCGCCGTGGAATCATGGC
TKA9	GCCATGATTCCACGGCGCTGCGCAACCCGACAG
TKB1	GGTTGCGCAGAACCGTGGGCGCATGGCAAAACATTAC
TKB2	GTGAATGTTTTGCCATGCGCCACGGTTCTGCGCAACC
TKB3	GCGCAGAACCGTGGAATGCGGGCAAAACATTACCTG
TKB4	CAGGTGAATGTTTTGCCCGATTCCACGGTTCTGCGC
TKB7	CGAAAGATGTTCTGGTGGCGTGGCTGCAGGGAAGCC
TKB8	GGCTTCCCTGCAGCCACGCCACCAGAACATCTTTCG
TKC1	TGCAGGGAAGCCAAGCGCTGCCCCGTGAAAAG
TKC2	CTTTTCACGGGGCAGCGCTTGGCTTCCCTGCA
TKC5	GATACGTTCACTGCGCGGTGGGCCATGAGGC
TKC6	GCCTCATGGCCACCGCGCAGCTGAACGTATC
TKD1	ATGGTGGGCCATGCGGCACTTCCGCTG
TKD2	CAGCGGAAGTGCCGCATGGCCACCAT
TKD5	GCCATGAGGCACTTCCGCGGCGCTTTACTCAAAAAAC
TKD6	GTTTTTTGAGTAAAGGCCGCGGAAGTGCCTCATGGC
TKE1	GAGGCACTTCCGCTGGCCGCGACTCAAAAACTATTGATC
TKE2	GATCAATAGTTTTTTGAGTCGCGGCCAGCGGAAGTGCCTC
WK209	CGAGGCTGATCAGCGAGCT
WK314	TGATCTAGAAGCTCGCTGATCAGCCTC
WK346	GCCTTTCTCTCCACAGGCGCGCACTCCGTGCCGAGCACCCCCC
WK347	CGAGGCTGATCAGCGAGCTTCTAGATCAGTGATGGTGATGATGGTGTGTTGCCC
WK353	GGACAATGGTCACCGTCTCCTCAGCGAGCCCGACGTCTCC
WK354	GGCTGATCAGCGAGCTTCTAGATCATTTGCCCGCCAGACGATCAATAGTTTTTTGAGTAAAGGCCA GCGG
WK364	ACCGTCAGTCTTCTCTTCCCCCGCGTTGGAAGACCTTCTGCTTGGTAGCGAAGCGAATGGCGT CACATGCGTGGTGGTGGA
WK366	CCCATCGAGAAAACCATCTCCAAAGCCAGCGGCAACACCTTCAGACC
WK370	TCAGTCTTCCTCTTCCCCCAGCCCTGGAGGACTTGCTG
WK385	CGTACCGTGTGGTCAGCGTCTCCCTGGATGTGCCGAGCCTTGAATCACGGCAAGGAGTACAAG TGCAAGGTCTC
WK386	CCTGTCGATGGTCTTCTGGGTGAAGGC
WK425	TGAGCGGCCGCTCGAG
WK426	AACTGGACACCTTTGAGCACAGC
WK448	CGCTGTGCTCAAAGGTGTCCAGTGTCAGCTGCTCCCCAAAGGCTG
WK450	CGCTGTGCTCAAAGGTGTCCAGTGTCAGCTGCTCCCCAAAGG
WK459	CGCTGTGCTCAAAGGTGTCCAGTGTCAGGAAGGGGACTTTCCCATGCC

WK460	GTGGTGATGGTGATGATGGTTCTGCGTCGTGTAATCTTGGTGATG
WK461	GTGGTGATGGTGATGATGCCCCATTGGTGAAGAGCTGCCC
WK462	GTGGTGATGGTGATGATGGGGAGCTTGGACAGTGATGGTCAC
WK463	CGCCTTATCCGGTAACTATCGTCTTG
WK464	GACTCAAGACGATAGTTACCGGATAA

Table A.3: Oligonucleotides Used in Chapter 2.

Primer Name	Oligonucleotide sequence (5' → 3')
WK188	TTTCTCTCCACAGGCGCGCACTCCGACAAAACCTCACACATGCCACCGTGCCAGCACCTGAACTC CTGGGGGGACCGTCAGTCTTCTCTTCC
WK190	GGTCTTCGTGGCTCACGTCCACCACCACGCATGTGACCTCAGGGGTCCGGGAGATCATGAGGGTG TCCTTGGGTTTTGGGGGGAAGAGGAAGACTGACGGTCCC
WK191	GGTCTTCGTGGCTCACGTCCACCACCACGCACGTACGTTGGCCTCGCTGCCAGCAGCAAGTCCT CCAGGGCTGGGGGGAAGAGGAAGACTGACGGTCCC
WK192	GGTCTTCGTGGCTCACGTCCACCACCACGCACGTACGCCGTTGGCCTCGCTGCCAGCAGCAAG TCCTCCAGGGCTGGGGGGAAGAGGAAGACTGACGGTCCC
WK194	GTGGACGTGAGCCACGAAGACCCTGAGGTCAAGTTCAACTGGTACGTGGACGGCGTGAGGTGC ATAATGCCAAGACAAAGCCGCGGGAGGAGCAGTAC
WK196	GGAGACCTTGCACTTGTA CTCTTGCCATT CAGCCAGTCTGGTGCAGGACGGTGAGGACGCTGA CCACACGGTACGTGCTGTTGTA CTCTCTCCCGCGG
WK198	GCAAGGAGTACAAGTGCAAGGTCTCCAACAAAGCCCTCCCAGCCCCATCGAGAAAACCATCTCC AAAGCCAGCGGCAACACCTTCAGACCCGAGGTGCATCTGC
WK200	GCACGTCTTGGGGCTGAAGCCCCTCGCAAGGCAGGTGAGAGTGACCAGCTCGTTCAGGGCGAG CTCCTCGCTGGGAGGGGGCAGCAGATGCACCTCGGGTCTGAAG
WK202	CTTCAGCCCCAAGGACGTGCTCGTGAGGTGGCTGCAGGGCTCCCAGGAGCTGCCAGGGAGAAG TACCTGACCTGGGCCAGCAGGCAGGAGCCAGCCAAGGCACC
WK204	CCTCGTGGCCAACCATGCAAGAGAAAGTGTGCCCCTTCTTCAGTCTCCGACGCGACCCTCAGGA TGCTGGTGACGGCGAAGGTGGTGGTGCCTTGGCTGGGCTC
WK206	CTTGATGGTTGGCCACGAGGCCCTGCCCTGGCCTTACCCAGAAGACCATCGACAGGCACCAC CATCATCACTGATCTAGAAGC
WK207	CGAGGCTGATCAGCGAGCTTCTAGATCAGTGGTGATGATGGTGGTG
WK188	TTTCTCTCCACAGGCGCGCACTCCGACAAAACCTCACACATGCCACCGTGCCAGCACCTGAACTC CTGGGGGGACCGTCAGTCTTCTCTTCC
WK190	GGTCTTCGTGGCTCACGTCCACCACCACGCATGTGACCTCAGGGGTCCGGGAGATCATGAGGGTG TCCTTGGGTTTTGGGGGGAAGAGGAAGACTGACGGTCCC
WK191	GGTCTTCGTGGCTCACGTCCACCACCACGCACGTACGTTGGCCTCGCTGCCAGCAGCAAGTCCT CCAGGGCTGGGGGGAAGAGGAAGACTGACGGTCCC
WK192	GGTCTTCGTGGCTCACGTCCACCACCACGCACGTACGCCGTTGGCCTCGCTGCCAGCAGCAAG TCCTCCAGGGCTGGGGGGAAGAGGAAGACTGACGGTCCC
WK194	GTGGACGTGAGCCACGAAGACCCTGAGGTCAAGTTCAACTGGTACGTGGACGGCGTGAGGTGC ATAATGCCAAGACAAAGCCGCGGGAGGAGCAGTAC
WK196	GGAGACCTTGCACTTGTA CTCTTGCCATT CAGCCAGTCTGGTGCAGGACGGTGAGGACGCTGA CCACACGGTACGTGCTGTTGTA CTCTCTCCCGCGG
WK198	GCAAGGAGTACAAGTGCAAGGTCTCCAACAAAGCCCTCCCAGCCCCATCGAGAAAACCATCTCC AAAGCCAGCGGCAACACCTTCAGACCCGAGGTGCATCTGC
WK200	GCACGTCTTGGGGCTGAAGCCCCTCGCAAGGCAGGTGAGAGTGACCAGCTCGTTCAGGGCGAG

WK202	CTCCTCGCTGGGAGGGGGCAGCAGATGCACCTCGGGTCTGAAG CTTCAGCCCCAAGGACGTGCTCGTGAGGTGGCTGCAGGGCTCCCAGGAGCTGCCAGGGAGAAG TACCTGACCTGGGCCAGCAGGCAGGAGCCCAGCCAAGGCACC
WK204	CCTCGTGGCCAACCATGCAAGAGAAAAGTGTGCCCCTTCTTCAGTCCTCCGCAGCGACCCTCAGGA TGCTGGTGACGGCGAAGGTGGTGGTGCCTTGGCTGGGCTC
WK206	CTTGCATGGTTGGCCACGAGGCCCTGCCCCTGGCCTTCACCCAGAAGACCATCGACAGGCACCAC CATCATCACCCTGATCTAGAAGC
WK207	CGAGGCTGATCAGCGAGCTTCTAGATCAGTGGTGATGATGGTGGTG

Figure A.1: SDS-PAGE Gel Showing Expression of IgA Fc Alanine Scanning Mutants Expressed in HEK293F Cells.

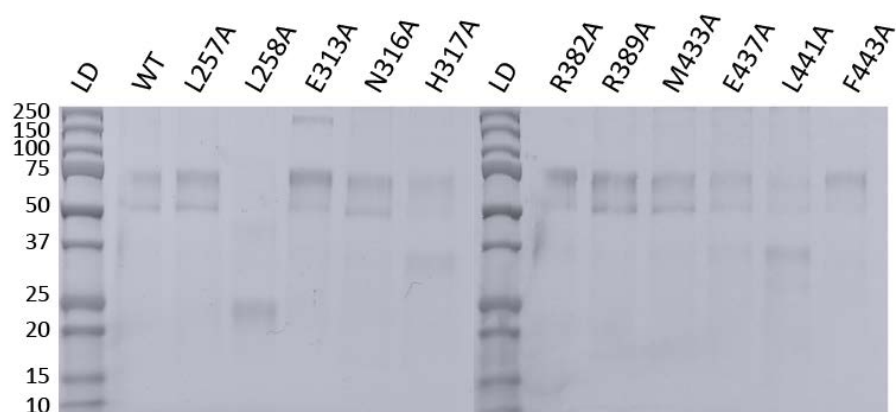


Figure A.2: Characterization of Aglycosylated IgA Expressed in Bacteria.  
A) ELISA analysis of completely aglycosylated IgA Fc domain binding to Fc $\alpha$ RI as compared to full length glycosylated IgA from human serum. B) 4-20% SDS-PAGE gel analysis of aglycosylated IgA.

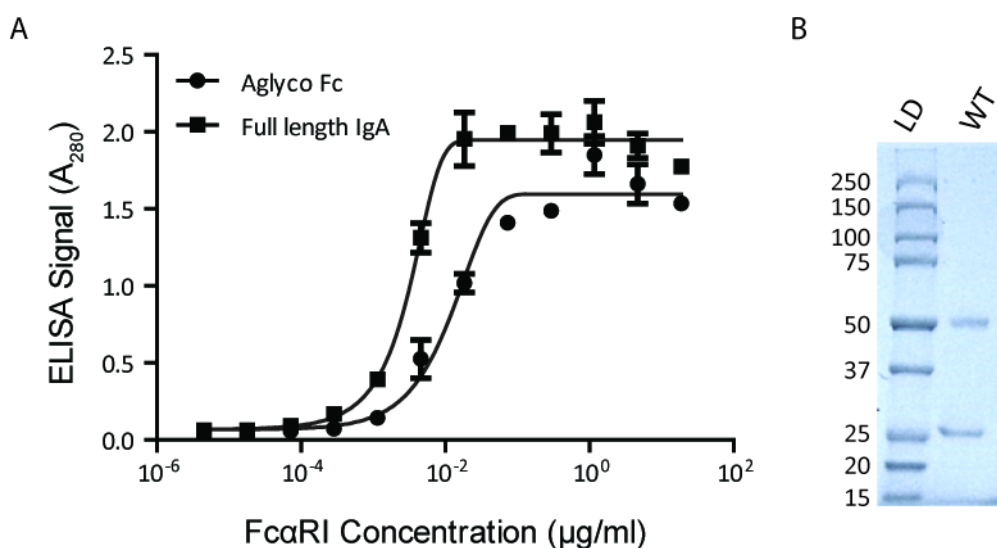


Figure A.3: Sequence Alignment of IgA/G Variants with Wild Type IgG.

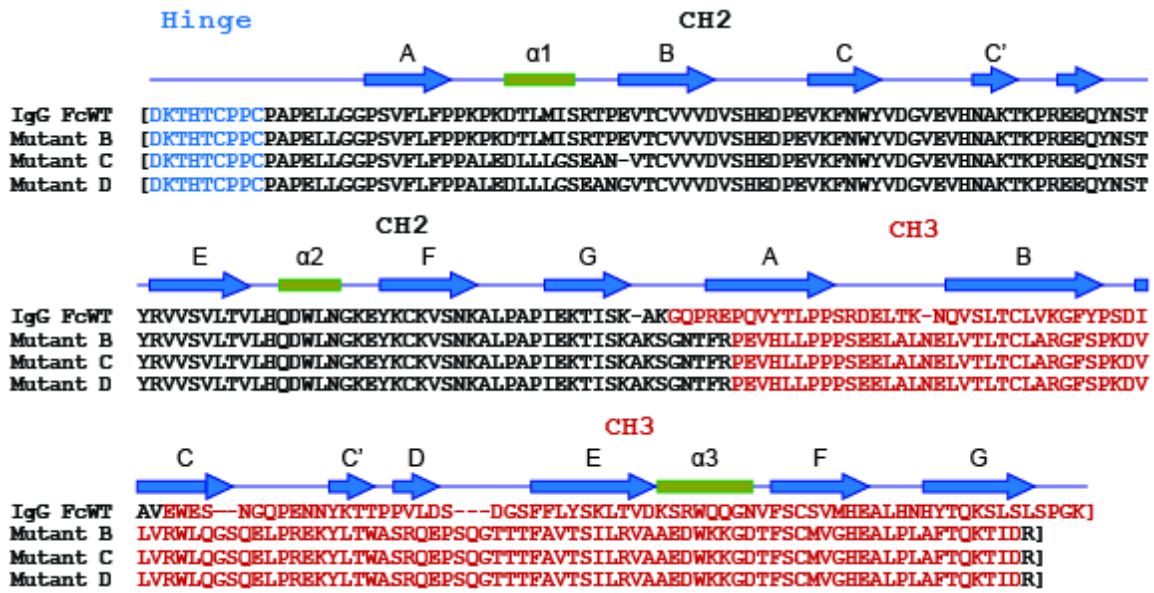


Figure A.4: Characterization of IgA/G Domain Swap Variants.

A) 4-20 % SDS-PAGE of variants expressed in HEK293F cells, B) ELISA analysis of variant binding to dimeric FcαRI-GST

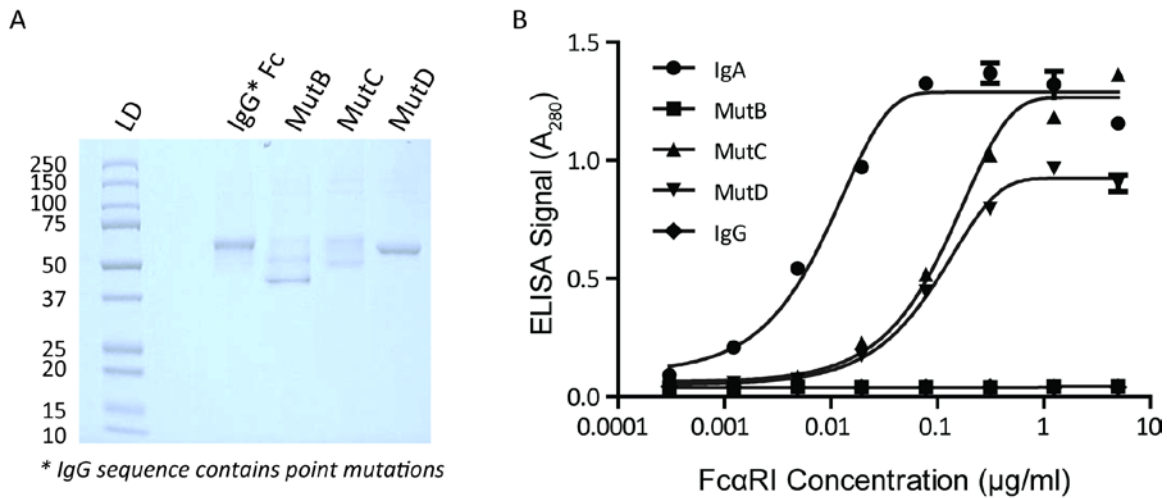


Figure A.5: SPR Analysis of MutD Affinity for FcγRIIa, FcγRIIb and FcαRI at Equilibrium.

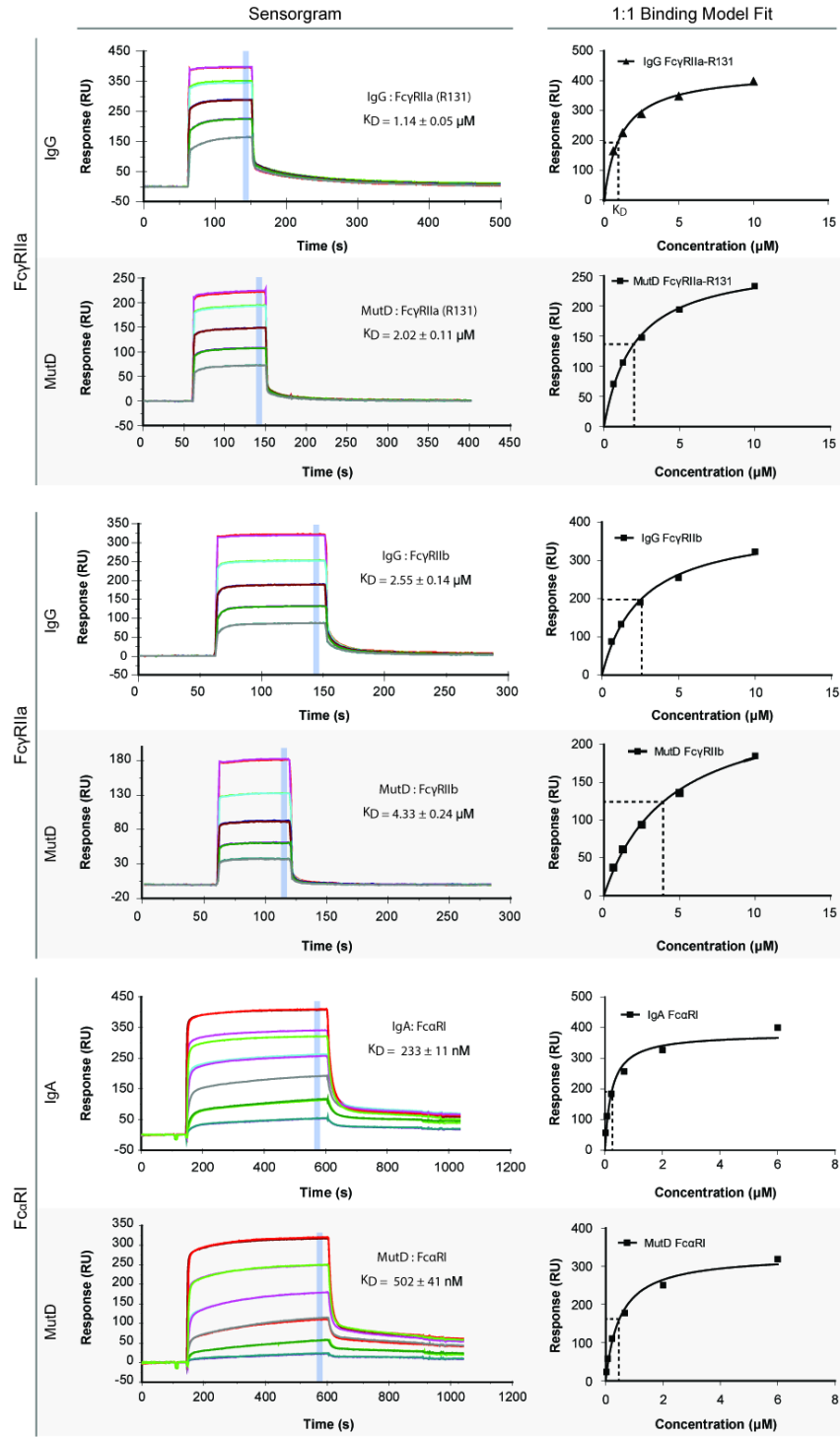


Figure A.6: Kinetic Analysis of MutD Affinity for FcγRI by SPR.

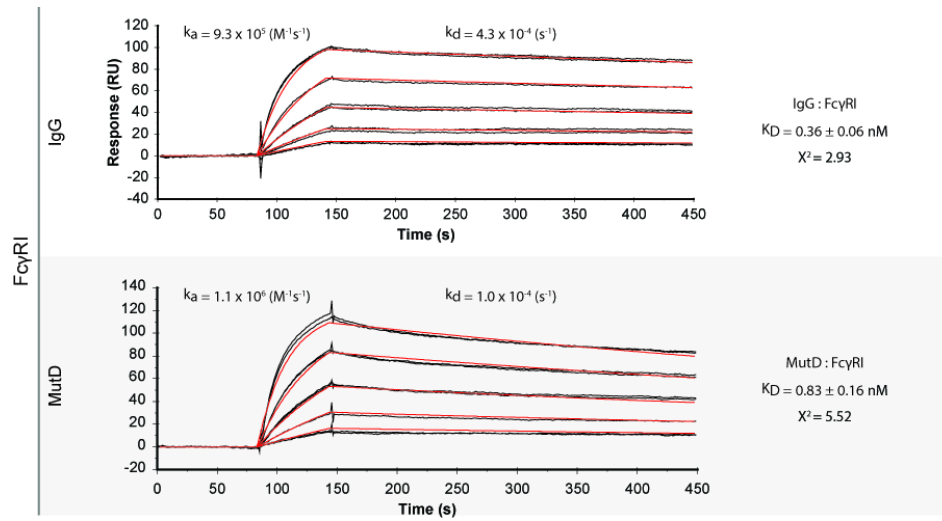
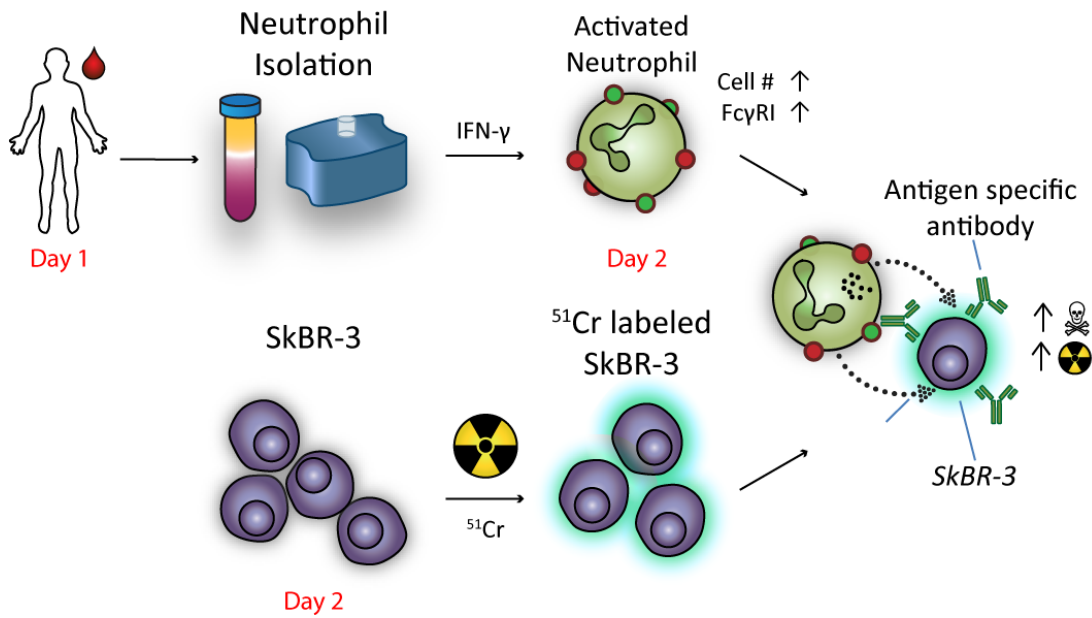


Figure A.7: Experimental Workflow for Neutrophil ADCC Assays.



## Appendix B

### MATERIALS AND METHODS

#### Molecular Biology Techniques

All plasmids and primers used in this study are described in Table B1 and B2. A gene encoding the human IgG1 Fc (comprising the hinge, CH2, and CH3 domains), was ligated into pPelBFLAG on *Sfi*I restriction endonuclease sites to generate pPelBFLAG-Fc. pTrc99A-DsbA-Fc2a-FLAG was constructed by PCR amplification of the Fc2a gene containing mutations S298G and T299A in the CH2 region using two primers (STJ#422 and STJ#147) with the template pTrc99A-DsbA-Fc-FLAG [172], and ligated into *Sac*II / *Hind*III restriction enzyme-treated pTrc99A-DsbA-Fc-FLAG. To construct pSTJ4-AglycoT-Fc2a, the Fc2a gene was amplified by primers STJ#290 and STJ#291, with pTrc99A-DsbA-Fc2a-FLAG as a template. The amplified PCR fragments were ligated into *Sal*I / *Eco*RV digested pSTJ4-AglycoT to generate pSTJ4-AglycoT-Fc2a. pSTJ4-AglycoT-Fc5-2a (E382V/M428I/S298G/T299A) was generated by amplifying the Fc5-2a gene using two primers (STJ#490 and STJ#220) and pSTJ4-AglycoT-Fc5 as a template, followed by *Sac*II / *Eco*RI restriction enzyme digestion, and ligation into digested pSTJ4-AglycoT.

Trastuzumab heavy chains encoding either wild type human Fc or the Fc5, Fc2a, or Fc5-2a mutants were amplified using the primers STJ#474 and STJ#67 with the respective templates pSTJ4-AglycoT, pSTJ4-AglycoT-Fc5, pSTJ4-AglycoT-Fc2a, or pSTJ4-AglycoT-Fc5-2a. Each fragment was ligated into the pPelBFLAG vector using the *Sfi*I restriction enzyme sites to generate pPelB-AglycoT(H)-FLAG, pPelB-AglycoT(H)-Fc5-FLAG, pPelB-AglycoT(H)-Fc2a-FLAG, and pPelB-AglycoT(H)-Fc5-2a-FLAG. pBADNlpAHis-M18 was constructed by ligating the NlpA fused M18 scFv gene amplified from pMoPac1-FLAG-M18 [218], and digested with *Xba*I–*Hind*III restriction



enzymes, into pBAD30-KmR [218] digested with the same restriction endonucleases. Ligation of the trastuzumab VL-C $\kappa$  gene, amplified using two primers (STJ#475 and STJ#476) and template pSTJ4-AglycoT, into pBADNlpAHis-M18 using SfiI restriction sites generated pBADNlpA-VL-C $\kappa$ -His. The PelB leader peptide-fused trastuzumab VL-C $\kappa$  gene was amplified with primers STJ#16 and STJ#340 from pSTJ4-AglycoT as the template, digested with XbaI / HindIII endonucleases, and ligated into pBADNlpA-VL-C $\kappa$ -His digested with the same endonucleases to generate pBADPelB-VL-C $\kappa$ . pBAD-AglycoT(L)-His was constructed by ligating XbaI digested PCR fragments amplified using the primers STJ#70 and STJ#332 with pBADPelB-VL-C $\kappa$  as a template into XbaI digested pBADNlpA-VL-C $\kappa$ -His.

The Fc1001, Fc1002, Fc1003, Fc1004, FcG236A, and FcN297D genes were PCR amplified from AglycoT(H)-Fc1001-FLAG, AglycoT(H)-Fc1002-FLAG, AglycoT(H)-Fc1003-FLAG, AglycoT(H)-Fc1004-FLAG, AglycoT(H)-FcG236A-FLAG, and AglycoT(H)-FcN297D-FLAG, respectively by using the primers STJ#290 and STJ#498, then digested with *SalI* and *XbaI* restriction enzymes, and ligated into the mammalian expression vector, pMAZ-IgH-GlycoT [172], to generate pMAZ-IgH-GlycoT-Fc1001, pMAZ-IgH-GlycoT-Fc1002, pMAZ-IgH-GlycoT-Fc1003, pMAZ-IgH-GlycoT-Fc1004, pMAZ-IgH-GlycoT-FcG236A, and pMAZ-IgH-GlycoT-FcN297D, respectively.

For 2B6-N297D gene synthesis [219], 2B6 variable domains from heavy and light chains were gene assembled by PCR with Phusion polymerase (New England Biolabs) from primers WK#158 – WK#169 for the light chain and WK#172 – WK#187 for the heavy chain (25 cycles with 98 °C denaturation 1 min, 55 °C denaturation 1 min and 72 °C extension 2 min were performed before a 10 min final extension step). Correctly assembled genes were amplified with the light chain primers WK#158, WK#170 and heavy chain primers WK#171, WK#187 by overlap extension (OLE) PCR

[220]. Briefly, the megaprimer generated in the previous step was added with Phusion polymerase at a 1:250 molar ratio to heavy chain template (pMAZ-IgH-GlycoT-FcN297D) and light chain template (pMAZ-IgL-GlycoT) (25 cycles of amplification were performed with 98 °C denaturation 1 min, 55 °C denaturation 1 min and 72 °C extension 10 min steps). Remaining template plasmid in the PCR reaction was digested with DpnI endonuclease for 1 h at 37 °C and the final mixture was transformed into Jude-1 cells (F' [Tn10(Tet<sup>r</sup>) proAB<sup>+</sup> lacI<sup>q</sup> Δ(lacZ)M15] mcrA Δ(mrr-hsdRMS-mcrBC) 80dlacZΔM15 ΔlacX74 deoR recA1 araD139 Δ(ara leu)7697 galU galK rpsL endA1 nupG) [221].

pMAZ-FcγRIIa<sub>H131</sub>-GST was cloned by the OLE PCR method as described above using a megaprimer generated with primers WK#100 and WK#101 from pDNR-LIB-FcγRIIa (ATCC: MGC-23887). The second PCR step cloned this megaprimer fragment in place of FcγRI in pMAZ-FcγRI-GST, a plasmid derived by OLE PCR from pMAZ-IgH GlycoT by cloning the FcγRI-GST cassette from pcDNA3(oriP)-FcγRI [170] with primers WK#56 and WK#57. pMAZ-FcγRIIa<sub>R131</sub>-GST was generated by OLE PCR using pMAZ-FcγRIIa<sub>H131</sub>-GST as a template to generate a megaprimer with primers (WK#100 and WK#116).

For the construction of pPelBHis-FcγRIIIa<sub>V158</sub>, the FcγRIIIa<sub>V158</sub> gene was PCR amplified using primers STJ#76 and STJ#82 and the template pCMV-SPORT6-FcγRIIIa (ATCC: MGC-45020), and then ligated into pPelBHis [172] using the *Sfi*I sites. pMAZ-FcγRIIIa<sub>V158</sub>-GST was cloned by OLE PCR from pMAZ-FcγRIIIa<sub>V158</sub>, a monomeric mammalian derivative of pPelBHis-FcγRIIIa<sub>V158</sub>, with primers WK#91 and WK#92 used to generate the megaprimer. The recipient vector was pMAZ-FcγRIIa<sub>H158</sub>-GST. pMAZ-FcγRIII<sub>F158</sub>-GST was likewise cloned by OLE PCR from pMAZ-FcγRIIIa<sub>V158</sub>-GST with

primers WK#91 and WK#94 used for megaprimer synthesis and pMAZ-FcγRIIIa<sub>V158</sub>-GST as the recipient vector.

### **IgG Display in *E. coli* for FcγR Binding**

pBAD-AglycoT(L)-His was transformed with either pPelB-AglycoT(H)-FLAG, pPelB-AglycoT(H)-Fc5-FLAG, pPelB-AglycoT(H)-Fc2a-FLAG, or pPelB-AglycoT(H)-Fc5-2a-FLAG for wild type trastuzumab, trastuzumab-Fc5, trastuzumab-Fc2a, or trastuzumab-Fc5-2a, respectively into *E. coli* JUDE-1. The transformed *E. coli* cells were cultured overnight at 37 °C with 250 rpm shaking in TB (Terrific Broth; Becton Dickinson Diagnostic Systems Difco™) supplemented with 2% (wt/vol) glucose, chloramphenicol (40 µg/mL) and kanamycin (50 µg/mL). The overnight cultured cells were diluted 1:100 in fresh 7 mL of TB medium with chloramphenicol (40 µg/mL) and kanamycin (50 µg/mL) in 125 mL Erlenmeyer flask. After incubation at 37 °C for 2 h and cooling at 25 °C for 20 min with 250 rpm shaking, protein expression was induced with 1 mM of isopropyl-1-thio-D-galactopyranoside (IPTG). 20 h after IPTG induction, 6 mL of the culture broth was harvested by centrifugation and washed two times in 1 mL of cold 10 mM Tris-HCl (pH 8.0). After re-suspension in 1 mL cold STE solution (0.5 M Sucrose, 10 mM Tris-HCl, 10 mM EDTA, pH 8.0), the cells were incubated at 37 °C for 30 min on a tube rotator, pelleted by centrifugation at 12,000 x g for 1 min and washed in 1 mL of cold Solution A (0.5 M Sucrose, 20 mM MgCl<sub>2</sub>, 10 mM MOPS, pH 6.8). The washed cells were incubated in 1 mL Solution A with 1 mg/mL of hen egg lysozyme at 37 °C for 15 min. After centrifugation at 12,000 x g for 1 min, the resulting spheroplast pellets were resuspended in 1 mL of cold PBS. 300 µl of the spheroplasts were further diluted in 700 µl of PBS and labeled with 30 nM FcγRI-FITC to analyze binding. For FACS analysis of FcγRIIa binding, spheroplasts were incubated with 30 nM FcγRIIa C-

terminal fused to GST [170], washed in 1 mL of PBS, and labeled with polyclonal goat anti-GST-FITC (Abcam) diluted 1:200 in 1 mL of PBS. After incubation for 1 h with vigorous shaking at 25 °C protected from light, the mixture was pelleted by centrifugation at 12,000 x g for 1 min and resuspended in 1 ml of PBS. The fluorescently labeled spheroplasts were diluted in 2.5 mL of PBS and analyzed on BD FACSCalibur (BD Bioscience).

### **Protein Expression and Purification**

AglycoT-Fc1001, AglycoT-Fc1002, AglycoT-Fc1003, AglycoT-Fc1004, GlycoT-G236A, AglycoT-N297D and the N297D variant of an anti-FcγRIIb 2B6 antibody [219] were produced by transient transfection of HEK293F cells (Invitrogen). pMAZ-IgL and pMAZ-IgH vectors for each of the variants were purified from overnight *E. coli* cultures by Midiprep (Qiagen). 293Fectin Transfection Reagent (Invitrogen) was used to transfect cells cultured in GIBCO FreeStyle™ 293 Expression Medium (Invitrogen) following the manufacturer's instructions. After 6 days, the cells were pelleted by centrifugation at 2,000 rpm for 10 min and the supernatant was recovered. 25x PBS was added to the supernatant to make a 1x final concentration and the solution was passed through a 0.22 μm filter. Protein A high capacity agarose resin (Thermo Scientific) was added to a polypropylene column and allowed to settle. The packed slurry was equilibrated with 1x PBS before addition of the buffered supernatant. The flow through was collected and passed twice more through the column. Unbound proteins were washed away with >10 CV (Column Volume) of 1x PBS. IgGs were eluted with 3 mL of 100 mM glycine-HCl (pH 2.7) and immediately neutralized with 1 mL of 1 M Tris (pH 8.0). Samples were buffer-exchanged into 1x PBS using Amicon Ultra-4 (Millipore) spin columns with a 10

kDa cutoff. Purity of purified samples was assessed by 4-20% gradient SDS-PAGE gel (NuSep).

FcγRIIa-R131-GST, FcγRIIa-H131-GST, FcγRIIb-GST and FcγRIIIa-F158-GST were produced by transient transfection of HEK293F cells (Invitrogen) using the pMAZ-IgH expression vectors described. Receptors with GST fusion partners were purified by Glutathione Sepharose (GE Healthcare) affinity chromatography. 25x PBS was added to filtered supernatants to a 1x concentration and the mixture passed twice over the column. The column was washed with 100 mL of 1x PBS to remove nonspecifically bound protein. 4 mL of 1x PBS containing 10 mM reduced glutathione was used for elution into 10 kDa filter columns.

### **Construction and Parameterization of Mathematical Model**

A mathematical model was developed to better understand the interaction between Her2-expressing cells (SKOV-3 or MDA-MD-453) and macrophages. Within a “contact” area, Her2-bound IgG can bind to FcγRs, but this interaction is not possible outside of this region because of physical constraints imparted by the curvature of the two cells (Fig. 4A). This contact area was estimated to be 1/3 of the surface area of the smaller SKOV-3/MDA-MD-453 cells based on geometric considerations. A lower bound of 1/10 of the surface area has been calculated for a non-deforming bead [222], but the actual contact area is significantly higher because macrophages deform and spread around IgG-bound cells [223, 224]. Model nomenclature and parameter values are provided in Table B.4.

We considered three types of FcγRs on macrophages: FcγRIIa-H131, FcγRIIa-R131, and FcγRIIb. The number of FcγRIIa and FcγRIIb were experimentally quantified (Figure B.5B), and the FcγRIIa-H131 and FcγRIIa-R131 variants were assumed to exist

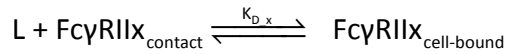
in 50/50 proportions [163]. FcγRs partitioned between the contact area and the free (non-contact) area with equilibrium constant  $K_{diff}$ :

$$\text{Fc}\gamma\text{RIIx}_{\text{free}} \xrightleftharpoons{K_{diff}} \text{Fc}\gamma\text{RIIx}_{\text{contact}}$$

where  $K_{diff} = \frac{[\text{Fc}\gamma\text{RIIx}_{\text{free}}]}{[\text{Fc}\gamma\text{RIIx}_{\text{contact}}]} = \frac{[\text{Macrophage Surface Area} - \text{Contact Area}]}{[\text{Contact Area}]}$

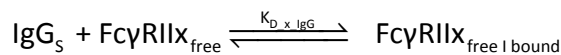
and  $\text{Fc}\gamma\text{RIIx} = \text{Fc}\gamma\text{RII-H131}, \text{Fc}\gamma\text{RII-R131}$  or  $\text{Fc}\gamma\text{RIIb}$

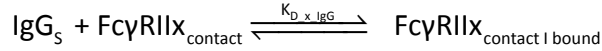
All Her2 receptors on SKOV-3 and MDA-MD-453 cells were considered to be evenly distributed and receptor numbers were calculated from experimental quantification of relative expression levels (Figure B.5A) and total absolute values from literature [225, 226]. The effective concentration of cell-bound IgG ( $[L_0]$ ) was calculated in an “effective contact volume,” defined as the product of contact\_area and cell\_gap. These cell-bound IgGs were free to interact with  $\text{Fc}\gamma\text{RIIx}_{\text{contact}}$  with ligand depletion:



where  $K_{D_x} = K_{D\_IIa-H131}, K_{D\_IIa-R131},$  or  $K_{D\_IIb}$  from SPR data for different Fc variants (Table B.3).

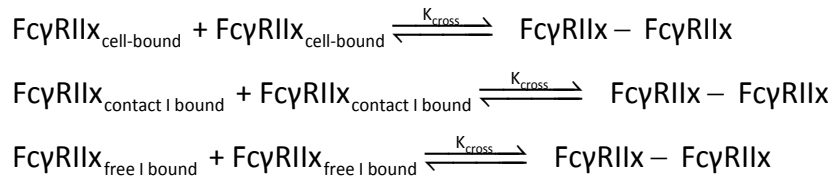
To mimic conditions in our *in vitro* experiments, as well as in normal physiology, 10 μM serum IgG ( $[\text{IgG}]_s$ ) was included in the system. Serum IgG was assumed to be in excess and could bind FcγRIIs anywhere on the macrophage surface without ligand depletion:





where  $K_{D_x \text{IgG}} = K_{D_{\text{IIa}} \text{IgG}}$  or  $K_{D_{\text{IIb}} \text{IgG}}$ .

Since receptor crosslinking leads to cell activation or inhibition, we assumed that dimers represent the minimal signaling unit (and serve as proxies for any higher-order receptor clusters). Any IgG-bound FcγRIIs were allowed to dimerize with equilibrium dissociation constant  $K_{\text{cross}}$ .  $K_{\text{cross}}$  was chosen to be  $2500 \text{ #}/\mu\text{m}^2$ , which maximizes the difference in the number of crosslinked receptors with and without MDA-MB-453 cells (chosen for this signal optimization since they express fewer Her2 molecules than SKOV-3 cells and therefore have lower signals). All possible combinations of dimers were allowed between the three FcγRII subunits with the same crosslinking constant, whether occupied by serum IgG or Her2-bound IgG. However, geometric constraints limited receptors in the contact area to only crosslink with those in the contact area, while receptors outside of the contact area could only crosslink with those outside:



No discrimination was made between crosslinked receptors in and out of the contact area because all of them could lead to an activating or inhibitory signal. However, local concentration effects made the density of dimers (and potentially higher-order clusters) much higher in the contact area.

The diffusion, binding, and crosslinking reactions above yield the following system of equations ( $x = \text{IIa-H131}$ ,  $\text{IIa-R131}$ , or  $\text{IIb}$ ):

$$[Fc\gamma RIIx]_{free} = K_{diff} [Fc\gamma RIIx]_{contact} \quad (E1, E2, E3)$$

$$\left( \frac{[L_0]_{SK/MD} - [Fc\gamma RIIx]_{cell-bound}}{(N_{AV} \times cell\_gap)} \right) \times [Fc\gamma RIIx]_{contact} = K_{D\_x} [Fc\gamma RIIx]_{cell-bound} \quad (E4, E5, E6)$$

$$[IgG]_S [Fc\gamma RIIx]_{free} = K_{D\_x\_IgG} [Fc\gamma RIIx]_{free \mid bound} \quad (E7, E8, E9)$$

$$[IgG]_S [Fc\gamma RIIx]_{contact} = K_{D\_x\_IgG} [Fc\gamma RIIx]_{contact \mid bound} \quad (E10, E11, E12)$$

$$[Fc\gamma RIIx]_{cell-bound} [Fc\gamma RIIx]_{cell-bound} = K_{cross} [Fc\gamma RIIx:Fc\gamma RIIx] \quad (E13 \text{ to } E18)$$

$$[Fc\gamma RIIx]_{contact \mid bound} [Fc\gamma RIIx]_{cell-bound} = K_{cross} [Fc\gamma RIIx:Fc\gamma RIIx] \quad (E19 \text{ to } E27)$$

$$[Fc\gamma RIIx]_{free \mid bound} [Fc\gamma RIIx]_{free \mid bound} = K_{cross} [Fc\gamma RIIx:Fc\gamma RIIx] \quad (E28 \text{ to } E33)$$

where  $[Fc\gamma RIIx]$  is in  $\#/\mu m^2$ . Conservation of mass gives:

all  $[Fc\gamma RIIx]$  in free area  $\times$  (macrophage total surface area – contact\_area)

+ all  $[Fc\gamma RIIx]$  in contact area  $\times$  contact\_area = Mac\_IIx

(E34, E35, E36)

This system of equations was solved in Matlab using *fsolve* to obtain the 36 unknowns. Finally, the resulting distribution of FcγRII dimers was correlated to the experimental output of ADCP. The relative contribution of activating/inhibiting homodimers to this cellular response is not known and, although there is evidence that heterodimers (FcγRIIa crosslinked with FcγRIIb) do form [227], it is not known whether they activate or inhibit. Therefore, we did not assign any *a priori* functions or signaling weights to these species, but rather allowed their contributions to be determined by the model by assigning an “intrinsic signaling potency” to each subunit. The signaling potency for FcγRIIb was fixed at -1 (negative for inhibitory) and the signaling potencies for FcγRIIa-H131 and FcγRIIa-R131 were allowed to vary freely. We then assumed that the signaling potency



of any given dimer was equal to the sum of potency of individual receptors. The overall response was calculated from:

$$\text{phagocytosis} \propto \sum (\text{Fc}\gamma\text{RII}x : \text{Fc}\gamma\text{RII}x \times \text{signaling potency of the respective dimer})$$

The level of phagocytosis was then compared to experimental data for only two Fc variants to obtain the intrinsic signaling potencies for Fc $\gamma$ RIIa-H131 and Fc $\gamma$ RIIa-R131. Fitted potency values are presented in Table B.5.

Table B.1: Plasmids Used in Chapter 3.

Plasmids	Relevant characteristics	Reference or Source
pPelBFLAG	Cm <sup>r</sup> , <i>lac</i> promoter, <i>tetA</i> gene, <i>skp</i> gene, C-terminal FL AG tag	[172]
pPelBFLAG-Fc	<i>IgG1-Fc</i> gene in pPelBFLAG	[172]
pTrc99A-DsbA-Fc-FLAG	<i>dsbA fused IgG1-Fc</i> gene, C-terminal FLAG tag in pTrc99A	[172]
pTrc99A-DsbA-Fc2a-FLAG	<i>dsbA fused IgG1-Fc2a</i> gene, C-terminal FLAG tag in pTrc99A	This study
pSTJ4-AglycoT	Trastuzumab IgG1 gene in pMAZ360	[172]
pSTJ4-AglycoT-Fc5	Trastuzumab IgG1-Fc5 gene in pMAZ360	[172]
pSTJ4-AglycoT-Fc2a	Trastuzumab IgG1-Fc2a gene in pMAZ360	This study
pSTJ4-AglycoT-Fc5-2a	Trastuzumab IgG1-Fc5-2a gene in pMAZ360	This study
pPelB-AglycoT(H)-FLAG	Trastuzumab IgG1 heavy chain gene in pPelBFLAG	This study
pPelB-AglycoT(H)-Fc5-FLAG	<i>IgG1-Fc5 heavy chain</i> gene in pPelB-AglycoT(H)-FLAG	This study
pPelB-AglycoT(H)-Fc2a-FLAG	<i>IgG1-Fc2a heavy chain</i> gene in pPelB-AglycoT(H)-FLAG	This study
pPelB-AglycoT(H)-Fc5-2a-FLAG	<i>IgG1-Fc5-2a heavy chain</i> gene in pPelB-AglycoT(H)-FLAG	This study
pPelB-AglycoT(H)-Fc1001-FLAG	<i>IgG1-Fc1001 heavy chain</i> gene in pPelB-AglycoT(H)-FLAG	This study
pPelB-AglycoT(H)-Fc1004-FLAG	<i>IgG1-Fc1004 heavy chain</i> gene in pPelB-AglycoT(H)-FLAG	This study
pPelB-AglycoT(H)-FcG236A-FLAG	<i>IgG1-FcG236A heavy chain</i> gene in pPelB-AglycoT(H)-FLAG	This study
pMoPac1-FLAG-M18	NlpA fused <i>M18 scFv</i> gene, C-terminal FLAG tag in pMoPac1	[218]
pBAD30-KmR	Km <sup>r</sup> , BAD promoter	[218]
pBADNlpAHis-M18	NlpA fused <i>M18 scFv</i> , C-terminal polyhistidine tag in pBAD30	This study
pBADNlpA-VL-Ck-His	NlpA fused <i>trastuzumab VL-Ck domain</i> , C-terminal polyhistidine tag and c-myc tag in pBAD30-KmR	This study
pBADPelB-VL-Ck-His	PelB fused <i>trastuzumab VL-Ck domain</i> , C-terminal polyhistidine tag and c-myc tag in pBAD30-KmR	This study
pBAD-AglycoT(L)-His	PelB fused <i>trastuzumab VL-Ck domain</i> followed by NlpA fused <i>trastuzumab VL-Ck-His</i> in pBAD30-KmR for dicistronic expression	This study
pMAZ-IgH-GlycoT	Trastuzumab IgG1 heavy chain gene in pMAZ-IgH-H23	[172]
pMAZ-IgH-GlycoT-Fc1001	<i>IgG1-Fc1001 heavy chain</i> gene in pMAZ-IgH-GlycoT	This study
pMAZ-IgH-GlycoT-Fc1002	<i>IgG1-Fc1002 heavy chain</i> gene in pMAZ-IgH-GlycoT	This study
pMAZ-IgH-GlycoT-Fc1003	<i>IgG1-Fc1003 heavy chain</i> gene in pMAZ-IgH-GlycoT	This study

pMAZ-IgH-GlycoT-Fc1004	IgG1-Fc1004 heavy chain gene in pMAZ-IgH-GlycoT	This study
pMAZ-IgH-GlycoT-FcG236A	IgG1-FcG236A heavy chain gene in pMAZ-IgH-GlycoT	This study
pMAZ-IgH-GlycoT-FcN297D	IgG1-FcN297D heavy chain gene in pMAZ-IgH-GlycoT	This study
pMAZ-IgH-2B6-N297D	2B6-N297D IgG1 heavy chain gene in pMAZ-IgH-GlycoT	This study
pMAZ-IgL-GlycoT	Trastuzumab IgG1 light gene in pMAZ-IgH-H23	[172]
pMAZ-IgL-2B6-N297D	2B6-N297D IgG1 light chain gene in pMAZ-IgH-GlycoT	[172]
pDNR-LIB-FcγRIIa	<i>FcγRIIa</i> <sub>H131</sub> gene in pMAZ-IgH-GlycoT	ATCC
pCMV-SPORT6-FcγRIIIa	<i>FcγRIIIa</i> <sub>V158</sub> gene in pMAZ-IgH-GlycoT	ATCC
pMAZ-FcγRI-GST	<i>FcγRI-GST</i> gene in pMAZ-IgH-GlycoT	This study
pMAZ-FcγRIIa <sub>R131</sub> -GST	<i>FcγRIIa</i> <sub>R131</sub> -GST gene in pMAZ-IgH-GlycoT	This study
pcDNA3(oriP)-FcγRI	<i>FcγRI</i> gene with C-Terminal GST fusion for mammalian expression	[170]
pMAZ-FcγRIIa <sub>H131</sub> -GST	<i>FcγRIIa</i> <sub>H131</sub> -GST gene in pMAZ-IgH-GlycoT	This study
pMAZ-FcγRIIIa <sub>V158</sub> -GST	<i>FcγRIIIa</i> <sub>V158</sub> -GST gene in pMAZ-IgH-GlycoT	This study
pMAZ-FcγRIIIa <sub>F158</sub> -GST	<i>FcγRIIIa</i> <sub>F158</sub> -GST gene in pMAZ-IgH-GlycoT	This study

Table B.2: Primers Used in Chapter 3.

Primer Name	Primer nucleotide sequence (5' → 3')
STJ#16	TTGTGAGCGGATAACAATTC
STJ#67	AATTC <u>GGCCCCGAGGCC</u> CTTTACCCGGGGACAGGGAGAGGCTCTTCTGCGTG
STJ#70	CTACCTGACGCTTTTATCGC
STJ#76	CGCAGCGAGGCCAGCCGGCCATGGCGGGCATGCGGACTGAAGATCTC
STJ#82	CGCAATTCGGCCCCGAGGCCCTTGGTACCCAGGTGGAAGAATG
STJ#147	GGCAAATTCTGTTTATCAGACCGCTTCTG
STJ#220	CAATTTGTCAGCCGCTGAGCAGAAG
STJ#290	TTTAGGGTTTTAGGGT <u>CGACA</u> AAGAAAGTTGAGCCCAAATCTTGACAAAACCTCACACATGCCC ACCG
STJ#290	TTTAGGGT <u>CGACA</u> AAGAAAGTTGAGCCCAAATCTTGACAAAACCTCACACATGCCCACCG
STJ#291	GGCCACCGGATATCTTATTATTTACCCGGGGACAGGGAGAGG
STJ#332	GGGAATCTAGACTATTAGCACTCTCCCCTGTTGAAGCTCTTTG
STJ#340	TTTAAGGGAAGCTTCTATTAGCACTCTCCCCTGTTGAAGCTCTTTG
STJ#422	CTAGGGAGCGCGGAGGAGCAGTACAACGGCGCGTACCGTGTGGTCAGCGTCCTC
STJ#474	CGCAGCGAGGCCAGCCGGCCATGGCGGAGGTTCAATTAGTGGAATCTG
STJ#475	CGCAGCGAGGCCAGCCGGCCATGGCGGATATTCAAATGACCCAAAGCCCG
STJ#476	CGCAATTCGGCCCCGAGGCCCGCACTCTCCCCTGTTGAAGCTCTTTG
STJ#490	CTAGGGAGCGCGGAGGAGCAGTACAACGGCGCGTACCGTGTGGTCAGTGTCTCT
STJ#498	TTTAGGGTCTAGATCATTTACCCGGGGACAGGGAGAGG
WK#56	TCCACAGGCGCGCACTCCCAAGTGGACACCACAAAGGCAGTG
WK#57	GGCTGATCAGCGAGCTTCTAGATCAGGATCTTTTGGAGGATGGTCGC
WK#91	CTCCACAGGCGCGCACTCCGGCATGCGGACTGAAGATCTCCC
WK#92	CCACGCGGAACCACTCGAGTTGGTACCCAGGTGGAAGAATGATG
WK#94	GTTACAGTCTCTGAAGACACATTTTACTCCCGAAAAGCCCCCTGCAGAAG
WK#100	CTCTCCACAGGCGCGCACTCCCAAGCTGCTCCCCAAAGGCTGT
WK#101	CCACGCGGAACCACTCGAGCCCCATTGGTGAAGAGCTGCCC
WK#116	GCTTGTGGGATGGAGAAGGTGGGATCCAACCGGGAGAATTTCTGGG
WK#158	CTCCACAGGCGCGCACTCCGAAATTGTGCTGACTCAGTCTCCAGACTTTC
WK#159	GGTGACTTTCTCCTTTGGTGTACGCTCTGAAAGTCTGGAGACTGAGTCAGCACAATTC
WK#160	AGAGCGTGACACAAAGGAGAAAGTCACCATCACCTGCAGGACCACTCAGAGC
WK#161	GCTGGTACCAATGTATGTTTGTGCCAATGCTCTGACTGGTCTGCAGGTGAT
WK#162	ATTGGCACAACATACATTGGTACCAGCAGAAACCAGATCAGTCTCCAAAGCTCC
WK#163	GACTCCAGAGATAGACTCAGAAACATACTTGATGAGGAGCTTTGGAGACTGATCTGGTTTCT
WK#164	TCATCAAGTATGTTTCTGAGTCTATCTCTGGAGTCCCATCGAGGTTCACTGGCAGTGG
WK#165	GGTGAGGGTGAAATCTGTCCCTGATCCACTGCCACTGAACCTCGATGG
WK#167	ATCAGGGACAGATTTACCCTCACCATCAATAGCCTGGAAGCTGAAGATGCTG
WK#168	GCCAGGTATTACTTTGTTGACAGTAATACGTTGCAGCATCTTCAGCTTCCAGGCTATTGAT
WK#169	CAACGTATTACTGTCAACAAAGTAATACCTGGCCGTTACGTTCCGGCGGAGG
WK#170	CGATGGGCCCTTGGTGCTAGCTTTGATCTCCACCTTGGTCCCTCCGCCGAACGTGAACG
WK#171	GCGGCCGCGTGCGTTTGATCTCCACCTTGGTC
WK#172	CTCCACAGGCGCGCACTCC
WK#173	CTCCACAGGCGCGCACTCCAGGTTCACTGGTGCACTCTGG
WK#174	CCCCAGGCTTCTTCACCTCAGCTCCAGACTGCACCACTGAACCTG
WK#175	AGCTGAGGTGAAGAAGCCTGGGGCCTCAGTGAAGGTCTCCTGCAAGG
WK#176	GTATCCAGTAGTTGGTAAAGGTGTAACCAGAAGCCTTGACAGGAGACCTTCACTGAGG

WK#177	CTTCTGGTTACACCTTTACCAACTACTGGATACTGGGTGCGACAGGCGCC
WK#178	CCATCCACTCAAGCCCTTGTCAGGCGCCTGTCGCACCCAGT
WK#179	TGGACAAGGGCTTGAGTGGATGGGAGTGATTGATCCTTCTGATACTTATCCAAATTAC
WK#180	CATGGTGACTCTGCCCTTGAACTTTTATTGTAATTTGGATAAGTATCAGAAGGATCAATCACTC
WK#181	AATAAAAAGTTCAAGGGCAGAGTCACCATGACCACAGACACATCCACGAGCACAG
WK#182	CTCAGGCTCCTCAGCTCCATGTAGGCTGTGCTCGTGGATGTGTCTGTGGT
WK#183	CCTACATGGAGCTGAGGAGCCTGAGATCTGACGACACGGCCGTGTATTAC
WK#184	CGGAATCACCGTTTCTCGCACAGTAATACACGGCCGTGTCGTCAGAT
WK#185	TGTGCGAGAAACGGTGATTCCGATTATTACTCTGGTATGGACTACTGGGGGC
WK#186	GAGACGGTGACCGTGGTCCCTTGCCCCAGTAGTCCATACCAGAGTAATAAT
WK#187	AAGGGACCACGGTCACCGTCTCCTCAGCTAGCACCAAGGGCCCATCG

---

Table B.3. Kinetic On and Off Rates for Trastuzumab Fc Variant Binding to FcγRs as Determined by SPR Analysis.

Variant	FcγRI			FcγRIIa-H131		
	$k_{on}$ ( $M^{-1} s^{-1}$ )	$k_{off}$ ( $s^{-1}$ )	$K_D$ (nM)	$k_{on}$ ( $M^{-1} s^{-1}$ )	$k_{off}$ ( $s^{-1}$ )	$K_D$ ( $\mu M$ )
Herceptin	$1.8 \times 10^5$	$2.7 \times 10^{-4}$	1.5 <sup>#</sup>	$7.2 \times 10^5$	$8.5 \times 10^{-2}$	0.12
AglycoT-Fc5-2a	$1.5 \times 10^5$	$2.3 \times 10^{-3}$	16	$3.1 \times 10^5$	$1.2 \times 10^{-1}$	0.37
AglycoT-Fc1001	$4.3 \times 10^5$	$3.3 \times 10^{-2}$	77	$2.6 \times 10^5$	$5.4 \times 10^{-2}$	0.20
AglycoT-Fc1002	N/A	N/A	N/A	$1.5 \times 10^5$	$2.8 \times 10^{-2}$	0.19
AglycoT-Fc1003	N/A	N/A	N/A	$3.3 \times 10^5$	$5.9 \times 10^{-2}$	0.18
AglycoT-Fc1004	$4.0 \times 10^5$	$2.6 \times 10^{-2}$	64	$5.3 \times 10^5$	$1.1 \times 10^{-2}$	0.021

Variant	FcγRIIa-R131			FcγRIIb		
	$k_{on}$ ( $M^{-1} s^{-1}$ )	$k_{off}$ ( $s^{-1}$ )	$K_D$ ( $\mu M$ )	$k_{off}$ ( $s^{-1}$ )	$k_{on}$ ( $M^{-1} s^{-1}$ )	$K_D$ ( $\mu M$ )
Herceptin	$1.2 \times 10^5$	$3.7 \times 10^{-2}$	0.31	$3.7 \times 10^{-2}$	$1.2 \times 10^5$	1.3
AglycoT-Fc5-2a	$1.3 \times 10^5$	$3.6 \times 10^{-2}$	0.27	$3.6 \times 10^{-2}$	$1.3 \times 10^5$	1.6
AglycoT-Fc1001	$2.6 \times 10^5$	$3.9 \times 10^{-3}$	0.015	$3.9 \times 10^{-3}$	$2.6 \times 10^5$	0.47
AglycoT-Fc1002	$1.8 \times 10^5$	$4.0 \times 10^{-2}$	0.22	$4.0 \times 10^{-2}$	$1.8 \times 10^5$	1.9
AglycoT-Fc1003	$2.6 \times 10^5$	$3.2 \times 10^{-2}$	0.12	$3.2 \times 10^{-2}$	$2.6 \times 10^5$	1
AglycoT-Fc1004	$3.2 \times 10^5$	$6.2 \times 10^{-4}$	0.0019	$6.2 \times 10^{-4}$	$3.2 \times 10^5$	0.2

<sup>#</sup> Affinity reported in previous study [172], using the same method.

Table B.4: Parameters Used to Generate FcγRIIa/b Activation Model.

Parameter	Description	Value	Reference or Source
<b>Physical parameters</b>			
SK_dia	Diameter of SKOV-3 cell	10 μm	[228]
MD_dia	Diameter of MDA-MB-453 cell	10 μm	[168, 228]
Mac_dia	Diameter of macrophage	21 μm	[229]
Cell_gap	Gap distance between SKOV-3/MDA-MB-453 cell and macrophage	12 nm	[230, 231]
Contact_area	Contact area of FcγRII receptors on macrophage	104.7 μm <sup>2</sup>	[222-224]
<b>Expression level parameters</b>			
SK_HER2	HER2 expression level on SKOV-3	7.36 x 10 <sup>5</sup>	[225, 226]
MD_HER2	HER2 expression level on MDA-MB-453	4.00 x 10 <sup>5</sup>	[225, 226]
Mac_IlaH	Number of FcγRIIa-H131 on macrophage	171271	This work
Mac_IlaR	Number of FcγRIIa-R131 on macrophage	171271	This work
Mac_Ilb	Number of FcγRIIb on macrophage	291150	This work
[IgG] <sub>s</sub>	Free serum IgG concentration	10 μM	This work
[L <sub>0</sub> ] <sub>SK</sub>	SKOV-3 Her2-bound IgG effective concentration	324.2 μM	This work
[L <sub>0</sub> ] <sub>MD</sub>	MDA-MB-453 Her2-bound IgG effective concentration	176.2 μM	This work
<b>Affinity parameters</b>			
K <sub>diff</sub>	Equilibrium constant for partitioning of FcγRII receptors in/out of the contact area on macrophage	16.64	This work
K <sub>cross</sub>	Equilibrium dissociation constant for the crosslinking of FcγRII receptors	2500 /μm <sup>2</sup>	This work
K <sub>D_Ila_IgG</sub>	Equilibrium dissociation constant between serum IgG and FcγRIIa-H131/FcγRIIa-R131	0.72 μM	[145]
K <sub>D_Ilb_IgG</sub>	Equilibrium dissociation constant between serum IgG and FcγRIIb	2.4 μM	[145]
K <sub>D_Ila-H131</sub>	Equilibrium dissociation constant between Fc variants and FcγRIIa-H131	(Table S3)	This work
K <sub>D_Ila-R131</sub>	Equilibrium dissociation constant between Fc variants and FcγRIIa-R131	(Table S3)	This work
K <sub>D_Ilb</sub>	Equilibrium dissociation constant between Fc variants and FcγRIIb	(Table S3)	This work

Table B.5: Intrinsic Signaling Potencies of FcγRIIa-H131, FcγRIIa-R131, and FcγRIIb.

ADCP data considered	Intrinsic signaling potency		
	FcγRIIa-H131	FcγRIIa-R131	FcγRIIb <sup>*</sup>
Fitting Herceptin and AglycoT-Fc1001 only	2.8	0.4	-1
Fitting Herceptin and AglycoT-Fc1004 only	2.0	0.3	-1
Fitting AglycoT-Fc1001 and AglycoT-Fc1004 only	11.3	0.1	-1

\* The signaling potency of FcγRIIb was always held fixed at -1, since the goal of each fit was to determine the *relative* potencies among the three receptor subunits.



Figure B.1: *E. coli* Bacterial Expression System for the Display of Full Length IgGs. (A) Expression cassettes for the display of covalently anchored full length IgGs. (B and C) Fluorescence histograms of spheroplasts expressing full length AglycoT-Fc5 (E382V/M428I) binding to 30 nM FcγRI-FITC (B) or AglycoT-2a (S298G/T299A) binding to 30 nM FcγRIIa-GST followed by 1:200 diluted goat anti-GST-FITC (C). (D) AglycoT-Fc5-2a shows high affinity binding for 30 nM FcγRI, FcγRIIa, and FcγRIIb.

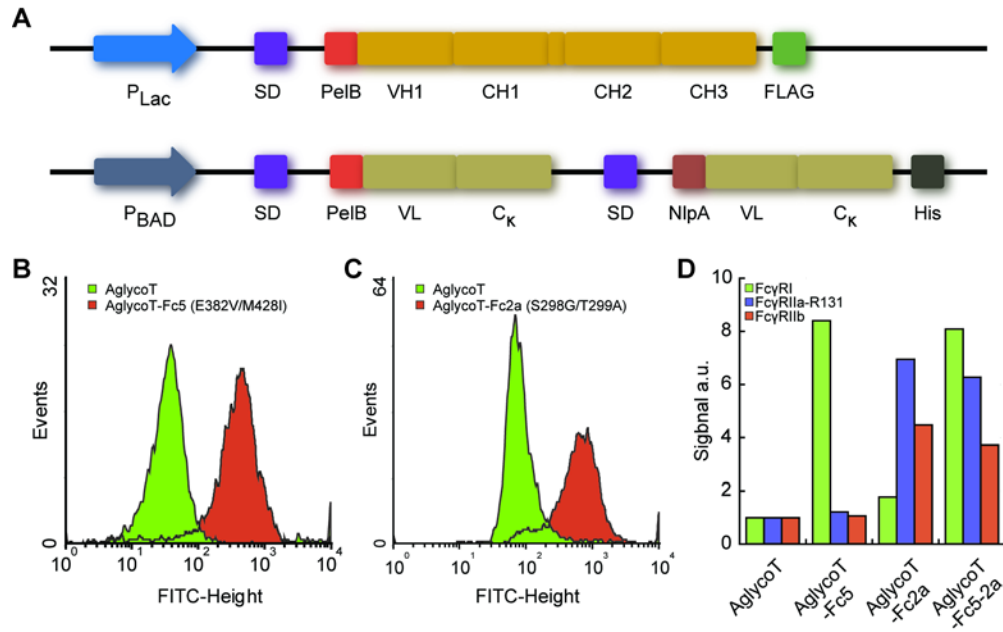


Figure B.2: Sequences and Corresponding FACS Signals for Isolated Fc Variants.

		Hinge								CH2							
		220	230	240	250	260	270	280	290								
FcWT	(75.76)	[-----]															ST
Fc5-2a	(135.76)	[DKTHTCPPC]	PAPELLGGPSVFLFPPKPKD	TL	MISRTPEV	TCVVVDVSHED	PEVKFNWYVD	GVGVHNAKTK	PREEQYNGA								
Fc1001	(408.55)	[-----]						P									K
Fc1002	(303.82)	[-----]															
Fc1003	(276.75)	[-----]															
Fc1004	(256.43)	[-----]															

		CH3							
		300	310	320	330	340	350	360	370
FcWT	(75.76)	YRVVSVLT	VLH	QDWLNGKEY	KCKVSNKALPAPIEKTISKAK				
Fc5-2a	(135.76)	YRVVSVLT	VLH	QDWLNGKEY	KCKVSNKALPAPIEKTISKAK		GQPREPQVY	TLPPSRDELTKNQVSLTCLVKGFYPSDIAV	
Fc1001	(408.55)								
Fc1002	(303.82)			D					
Fc1003	(276.75)								
Fc1004	(256.43)								

		CH3							
		380	390	400	410	420	430	440	
FcWT	(75.76)	--E						M	
Fc5-2a	(135.76)	EWSNGQPENNY	KTTTPPVLD	SDGSFFLYSKLT	VDKSRWQ	QGNVFSCSVIHE	ALHNHYTQKSLSLSPGK		
Fc1001	(408.55)						L		
Fc1002	(303.82)						L		
Fc1003	(276.75)		E	M			L		
Fc1004	(256.43)		D				L		

1) FACS mean values are indicated in the parenthesis

Figure B.3: Characterization of Isolated Aglycosylated Fc Variants.

(A) Fluorescent histogram of variant binding to 30 nM Fc $\gamma$ RIIa as detected by secondary goat anti-GST-FITC diluted at 1:200 from a 1 mg/mL stock. (B) SDS-PAGE showing full length trastuzumab Fc variants purified from HEK293F cells; M: molecular weight ladder, 1: AglycoT-Fc1001, 2: AglycoT-Fc1002, 3: AglycoT-Fc1003, and 4: AglycoT-Fc1004. (C and D) ELISA analysis of isolated aglycosylated Fc variants and Herceptin for (C) binding to Fc $\gamma$ RIIa, and (D) binding to FcRn at pH 6.0 and 7.4.

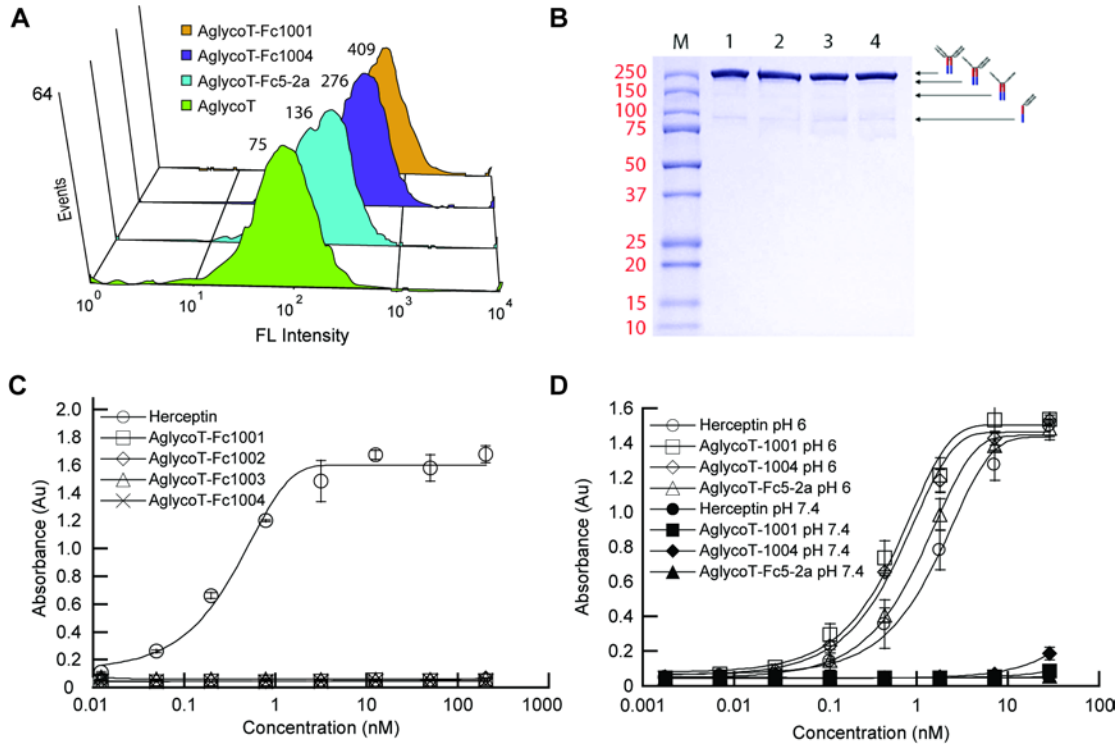


Figure B.4: Biacore Sensorgrams for FcγRIIa-R131-GST, FcγRIIa-H131-GST and FcγRIIb-GST Binding to Aglycosylated Mutants.

Antibody variants were immobilized on CM5 chips and soluble dimeric FcγRs used as analytes. A bivalent kinetic model was used to fit a minimum of four concentrations in duplicate for each variant.

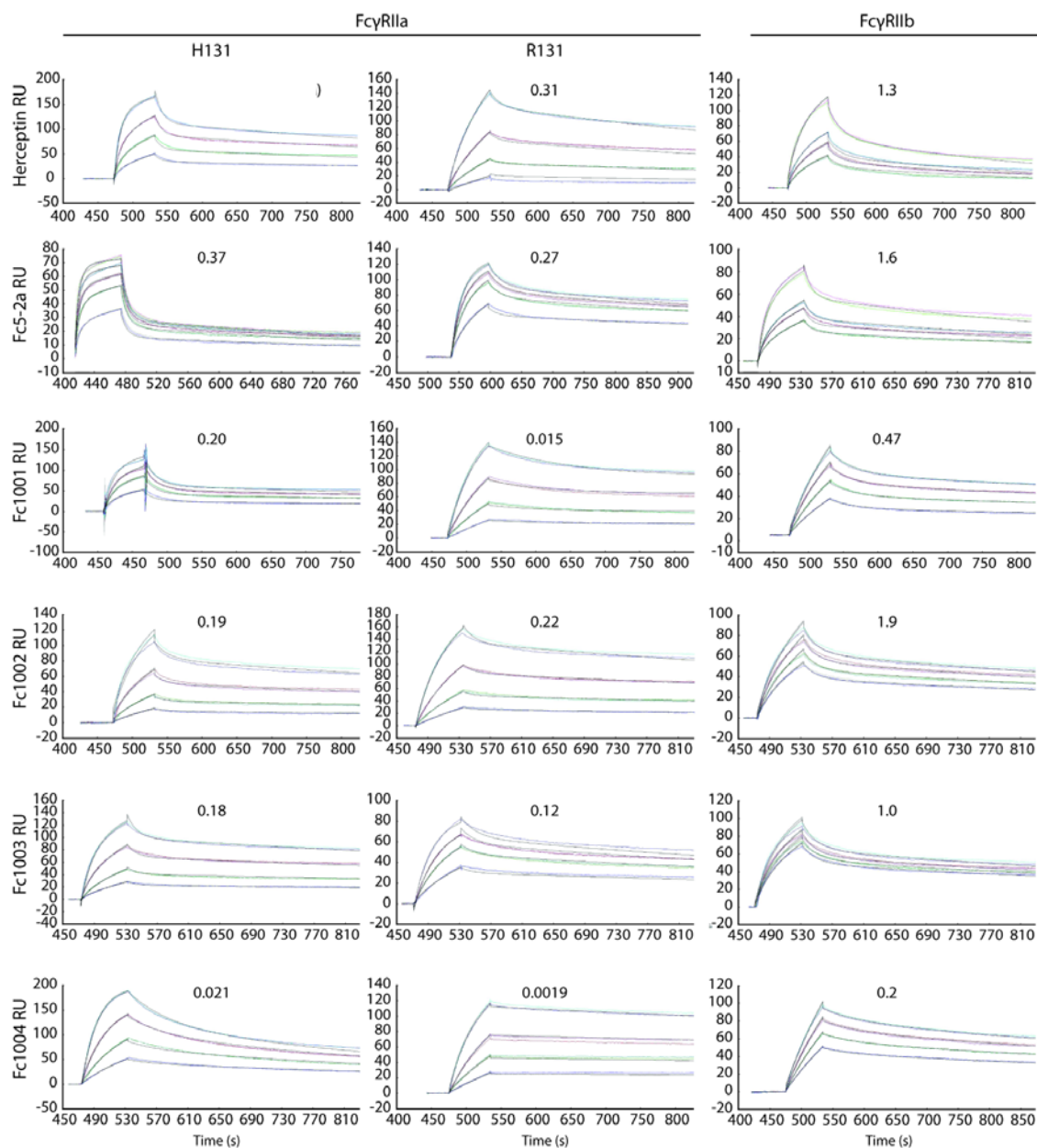


Figure B.5: Expression Level of Her2 and FcγR on Tumor Cell Lines and Macrophages for ADCP Assay.

(A) Her2 expression level on tumor cell lines used for ADCP was serum followed by fluorescent donkey anti-human IgG (H+L) FITC Fab at a 1:50 dilution. (B) FcγR counts on macrophages were determined using a fluorescent Quantum Simply Cellular bead assay. Macrophages were labeled with 20 μg/mL anti-FcγRI-FITC, 10 μg/mL anti-FcγRIIa-FITC, 1 μg/mL 2B6-N297D-FITC and 20 μg/mL anti-FcγRIII-FITC

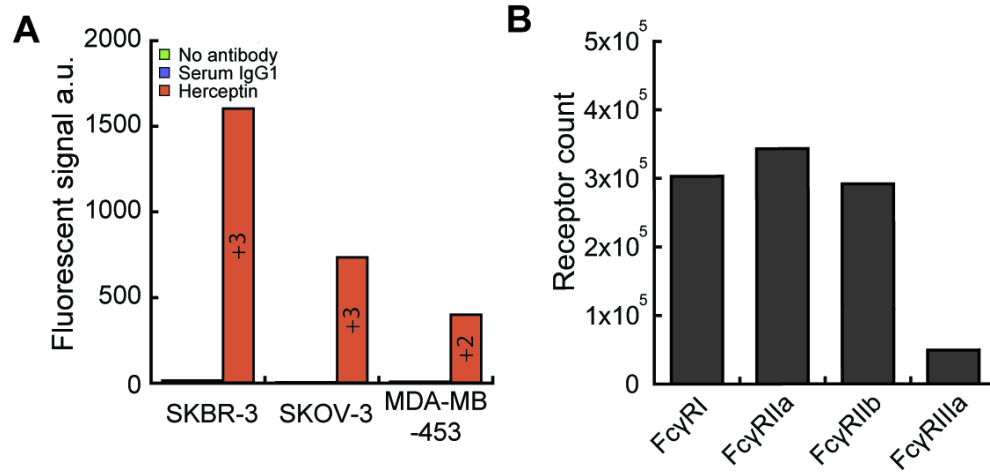


Figure B.6: ADCP Analysis for Ovarian Cancer Cells Expressing Medium HER2 Density (SKOV-3) and Low HER2 Density (MDA-MB-453).

Tumor cells were labeled with PKH67 membrane dye, opsonized with 0.5  $\mu\text{g/mL}$  antibody and mixed with macrophages at a 1:5 ratio for MDA-MB-453 and 1:10 for SKOV-3 tumor cells. Macrophages were labeled with 10  $\mu\text{g/mL}$  anti-CD11b-APC and 10  $\mu\text{g/mL}$  anti-CD14-APC before FACS interrogation. (A - F) FACS dot plots for SKOV-3 with No Ab (A), AglycoT-N297D (B), Herceptin (C), GlycoT-G236A (D), AglycoT-Fc1001 (E), and AglycoT-Fc1004 (F). Blue population = macrophages, Red population = SKOV-3 cells, green = double positive phagocytosed SKOV-3 cells. (G - L) FACS dot plots for MDA-MB-453 with No Ab (G), AglycoT-N297D (H), Herceptin (I), GlycoT-G236A (J), AglycoT-Fc1001 (K), and AglycoT-Fc1004 (L). Blue population = macrophages, Red population = MDA-MB-453 cells, green = double positive phagocytosed MDA-MB-453 cells.

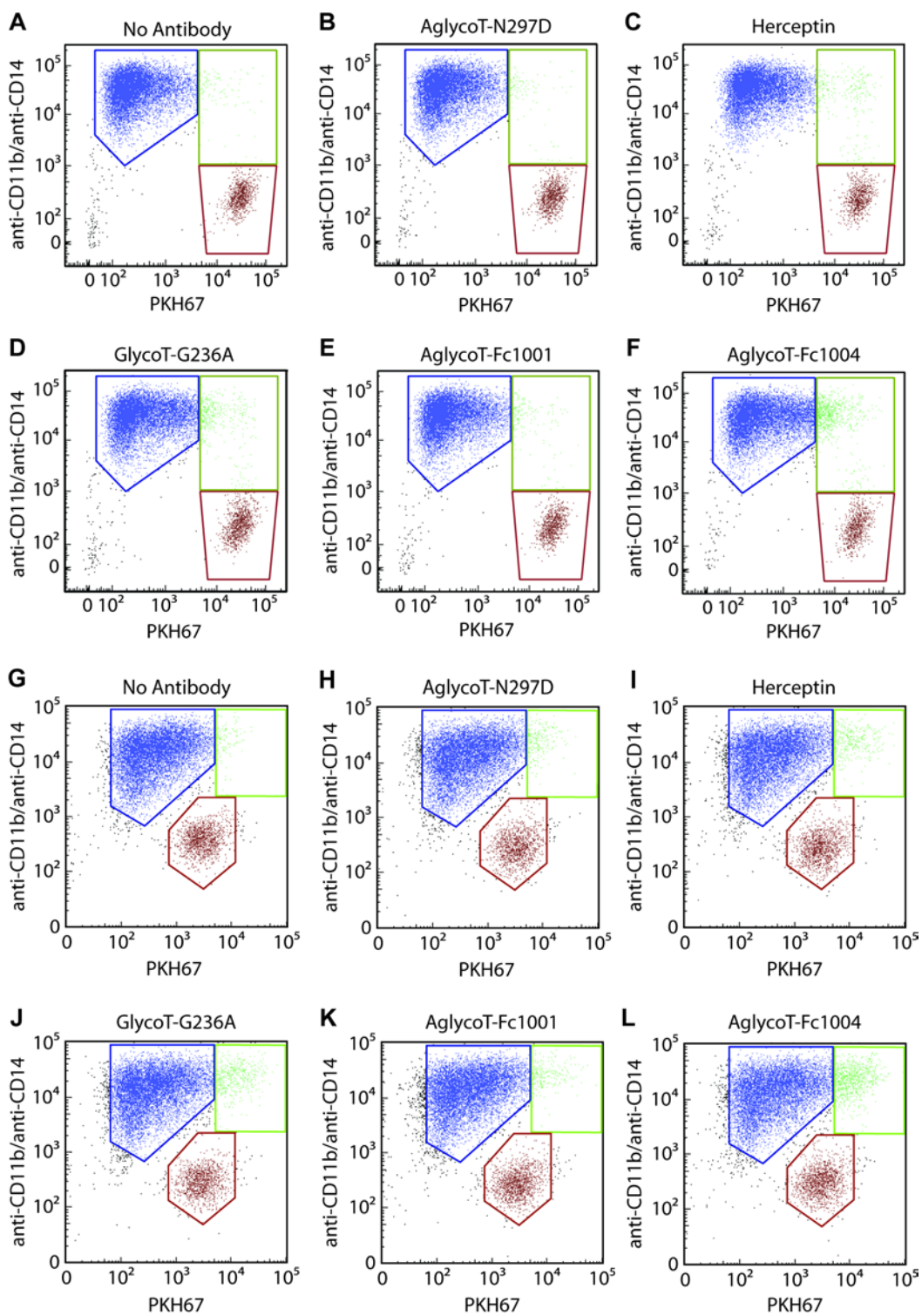
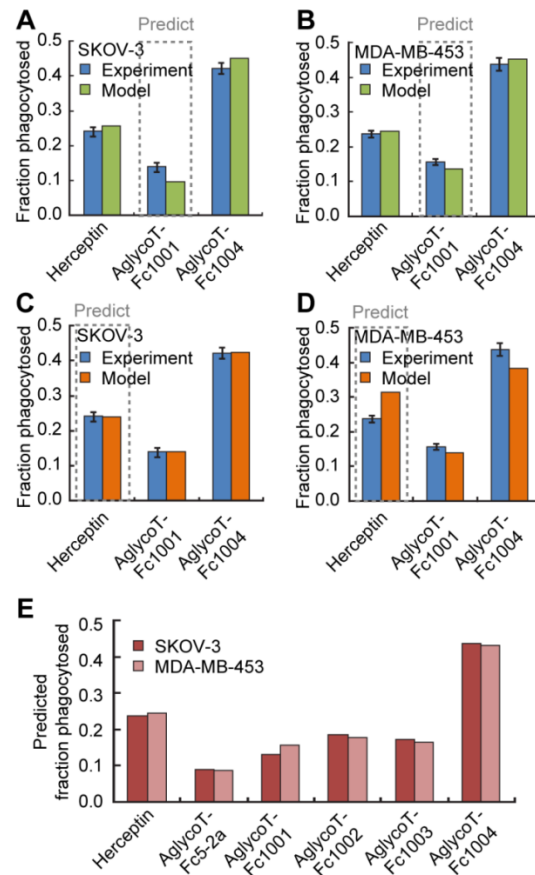


Figure B.7. The Model Returns Similar Predictions for Receptor Signaling Potency Independent of Experimental Data Used for Parameterization.

(A and B) ADCP data for Herceptin and AglycoT-Fc1004 were used to obtain intrinsic signaling potency values in the model, which was then used to predict phagocytic response of AglycoT-Fc1001 with both SKOV-3 cells (A) and MDA-MB-453 cells (B). Blue bars represent experimental values and green bars represent model predictions. (C and D) ADCP data for AglycoT-Fc1001 and AglycoT-Fc1004 were used to obtain intrinsic signaling potency values in the model, which was then used to predict phagocytic potency of AglycoT-Fc1001 with both SKOV-3 cells (C) and MDA-MB-453 cells (D). Blue bars represent experimental values and orange bars represent model predictions. (E) Predicted phagocytic responses of other Fc variants. Based on KD<sub>Ila</sub>-H131, KD<sub>Ila</sub>-R131, and KD<sub>Iib</sub> values from SPR analysis (Table S3), phagocytic response was predicted by the mathematical model for both SKOV-3 cells (dark red bar) and MDA-MB-453 cells (light red bar). Intrinsic signaling potencies for FcγRIIa-H131, FcγRIIa-R131 and FcγRIIb were the same as in Fig. 4 (2.8, 0.4, and -1 respectively).





## Appendix C

Table C.1: Plasmids Used in Chapter 4.

Plasmids	Relevant characteristics	Reference or Source
pMaz-IgH-FcγRIIaR131-GST	FcγRIIa gene in pMaz-IgH for dimeric mammalian expression	[96]
pMaz-IgH-FcγRIIaH131-GST	FcγRIIa gene in pMaz-IgH for dimeric mammalian expression	[96]
pMaz-IgH-N297D-trastuzumab	IgG1 trastuzumab heavy chain mammalian expression vector with glycosylation knockout at N297	[96]
pMaz-IgH-Fc1004-trastuzumab	IgG1 trastuzumab heavy chain mammalian expression vector with Fc1004 Fc domain	[96]
pMaz-IgL-trastuzumab	Wild type IgG1 trastuzumab kappa light chain mammalian expression vector	[96]
pcDNA3.4-IgH-Fc1004-trastuzumab	IgG1 trastuzumab heavy chain mammalian expression vector with Fc1004 Fc domain	This study
pcDNA3.4-IgL- trastuzumab	IgG1 trastuzumab light chain mammalian expression vector	This study

Table C.2: Primers Used in Chapter 4.

Primer Name	Primer nucleotide sequence (5' → 3')
WK124	CCAGAATGGAAAATCCCAGAAATTCTCTCA
WK125	CCAGAATGGAAAATCCCAGAAATTCTCTCG
WK126	CCATTGGTGAAGAGCTGCCCATGCTGGGCA
WK127	CCAGAATGGAAAATCCCAGAAATTCTCTCT
WK425	TGAGCGGCCGCTCGAG
WK426	ACACTGGACACCTTTGAGCACAGC
WK427	TAGCGGCCGCTATAAGGGTTCGAT
WK428	GGCACATCTGGCACCTGGGAG
WK429	CTGTGCTCAAAGGTGTCCAGTGTGAAATGGCGGAGGTTCAATTAGTGG
WK430	CTCTCCCTGTCCCCGGGTAAATGAGCGGCCGCTCGAGG
WK431	CCCAGGTGCCAGATGTGCCGAAATGGCGGATATTCAAATGACCCAAAGC
WK432	CCGGTAGGGATCGAACCCTTAACACTCTCCCCTGTTGAAGCTCTTTG

Table C.3: Genotypes of Anonymous Donors and Frequencies of Observed Alleles

Donor genotype	Number	Frequency
Homozygous R/R	5	0.28
Heterozygous H/R	8	0.44
Homozygous H/H	5	0.28
	<b>18</b>	

## **Appendix D**

### **MATERIALS AND METHODS**

#### **Transgenic Mouse ADCP Assay**

Bone marrow was isolated from C57BL/6 FcγR null mice transgenic for human FcγRIIa-R131 and FcγRIIb (Rockefeller University). The cells were resuspended in RPMI (Invitrogen) containing 10 % FBS and passed through a 70 μM filter (BD Biosciences) for seeding in T75 flasks (Corning). The culture was supplemented with 20 ng/mL of murine GM-CSF and incubated at 37 °C in 5 % CO<sub>2</sub>. On days 2 and 5 of culture the growth media was exchanged and non-adherent cells were aspirated. After 7 days, the plate was washed with Dulbecco's PBS (Mediatech) and 10 mL HyQTase (Thermo Scientific) solution was added for 15 min at 37 °C for the detachment of macrophages from the plate surface. Recovered cells were washed with 50 mL RPMI media and resuspended in RPMI containing 10 % FBS. MDA-MB-453 tumor cells were grown in DMEM containing 10 % FBS. Cells were recovered from culture flasks by trypsinization, labeled with PKH67 (Sigma-Aldrich) according to the manufacturer's instructions and resuspended in RPMI with 10 % human AB serum. These cells were seeded at  $5 \times 10^3$  per well in 96 well V-bottom plates (Corning) followed by addition of macrophages at the appropriate effector: tumor cell ratio (1:5 MDA-MB-453) and antibodies, to a final concentration of 5 μg/mL. The plate was briefly spun at 2,000 rpm for 1 min and incubated at 37 °C with 5 % CO<sub>2</sub> for 2 h (MDA-MB-453). Cells were stained with 5 μg/mL anti-CD11b-PE/Cy7 (Clone M1/70, Biolegend) on ice for 1 h. Phagocytosis was evaluated by FACS on an LSRFortessa (BD Bioscience), and reported as the fraction of double positive cells over the total number of tumor cells in the sample.

## References

1. LaMerie, *Blockbuster Biologics* 2012. 2013.
2. Reichert, J.M. *Therapeutic monoclonal antibodies approved or in review in the European Union or United States*. 2013; Available from: [http://www.antibodysociety.org/news/approved\\_mabs.php](http://www.antibodysociety.org/news/approved_mabs.php).
3. Behring, E. and S. Kitasato, *Ueber das zustandekommen der diphtherie-immunitat und der tetanus-immunitat bei thieren*. Dtsch med Wochenschr, 1890. **16**(06): p. 1113-1114.
4. Llewelyn, M.B., R.E. Hawkins, and S.J. Russell, *Discovery of antibodies*. BMJ: British Medical Journal, 1992. **305**(6864): p. 1269.
5. Edelman, G. and J. Gally, *A model for the 7S antibody molecule*. Proceedings of the National Academy of Sciences of the United States of America, 1964. **51**(5): p. 846.
6. Edelman, G.M., et al., *The covalent structure of an entire  $\gamma$ G immunoglobulin molecule*. Proceedings of the National Academy of Sciences, 1969. **63**(1): p. 78-85.
7. Jefferis, R. and D. Kumararatne, *Selective IgG subclass deficiency: quantification and clinical relevance*. Clinical and Experimental Immunology, 1990. **81**(3): p. 357.
8. Shakib, F. and D.R. Stanworth, *Human IgG subclasses in health and disease (A review) Part I*. Ricerca in clinica e in laboratorio, 1980. **10**(3): p. 463-479.
9. Morell, A., et al., *Metabolic properties of human IgA subclasses*. Clinical and Experimental Immunology, 1973. **13**(4): p. 521.
10. Manz, R.A., et al., *Maintenance of serum antibody levels*. Annual Review of Immunology, 2005. **23**(1): p. 367-386.
11. Achatz, G., et al., *The Biology of IgE: Molecular Mechanism Restraining Potentially Dangerous High Serum IgE Titres In Vivo*, in *Cancer and IgE*, M.L. Penichet and E. Jensen-Jarolim, Editors. 2010, Humana Press. p. 13-36.
12. Gonzalez-Quintela, A., et al., *Serum levels of immunoglobulins (IgG, IgA, IgM) in a general adult population and their relationship with alcohol consumption, smoking and common metabolic abnormalities*. Clinical and Experimental Immunology, 2008. **151**(1): p. 42.
13. Buckley, R.H. and S.A. Fiscus, *Serum IgD and IgE concentrations in immunodeficiency diseases*. The Journal of Clinical Investigation, 1975. **55**(1): p. 157-165.
14. Rogentine Jr, G.N., et al., *Metabolism of human immunoglobulin D (IgD)*. Journal of Clinical Investigation, 1966. **45**(9): p. 1467.
15. Harry, W.S. and C. Lisa, *Structure and function of immunoglobulins*. The Journal of allergy and clinical immunology, 2010. **125**(2): p. S41-S52.
16. Kerr, M.A., *The structure and function of human IgA*. Biochem. J, 1990. **271**: p. 285-296.
17. Snoeck, V., I.R. Peters, and E. Cox, *The IgA system: a comparison of structure and function in different species*. Vet. Res., 2006. **37**(3): p. 455-467.

18. Pasquier, B., et al., *Identification of FcαRI as an Inhibitory Receptor that Controls Inflammation Dual Role of FcR ITAM*. *Immunity*, 2005. **22**(1): p. 31-42.
19. Woof, J. and J. Mestecky, *Mucosal immunoglobulins*. *Immunological reviews*, 2005. **206**(1): p. 64-82.
20. Gould, H.J. and B.J. Sutton, *IgE in allergy and asthma today*. *Nature Reviews Immunology*, 2008. **8**(3): p. 205-217.
21. Jung, S.T., et al., *Bypassing glycosylation: Engineering aglycosylated full-length IgG antibodies for human therapy*. *Current Opinion in Biotechnology*, 2011.
22. Liu, H., G.-G. Bulseco, and J. Sun, *Effect of posttranslational modifications on the thermal stability of a recombinant monoclonal antibody*. *Immunology letters*, 2006. **106**(2): p. 144-153.
23. Cox, K.M., et al., *Glycan optimization of a human monoclonal antibody in the aquatic plant *Lemna minor**. *Nature biotechnology*, 2006. **24**(12): p. 1591-1597.
24. Li, H., et al., *Optimization of humanized IgGs in glycoengineered *Pichia pastoris**. *Nature biotechnology*, 2006. **24**(2): p. 210-215.
25. van Berkel, P.H.C., et al., *N-linked glycosylation is an important parameter for optimal selection of cell lines producing biopharmaceutical human IgG*. *Biotechnology Progress*, 2009. **25**(1): p. 244-251.
26. Shields, R.L., et al., *Lack of Fucose on Human IgG1 N-Linked Oligosaccharide Improves Binding to Human FcγRIII and Antibody-dependent Cellular Toxicity*. *Journal of Biological Chemistry*, 2002. **277**(30): p. 26733-26740.
27. Anthony, R. and J. Ravetch, *A Novel Role for the IgG Fc Glycan: The Anti-inflammatory Activity of Sialylated IgG Fcs*. *Journal of Clinical Immunology*, 2010. **30**(1): p. 9-14.
28. Burrows, P.D., et al., *Chapter 9 - The Development of Human B Lymphocytes*, in *Molecular Biology of B Cells*, H. Tasuku, et al., Editors. 2003, Academic Press: Burlington. p. 141-154.
29. Pieper, K., B. Grimbacher, and H. Eibel, *B-cell biology and development*. *Journal of Allergy and Clinical Immunology*, 2013.
30. Cogné, M. and B.K. Birshstein, *Chapter 19 - Regulation of Class Switch Recombination*, in *Molecular Biology of B Cells*, H. Tasuku, et al., Editors. 2003, Academic Press: Burlington. p. 289-305.
31. Vos, Q., et al., *B-cell activation by T-cell-independent type 2 antigens as an integral part of the humoral immune response to pathogenic microorganisms*. *Immunological reviews*, 2000. **176**: p. 154-170.
32. Di Noia, J.M. and M.S. Neuberger, *Molecular mechanisms of antibody somatic hypermutation*. *Annu. Rev. Biochem.*, 2007. **76**: p. 1-22.
33. Veselinovic, M., et al., *Topical gel formulation of broadly neutralizing anti-HIV-1 monoclonal antibody VRC01 confers protection against HIV-1 vaginal challenge in a humanized mouse model*. *Virology*, 2012. **432**(2): p. 505-510.
34. Nimmerjahn, F. and J. Ravetch, *Antibody-mediated modulation of immune responses*. *Immunol Rev*, 2010. **236**(1): p. 265-275.
35. Nimmerjahn, F. and J.V. Ravetch, *Fc[γ] Receptors: Old Friends and New Family Members*. *Immunity*, 2006. **24**(1): p. 19-28.

36. Nimmerjahn, F. and J.V. Ravetch, *Fc[gamma] receptors as regulators of immune responses*. Nat Rev Immunol, 2008. **8**(1): p. 34-47.
37. van der Poel, C.E., et al., *Functional Characteristics of the High Affinity IgG Receptor, FcγRI*. The Journal of Immunology, 2011. **186**(5): p. 2699-2704.
38. Kerst, J.M., et al., *Granulocyte colony-stimulating factor induces hFc gamma RI (CD64 antigen)-positive neutrophils via an effect on myeloid precursor cells*. Blood, 1993. **81**(6): p. 1457-1464.
39. Weng, W.K. and R. Levy, *Two immunoglobulin G fragment C receptor polymorphisms independently predict response to rituximab in patients with follicular lymphoma*. J Clin Oncol, 2003. **21**(21): p. 3940-3947.
40. Tamura, K., et al., *FcγR2A and 3A polymorphisms predict clinical outcome of trastuzumab in both neoadjuvant and metastatic settings in patients with HER2-positive breast cancer*. Ann Oncol, 2011. **22**(6): p. 1302-1307.
41. Zhang, W., et al., *FCGR2A and FCGR3A polymorphisms associated with clinical outcome of epidermal growth factor receptor-expressing metastatic colorectal cancer patients treated with single-agent cetuximab*. J Clin Oncol, 2007. **25**(24): p. 3712-3718.
42. Weiner, G.J. *Rituximab: mechanism of action*. in *Seminars in hematology*. 2010. Elsevier.
43. Arnould, L., et al., *Trastuzumab-based treatment of HER2-positive breast cancer: an antibody-dependent cellular cytotoxicity mechanism?* British journal of cancer, 2006. **94**(2): p. 259-267.
44. Hogarth, P.M. and G.A. Pietersz, *Fc receptor-targeted therapies for the treatment of inflammation, cancer and beyond*. Nat Rev Drug Discov, 2012. **11**(4): p. 311-331.
45. Takai, T., *Roles of Fc receptors in autoimmunity*. Nature Reviews Immunology, 2002. **2**(8): p. 580-592.
46. Biburger, M., et al., *FcγRIIB: a modulator of cell activation and humoral tolerance*. Expert Review of Clinical Immunology, 2012. **8**(3): p. 243+.
47. Bolland, S. and J. Ravetch, *Spontaneous autoimmune disease in Fc [gamma] RIIB-deficient mice results from strain-specific epistasis*. Immunity, 2000. **13**(2): p. 277-285.
48. Nimmerjahn, F. and J.V. Ravetch, *Divergent Immunoglobulin G Subclass Activity Through Selective Fc Receptor Binding*. Science, 2005. **310**(5753): p. 1510-1512.
49. Desjarlais, J., et al., *Optimizing engagement of the immune system by anti-tumor antibodies: an engineer's perspective*. Drug discovery today, 2007. **12**(21-22): p. 898-910.
50. Clynes, R.A., et al., *Inhibitory Fc receptors modulate in vivo cytotoxicity against tumor targets*. Nature medicine, 2000. **6**(4): p. 443-446.
51. Li, F. and J.V. Ravetch, *Inhibitory Fcγ Receptor Engagement Drives Adjuvant and Anti-Tumor Activities of Agonistic CD40 Antibodies*. Science, 2011. **333**(6045): p. 1030-1034.
52. Roopenian, D.C. and S. Akilesh, *FcRn: the neonatal Fc receptor comes of age*. Nat Rev Immunol, 2007. **7**(9): p. 715-725.

53. Baker, K., et al., *Neonatal Fc receptor for IgG (FcRn) regulates cross-presentation of IgG immune complexes by CD8-CD11b+ dendritic cells*. Proceedings of the National Academy of Sciences, 2011. **108**(24): p. 9927-9932.
54. Monteiro, R.C. and J.G.J. van de Winkel, *IgA Fc receptors*. Annual Review of Immunology, 2003. **21**: p. 177-204.
55. Wines, B.D. and P.M. Hogarth, *IgA receptors in health and disease*. Tissue Antigens, 2006. **68**(2): p. 103-114.
56. van Egmond, M., et al., *Human Immunoglobulin A Receptor (Fcalpha RI, CD89) Function in Transgenic Mice Requires Both FcR gamma Chain and CR3 (CD11b/CD18)*. Blood, 1999. **93**(12): p. 4387.
57. Mattu, T., et al., *The glycosylation and structure of human serum IgA1, Fab, and Fc regions and the role of N-glycosylation on Fc receptor interactions*. Journal of Biological Chemistry, 1998. **273**(4): p. 2260.
58. Jacob, C., et al., *Autoimmunity in IgA deficiency: revisiting the role of IgA as a silent housekeeper*. Journal of Clinical Immunology, 2008. **28**: p. 56-61.
59. Morton, H.C., et al., *Functional Association between the Human Myeloid Immunoglobulin A Fc Receptor (CD89) and FcR [IMAGE] Chain*. Journal of Biological Chemistry, 1995. **270**(50): p. 29781.
60. Otten, M.A. and M. van Egmond, *The Fc receptor for IgA (Fc RI, CD89)*. Immunology letters, 2004. **92**(1-2): p. 23-31.
61. Zhou, X., W. Hu, and X. Qin, *The Role of Complement in the Mechanism of Action of Rituximab for B-Cell Lymphoma: Implications for Therapy*. The Oncologist, 2008. **13**(9): p. 954-966.
62. Köhler, G. and C. Milstein, *Continuous cultures of fused cells secreting antibody of predefined specificity*. Nature, 1975. **256**(5517): p. 495-497.
63. Morrison, S.L., et al., *Chimeric human antibody molecules: mouse antigen-binding domains with human constant region domains*. Proceedings of the National Academy of Sciences, 1984. **81**(21): p. 6851-6855.
64. Jones, P.T., et al., *Replacing the complementarity-determining regions in a human antibody with those from a mouse*. 1986.
65. Beck, A., et al., *Strategies and challenges for the next generation of therapeutic antibodies*. Nature Reviews Immunology, 2010. **10**(5): p. 345-352.
66. McLaughlin, P., et al., *Rituximab chimeric anti-CD20 monoclonal antibody therapy for relapsed indolent lymphoma: half of patients respond to a four-dose treatment program*. Journal of clinical oncology, 1998. **16**(8): p. 2825-2833.
67. Slamon, D.J., et al., *Use of chemotherapy plus a monoclonal antibody against HER2 for metastatic breast cancer that overexpresses HER2*. New England Journal of Medicine, 2001. **344**(11): p. 783-792.
68. Strohl, W., *Optimization of Fc-mediated effector functions of monoclonal antibodies*. Current opinion in biotechnology, 2009. **20**(6): p. 685-691.
69. Kubota, T., et al., *Engineered therapeutic antibodies with improved effector functions*. Cancer science, 2009. **100**(9): p. 1566-1572.
70. Mavilio, D., L. Galluzzi, and E. Lugli, *Novel multifunctional antibody approved for the treatment of breast cancer*. OncoImmunology, 2013. **2**(3): p. e24567.

71. Shields, R., et al., *High resolution mapping of the binding site on human IgG1 for FcγRI, FcγRII, FcγRIII, and FcγRn and design of IgG1 variants with improved binding to the FcγRIIIb*. J Biol Chem, 2001. **276**(9): p. 6591-6604.
72. Lazar, G., et al., *Engineered antibody Fc variants with enhanced effector function*. Proc Natl Acad Sci USA, 2006. **103**(11): p. 4005-4010.
73. Horton, H.M., et al., *Potent In vitro and In vivo Activity of an Fc-Engineered Anti-CD19 Monoclonal Antibody against Lymphoma and Leukemia*. Cancer research, 2008. **68**(19): p. 8049-8057.
74. ClinicalTrials.gov. 2013; Available from: <http://www.clinicaltrials.gov>.
75. Richards, J., et al., *Optimization of antibody binding to FcγRIIIa enhances macrophage phagocytosis of tumor cells*. Mol Cancer Ther, 2008. **7**(8): p. 2517-2527.
76. Boder, E.T. and K.D. Wittrup, *Yeast surface display for screening combinatorial polypeptide libraries*. Nature biotechnology, 1997. **15**(6): p. 553-557.
77. Boder, E.T. and K.D. Wittrup, *Yeast surface display for directed evolution of protein expression, affinity, and stability*. Methods in enzymology, 2000. **328**: p. 430-444.
78. Stavenhagen, J.B., et al., *Fc optimization of therapeutic antibodies enhances their ability to kill tumor cells in vitro and controls tumor expansion in vivo via low-affinity activating Fcγ receptors*. Cancer research, 2007. **67**(18): p. 8882-8890.
79. Chu, S.Y., et al., *Inhibition of B cell receptor-mediated activation of primary human B cells by coengagement of CD19 and FcγRIIb with Fc-engineered antibodies*. Molecular immunology, 2008. **45**(15): p. 3926-3933.
80. Cemurski, S., et al., *Suppression of mast cell degranulation through a dual-targeting tandem IgE-IgG Fc domain biologic engineered to bind with high affinity to FcγRIIb*. Immunology Letters, 2012. **143**(1): p. 34-43.
81. Mimoto, F., et al., *Engineered antibody Fc variant with selectively enhanced FcγRIIb binding over both FcγRIIaR131 and FcγRIIaH131*. Protein Engineering Design and Selection, 2013.
82. Cox, K.M., et al., *Glycan optimization of a human monoclonal antibody in the aquatic plant Lemna minor*. Nat Biotech, 2006. **24**(12): p. 1591-1597.
83. Schuster, M., et al., *In vivo glyco-engineered antibody with improved lytic potential produced by an innovative non-mammalian expression system*. Biotechnology journal, 2007. **2**(6): p. 700-708.
84. Strasser, R., et al., *Generation of glyco engineered Nicotiana benthamiana for the production of monoclonal antibodies with a homogeneous human like N glycan structure*. Plant biotechnology journal, 2008. **6**(4): p. 392-402.
85. Bowles, J., et al., *Anti-CD20 monoclonal antibody with enhanced affinity for CD16 activates NK cells at lower concentrations and more effectively than rituximab*. Blood, 2006. **108**(8): p. 2648.
86. Naso, M.F., et al., *Engineering host cell lines to reduce terminal sialylation of secreted antibodies*. mAbs, 2010. **2**(5): p. 519-27.



87. Yamane-Ohnuki, N. and M. Satoh, *Production of therapeutic antibodies with controlled fucosylation*. mAbs, 2009. **1**(3): p. 230-6.
88. Geijtenbeek, T.B., et al., *Identification of DC-SIGN, a novel dendritic cell-specific ICAM-3 receptor that supports primary immune responses*. cell, 2000. **100**(5): p. 575-585.
89. Anthony, R.M., et al., *Identification of a receptor required for the anti-inflammatory activity of IVIG*. Proceedings of the National Academy of Sciences, 2008. **105**(50): p. 19571-19578.
90. Kaneko, Y., F. Nimmerjahn, and J.V. Ravetch, *Anti-Inflammatory Activity of Immunoglobulin G Resulting from Fc Sialylation*. Science, 2006. **313**(5787): p. 670-673.
91. Sonderrmann, P., et al., *General mechanism for modulating immunoglobulin effector function*. Proceedings of the National Academy of Sciences, 2013. **110**(24): p. 9868-9872.
92. Crispin, M., X. Yu, and T.A. Bowden, *Crystal structure of sialylated IgG Fc: Implications for the mechanism of intravenous immunoglobulin therapy*. Proceedings of the National Academy of Sciences, 2013. **110**(38): p. E3544-E3546.
93. Sonderrmann, P., et al., *Reply to Crispin et al.: Molecular model that accounts for the biological and physical properties of sialylated Fc*. Proceedings of the National Academy of Sciences, 2013. **110**(38): p. E3547.
94. van Oers, M.H.J., *CD20 antibodies: type II to tango?* Blood, 2012. **119**(22): p. 5061-5063.
95. Jung, S., et al., *Aglycosylated IgG variants expressed in bacteria that selectively bind Fc RI potentiate tumor cell killing by monocyte-dendritic cells*. Proceedings of the National Academy of Sciences, 2010. **107**(2): p. 604.
96. Jung, S.T., et al., *Effective Phagocytosis of Low Her2 Tumor Cell Lines with Engineered, Aglycosylated IgG Displaying High FcγRIIIa Affinity and Selectivity*. ACS Chemical Biology, 2012.
97. Keymeulen, B., et al., *Insulin needs after CD3-antibody therapy in new-onset type 1 diabetes*. New England Journal of Medicine, 2005. **352**(25): p. 2598.
98. Tran, M., et al., *Synthesis and assembly of a full length human monoclonal antibody in algal chloroplasts*. Biotechnology and bioengineering, 2009. **104**(4): p. 663-673.
99. Adair, J., *Engineering antibodies for therapy*. Immunological reviews, 1992. **130**(1): p. 5-40.
100. Hale, G., et al., *Pharmacokinetics and Antibody Responses to the CD3 Antibody Otelixizumab Used in the Treatment of Type 1 Diabetes*. The Journal of Clinical Pharmacology, 2010. **50**(11): p. 1238-1248.
101. Wiczling, P., et al., *Pharmacokinetics and Pharmacodynamics of a Chimeric/Humanized Anti-CD3 Monoclonal Antibody, Otelixizumab (TRX4), in Subjects With Psoriasis and With Type 1 Diabetes Mellitus*. The Journal of Clinical Pharmacology, 2010. **50**(5): p. 494-506.

102. Keymeulen, B., et al., *Four-year metabolic outcome of a randomised controlled CD3-antibody trial in recent-onset type 1 diabetic patients depends on their age and baseline residual beta cell mass*. Diabetologia, 2010. **53**(4): p. 614-623.
103. Ng, C., et al., *Pharmacokinetics/pharmacodynamics of nondepleting anti-CD4 monoclonal antibody (TRX1) in healthy human volunteers*. Pharmaceutical research, 2006. **23**(1): p. 95-103.
104. Scheerens, H., et al., *MTRX1011A, a humanized anti-CD4 monoclonal antibody, in the treatment of patients with rheumatoid arthritis: a Phase I randomized, double-blind, placebo-controlled study incorporating pharmacodynamic biomarker assessments*. Arthritis Research & Therapy, 2011. **13**(5): p. R177.
105. Clarke, S., et al. *A phase I, pharmacokinetic (PK), and preliminary efficacy assessment of ALD518, a humanized anti-IL-6 antibody, in patients with advanced cancer*. in American Society of Clinical Oncology. 2009.
106. Eder, J.P., et al., *Novel Therapeutic Inhibitors of the c-Met Signaling Pathway in Cancer*. Clinical Cancer Research, 2009. **15**(7): p. 2207-2214.
107. Merchant, M., et al., *Monovalent antibody design and mechanism of action of onartuzumab, a MET antagonist with anti-tumor activity as a therapeutic agent*. Proceedings of the National Academy of Sciences, 2013. **110**(32): p. E2987-E2996.
108. Yap, T.A. and J.S. de Bono, *Targeting the HGF/c-Met Axis: State of Play*. Molecular Cancer Therapeutics, 2010. **9**(5): p. 1077-1079.
109. Spigel, D., et al., *Final efficacy results from OAM4558g, a randomized phase II study evaluating MetMab or placebo in combination with erlotinib in advanced NSCLC*. J Clin Oncol, 2011. **29**(15 Suppl): p. 7505.
110. Georgiou, G. and L. Segatori, *Preparative expression of secreted proteins in bacteria: status report and future prospects*. Current Opinion in Biotechnology, 2005. **16**(5): p. 538-545.
111. Krapp, S., et al., *Structural analysis of human IgG-Fc glycoforms reveals a correlation between glycosylation and structural integrity*. J Mol Biol, 2003. **325**(5): p. 979-989.
112. Borrok, M.J., et al., *Revisiting the Role of Glycosylation in the Structure of Human IgG Fc*. ACS Chemical Biology, 2012.
113. Correia, I., *Stability of IgG isotypes in serum*. mAbs, 2010. **2**(3): p. 221-232.
114. Rother, R.P., et al., *Discovery and development of the complement inhibitor eculizumab for the treatment of paroxysmal nocturnal hemoglobinuria*. Nature biotechnology, 2007. **25**(11): p. 1256-1264.
115. Natsume, A., et al., *Engineered Antibodies of IgG1/IgG3 Mixed Isotype with Enhanced Cytotoxic Activities*. Cancer Research, 2008. **68**(10): p. 3863-3872.
116. Bruhns, P., et al., *Specificity and affinity of human Fcγ receptors and their polymorphic variants for human IgG subclasses*. Blood, 2009. **113**(16): p. 3716-3725.
117. Igietseme, J.U., X. Zhu, and C.M. Black, *Chapter 15 - Fc Receptor-Dependent Immunity*, in *Antibody Fc*, A. Margaret, Editor. 2014, Academic Press: Boston. p. 269-281.

118. Takai, T., *Fc receptors and their role in immune regulation and autoimmunity*. Journal of clinical immunology, 2005. **25**(1): p. 1-18.
119. Hatjiharissi, E., et al., *Increased natural killer cell expression of CD16, augmented binding and ADCC activity to rituximab among individuals expressing the FcγRIIIa-158 V/V and V/F polymorphism*. Blood, 2007. **110**(7): p. 2561-2564.
120. Souto, J.C., L. Vila, and A. Brú, *Polymorphonuclear neutrophils and cancer: Intense and sustained neutrophilia as a treatment against solid tumors*. Medicinal Research Reviews, 2011. **31**(3): p. 311-363.
121. Albanesi, M., et al., *Neutrophils mediate antibody-induced anti-tumor effects in mice*. Blood, 2013.
122. Siders, W.M., et al., *Involvement of neutrophils and natural killer cells in the anti-tumor activity of alemtuzumab in xenograft tumor models*. Leukemia & lymphoma, 2010. **51**(7): p. 1293-1304.
123. van Egmond, M. and J.E. Bakema, *Neutrophils as effector cells for antibody-based immunotherapy of cancer*. Seminars in Cancer Biology, 2013(0).
124. Otten, M.A., et al., *Immature Neutrophils Mediate Tumor Cell Killing via IgA but Not IgG Fc Receptors*. The Journal of Immunology, 2005. **174**(9): p. 5472-5480.
125. Bakema, J.E., et al., *Targeting FcαRI on Polymorphonuclear Cells Induces Tumor Cell Killing through Autophagy*. The Journal of Immunology, 2011. **187**(2): p. 726-732.
126. Stockmeyer, B., et al., *Triggering Fcα-Receptor I (CD89) Recruits Neutrophils as Effector Cells for CD20-Directed Antibody Therapy*. The Journal of Immunology, 2000. **165**(10): p. 5954-5961.
127. van Spriel, A.B., et al., *Effective Phagocytosis and Killing of Candida albicans via Targeting FcγRI (CD64) or FcαRI (CD89) on Neutrophils*. Journal of Infectious Diseases, 1999. **179**(3): p. 661-669.
128. van Egmond, M., A. Hanneke van Vuuren, and J.G. van de Winkel, *The human Fc receptor for IgA (FcαRI, CD89) on transgenic peritoneal macrophages triggers phagocytosis and tumor cell lysis*. Immunology letters, 1999. **68**(1): p. 83-87.
129. Dechant, M., et al., *Chimeric IgA antibodies against HLA class II effectively trigger lymphoma cell killing*. Blood, 2002. **100**(13): p. 4574.
130. Dechant, M., et al., *Effector mechanisms of recombinant IgA antibodies against epidermal growth factor receptor*. The Journal of Immunology, 2007. **179**(5): p. 2936.
131. Beyer, T., et al., *Serum-free production and purification of chimeric IgA antibodies*. Journal of Immunological Methods, 2009.
132. Woof, J.M. and M.A. Kerr, *The function of immunoglobulin A in immunity*. The Journal of Pathology, 2006. **208**(2): p. 270-282.
133. Raju, T.S., *Terminal sugars of Fc glycans influence antibody effector functions of IgGs*. Current opinion in immunology, 2008. **20**(4): p. 471-478.
134. Mariño, K., et al., *A systematic approach to protein glycosylation analysis: a path through the maze*. Nature chemical biology, 2010. **6**(10): p. 713-723.

135. van Egmond, M., et al., *Enhancement of Polymorphonuclear Cell-mediated Tumor Cell Killing on Simultaneous Engagement of Fc  $\gamma$  RI (CD64) and Fc  $\alpha$  RI (CD89)*. Cancer Research, 2001. **61**(10): p. 4055.
136. Gibson, D.G., et al., *Enzymatic assembly of DNA molecules up to several hundred kilobases*. Nature methods, 2009. **6**(5): p. 343-345.
137. Bryksin, A. and I. Matsumura, *Overlap extension PCR cloning: a simple and reliable way to create recombinant plasmids*. BioTechniques, 2010. **48**: p. 463-465.
138. Sockolosky, J.T., M.R. Tiffany, and F.C. Szoka, *Engineering neonatal Fc receptor-mediated recycling and transcytosis in recombinant proteins by short terminal peptide extensions*. Proceedings of the National Academy of Sciences, 2012. **109**(40): p. 16095-16100.
139. Pleass, R.J., et al., *Identification of Residues in the CH2/CH3 Domain Interface of IgA Essential for Interaction with the Human Fc $\alpha$  Receptor (Fc $\alpha$ R) CD89*. Journal of Biological Chemistry, 1999. **274**(33): p. 23508-23514.
140. Herr, A.B., E.R. Ballister, and P.J. Bjorkman, *Insights into IgA-mediated immune responses from the crystal structures of human Fc RI and its complex with IgA1-Fc*. Nature, 2003. **423**(6940): p. 614-620.
141. Carayannopoulos, L., J.M. Hexham, and J.D. Capra, *Localization of the binding site for the monocyte immunoglobulin (Ig) A-Fc receptor (CD89) to the domain boundary between Calpha2 and Calpha3 in human IgA1*. The Journal of Experimental Medicine, 1996. **183**(4): p. 1579-1586.
142. Basset, et al., *Glycosylation of Immunoglobulin A Influences Its Receptor Binding*. Scandinavian Journal of Immunology, 1999. **50**(6): p. 572-579.
143. Williams, A.F. and A.N. Barclay, *The immunoglobulin superfamily-domains for cell surface recognition*. Annual Review of Immunology, 1988. **6**(1): p. 381-405.
144. Kabat, E.A., et al., *Sequences of proteins of immunological interest*. Vol. 1. 1992: Diane Publishing.
145. Maenaka, K., et al., *The human low affinity Fc $\gamma$  receptors IIa, IIb, and III bind IgG with fast kinetics and distinct thermodynamic properties*. J Biol Chem, 2001. **276**(48): p. 44898-44904.
146. Herr, A., et al., *Bivalent binding of IgA1 to Fc RI suggests a mechanism for cytokine activation of IgA phagocytosis*. Journal of molecular biology, 2003. **327**(3): p. 645-657.
147. Roos, A., et al., *Human IgA activates the complement system via the mannan-binding lectin pathway*. The Journal of Immunology, 2001. **167**(5): p. 2861-2868.
148. Perussia, B., et al., *Immune interferon induces the receptor for monomeric IgG1 on human monocytic and myeloid cells*. The Journal of Experimental Medicine, 1983. **158**(4): p. 1092-1113.
149. Aida, Y. and M.J. Pabst, *Neutrophil responses to lipopolysaccharide. Effect of adherence on triggering and priming of the respiratory burst*. The Journal of Immunology, 1991. **146**(4): p. 1271-6.
150. Lux, A., et al., *Impact of Immune Complex Size and Glycosylation on IgG Binding to Human Fc $\gamma$ Rs*. The Journal of Immunology, 2013.

151. Monteiro, R.C. and J.G. van de Winkel, *IgA Fc receptors*. Annual Review of Immunology, 2003. **21**(1): p. 177-204.
152. Deng, R., et al., *Pharmacokinetics of Humanized Monoclonal Anti-Tumor Necrosis Factor- $\alpha$  Antibody and Its Neonatal Fc Receptor Variants in Mice and Cynomolgus Monkeys*. Drug Metabolism and Disposition, 2010. **38**(4): p. 600-605.
153. Bakema, J.E. and M. van Egmond, *The human immunoglobulin A Fc receptor Fc[ $\alpha$ ]RI: a multifaceted regulator of mucosal immunity*. Mucosal Immunol, 2011. **4**(6): p. 612-624.
154. Reljic, R., *In search of the elusive mouse macrophage Fc-alpha receptor*. Immunology letters, 2006. **107**(1): p. 80-81.
155. Mantovani, A., et al., *Neutrophils in the activation and regulation of innate and adaptive immunity*. Nat Rev Immunol, 2011. **11**(8): p. 519-531.
156. Fridlender, Z.G., et al., *Polarization of tumor-associated neutrophil phenotype by TGF- $\beta$ : "N1" versus "N2" TAN*. Cancer cell, 2009. **16**(3): p. 183-194.
157. Launay, P., et al., *Fc $\alpha$  Receptor (Cd89) Mediates the Development of Immunoglobulin a (Iga) Nephropathy (Berger's Disease)*. The Journal of Experimental Medicine, 2000. **191**(11): p. 1999-2010.
158. Stavenhagen, J., et al., *Fc optimization of therapeutic antibodies enhances their ability to kill tumor cells in vitro and controls tumor expansion in vivo via low-affinity activating Fc $\gamma$  receptors*. Cancer Res, 2007. **67**(18): p. 8882-8890.
159. Yee, A.M.F., et al., *Association Between Fc $\gamma$ RIIa-R131 Allotype and Bacteremic Pneumococcal Pneumonia*. Clin Infect Dis, 2000. **30**(1): p. 25-28.
160. Sanders, L., et al., *Human immunoglobulin G (IgG) Fc receptor IIA (CD32) polymorphism and IgG2-mediated bacterial phagocytosis by neutrophils*. Infect Immun, 1995. **63**(1): p. 73-81.
161. Shashidharamurthy, R., et al., *Dynamics of the interaction of human IgG subtype immune complexes with cells expressing R and H allelic forms of a low-affinity Fc $\gamma$  receptor CD32A*. J Immunol, 2009. **183**(12): p. 8216-8224.
162. Karassa, F.B., T.A. Trikalinos, and J.P.A. Ioannidis, *Role of the Fc $\gamma$  receptor IIA polymorphism in susceptibility to systemic lupus erythematosus and lupus nephritis: A meta-analysis*. Arthritis Rheum, 2002. **46**(6): p. 1563-1571.
163. Reilly, A., et al., *Genetic diversity in human Fc receptor II for immunoglobulin G: Fc gamma receptor IIA ligand-binding polymorphism*. Clin Vaccine Immunol, 1994. **1**(6): p. 640-644.
164. Sullivan, K., et al., *Analysis of polymorphisms affecting immune complex handling in systemic lupus erythematosus*. Rheumatology, 2003. **42**(3): p. 446-452.
165. Ruffell, B., et al., *Leukocyte composition of human breast cancer*. Proc Natl Acad Sci USA, 2012. **109**(8): p. 2796-2801.
166. Sazinsky, S., et al., *Aglycosylated immunoglobulin G1 variants productively engage activating Fc receptors*. Proc Natl Acad Sci USA, 2008. **105**(51): p. 20167-20172.

167. Rankin, C.T., et al., *CD32B, the human inhibitory Fc-gamma receptor IIB, as a target for monoclonal antibody therapy of B-cell lymphoma*. *Blood*, 2006. **108**(7): p. 2384-2391.
168. Rhodes, A., et al., *Evaluation of HER-2/neu immunohistochemical assay sensitivity and scoring on formalin-fixed and paraffin-processed cell lines and breast tumors*. *Am J Clin Pathol*, 2002. **118**(3): p. 408-417.
169. Fromant, M., S. Blanquet, and P. Plateau, *Direct random mutagenesis of gene-sized DNA fragments using polymerase chain reaction*. *Anal Biochem*, 1995. **224**(1): p. 347-353.
170. Berntzen, G., et al., *Prolonged and increased expression of soluble Fc receptors, IgG and a TCR-Ig fusion protein by transiently transfected adherent 293E cells*. *J Immunol Methods*, 2005. **298**(1-2): p. 93-104.
171. Pabbisetty, K.B., et al., *Kinetic analysis of the binding of monomeric and dimeric ephrins to Eph receptors: Correlation to function in a growth cone collapse assay*. *Protein Sci*, 2007. **16**(3): p. 355-361.
172. Jung, S.T., et al., *Aglycosylated IgG variants expressed in bacteria that selectively bind FcγRI potentiate tumor cell killing by monocyte-dendritic cells*. *Proc Natl Acad Sci USA*, 2010. **107**(2): p. 604-609.
173. Harvey, B.R., et al., *Anchored periplasmic expression, a versatile technology for the isolation of high-affinity antibodies from Escherichia coli-expressed libraries*. *Proc Natl Acad Sci USA*, 2004. **101**(25): p. 9193-9198.
174. Hinton, P.R., et al., *An engineered human IgG1 antibody with longer serum half-life*. *J Immunol*, 2006. **176**(1): p. 346-356.
175. Moasser, M.M., et al., *The Tyrosine Kinase Inhibitor ZD1839 ("Iressa") Inhibits HER2-driven Signaling and Suppresses the Growth of HER2-overexpressing Tumor Cells*. *Cancer Res*, 2001. **61**(19): p. 7184-7188.
176. Reim, F., et al., *Immunoselection of breast and ovarian cancer cells with trastuzumab and natural killer cells: selective escape of CD44high/CD24low/HER2low breast cancer stem cells*. *Cancer Res*, 2009. **69**(20): p. 8058-8066.
177. Narayan, M., et al., *Trastuzumab-induced HER reprogramming in "resistant" breast carcinoma cells*. *Cancer Res*, 2009. **69**(6): p. 2191-2194.
178. Ramsland, P.A., et al., *Structural basis for FcγRIIa recognition of human IgG and formation of inflammatory signaling complexes*. *J Immunol*, 2011. **187**(6): p. 3208-3217.
179. Indik, Z., et al., *Human Fc gamma RII, in the absence of other Fc gamma receptors, mediates a phagocytic signal*. *The Journal of Clinical Investigation*, 1991. **88**(5): p. 1766-1771.
180. Jung, S.T., et al., *Bypassing glycosylation: engineering aglycosylated full-length IgG antibodies for human therapy*. *Curr Opin Biotech*, 2011. **22**(6): p. 858-867.
181. Umaña, P., et al., *Engineered glycoforms of an antineuroblastoma IgG1 with optimized antibody-dependent cellular cytotoxic activity*. *Nat Biotechnol*, 1999. **17**(2): p. 176-180.

182. Stavenhagen, J., et al., *Enhancing the potency of therapeutic monoclonal antibodies via Fc optimization*. Adv Enzyme Regul, 2008. **48**(1): p. 152-164.
183. Nimmerjahn, F. and J. Ravetch, *Divergent immunoglobulin g subclass activity through selective Fc receptor binding*. Science, 2005. **310**(5753): p. 1510.
184. Mellor, J.D., et al., *A critical review of the role of Fc gamma receptor polymorphisms in the response to monoclonal antibodies in cancer*. J Hematol Oncol, 2013. **6**(1).
185. Shashidharamurthy, R., et al., *Dynamics of the Interaction of Human IgG Subtype Immune Complexes with Cells Expressing R and H Allelic Forms of a Low-Affinity Fcγ Receptor CD32A*. The Journal of Immunology, 2009. **183**(12): p. 8216-8224.
186. Ruffell, B., et al., *Leukocyte composition of human breast cancer*. Proceedings of the National Academy of Sciences, 2012. **109**(8): p. 2796-2801.
187. Steidl, C., et al., *Tumor-Associated Macrophages and Survival in Classic Hodgkin's Lymphoma*. New England Journal of Medicine, 2010. **362**(10): p. 875-885.
188. Solinas, G., et al., *Tumor-associated macrophages (TAM) as major players of the cancer-related inflammation*. Journal of Leukocyte Biology, 2009. **86**(5): p. 1065-1073.
189. Bingle, L., N.J. Brown, and C.E. Lewis, *The role of tumour-associated macrophages in tumour progression: implications for new anticancer therapies*. The Journal of Pathology, 2002. **196**(3): p. 254-265.
190. Chen, J., et al., *CCL18 from Tumor-Associated Macrophages Promotes Breast Cancer Metastasis via PITPNM3*. Cancer Cell, 2011. **19**(4): p. 541-555.
191. Grugan, K.D., et al., *Tumor-Associated Macrophages Promote Invasion while Retaining Fc-Dependent Anti-Tumor Function*. The Journal of Immunology, 2012. **189**(11): p. 5457-5466.
192. Jensen, H.K., et al., *Presence of Intratumoral Neutrophils Is an Independent Prognostic Factor in Localized Renal Cell Carcinoma*. Journal of clinical oncology, 2009. **27**(28): p. 4709-4717.
193. Gregory, A.D. and A. McGarry Houghton, *Tumor-Associated Neutrophils: New Targets for Cancer Therapy*. Cancer Research, 2011. **71**(7): p. 2411-2416.
194. Smith, I., C. Vedeler, and A. Halstensen, *FcγRIIa and FcγRIIIb Polymorphisms Were Not Associated with Meningococcal Disease in Western Norway*. Epidemiology and Infection, 2003. **130**(2): p. 193-199.
195. Smith, P., et al., *Mouse model recapitulating human Fcγ receptor structural and functional diversity*. Proceedings of the National Academy of Sciences, 2012.
196. Rhodes, A., et al., *The use of cell line standards to reduce HER-2/neu assay variation in multiple European cancer centers and the potential of automated image analysis to provide for more accurate cut points for predicting clinical response to trastuzumab*. American journal of clinical pathology, 2004. **122**(1): p. 51-60.

197. Nesspor, T.C., et al., *Avidity confers FcγR binding and immune effector function to aglycosylated immunoglobulin G1*. Journal of Molecular Recognition, 2012. **25**(3): p. 147-154.
198. Hinton, P.R., et al., *Engineered Human IgG Antibodies with Longer Serum Half-lives in Primates*. Journal of Biological Chemistry, 2004. **279**(8): p. 6213-6216.
199. Tao, M.-H. and S.L. Morrison, *Studies of aglycosylated chimeric mouse-human IgG. Role of carbohydrate in the structure and effector functions mediated by the human IgG constant region*. The Journal of Immunology, 1989. **143**(8): p. 2595-2601.
200. Hobbs, S.M., L.E. Jackson, and J. Hoadley, *Interaction of aglycosyl immunoglobulins with the IgG Fc transport receptor from neonatal rat gut: Comparison of deglycosylation by tunicamycin treatment and genetic engineering*. Molecular immunology, 1992. **29**(7-8): p. 949-956.
201. Ohnishi, Y., et al., *Prolonged survival of mice with human gastric cancer treated with an anti-c-ErbB-2 monoclonal antibody*. British journal of cancer, 1995. **71**(5): p. 969.
202. Baselga, J., et al., *Recombinant humanized anti-HER2 antibody (Herceptin™) enhances the antitumor activity of paclitaxel and doxorubicin against HER2/neu overexpressing human breast cancer xenografts*. Cancer research, 1998. **58**(13): p. 2825-2831.
203. Pietras, R.J., et al., *Remission of human breast cancer xenografts on therapy with humanized monoclonal antibody to HER-2 receptor and DNA-reactive drugs*. Oncogene, 1998. **17**(17): p. 2235.
204. Colomer, R., et al., *Herceptin: from the bench to the clinic*. Cancer investigation, 2001. **19**(1): p. 49-56.
205. Nahta, R. and F.J. Esteva, *Herceptin: mechanisms of action and resistance*. Cancer Letters, 2006. **232**(2): p. 123-138.
206. Vu, T. and F.X. Claret, *Trastuzumab: updated mechanisms of action and resistance in breast cancer*. Frontiers in oncology, 2012. **2**.
207. Ursini-Siegel, J., et al., *Insights from transgenic mouse models of ERBB2-induced breast cancer*. Nature Reviews Cancer, 2007. **7**(5): p. 389-397.
208. Bruhns, P., *Properties of mouse and human IgG receptors and their contribution to disease models*. Blood, 2012. **119**(24): p. 5640-5649.
209. Clatworthy, M.R. and K.G. Smith, *FcγRIIb balances efficient pathogen clearance and the cytokine-mediated consequences of sepsis*. The Journal of experimental medicine, 2004. **199**(5): p. 717-723.
210. Singer, J. and E. Jensen-Jarolim, *IgE-based immunotherapy of cancer: challenges and chances*. Allergy, 2013: p. n/a-n/a.
211. Wilson, T.J., A. Fuchs, and M. Colonna, *Cutting Edge: Human FcRL4 and FcRL5 Are Receptors for IgA and IgG*. The Journal of Immunology, 2012. **188**(10): p. 4741-4745.
212. Dhodapkar, K., et al., *Antitumor monoclonal antibodies enhance cross-presentation of cellular antigens and the generation of myeloma-specific killer T*



- cells by dendritic cells. *The Journal of experimental medicine*, 2002. **195**(1): p. 125.
213. van Montfoort, N., et al., *Fcγ Receptor IIb Strongly Regulates Fcγ Receptor-Facilitated T Cell Activation by Dendritic Cells*. *The Journal of Immunology*, 2012. **189**(1): p. 92-101.
  214. Taylor, C., et al., *Augmented HER-2-Specific Immunity during Treatment with Trastuzumab and Chemotherapy*. *Clinical cancer research*, 2007. **13**(17): p. 5133.
  215. Simpson, T.R., et al., *Fc-dependent depletion of tumor-infiltrating regulatory T cells co-defines the efficacy of anti-CTLA-4 therapy against melanoma*. *The Journal of experimental medicine*, 2013. **210**(9): p. 1695-1710.
  216. Peggs, K.S., et al., *Blockade of CTLA-4 on both effector and regulatory T cell compartments contributes to the antitumor activity of anti-CTLA-4 antibodies*. *The Journal of experimental medicine*, 2009. **206**(8): p. 1717-1725.
  217. Allison, J. and M. Curran, *Methods and Compositions for Localized Secretion of Anti-CTLA-4 Antibodies*, 2007, Google Patents.
  218. Jung, S.T., et al., *Binding and enrichment of Escherichia coli spheroplasts expressing inner membrane tethered scFv antibodies on surface immobilized antigens*. *Biotechnol Bioeng*, 2007. **98**(1): p. 39-47.
  219. Veri, M.C., et al., *Monoclonal antibodies capable of discriminating the human inhibitory Fcγ-receptor IIB (CD32B) from the activating Fcγ-receptor IIA (CD32A): biochemical, biological and functional characterization*. *Immunology*, 2007. **121**(3): p. 392-404.
  220. Bryksin, A.V. and I. Matsumura, *Overlap extension PCR cloning: a simple and reliable way to create recombinant plasmids*. *BioTechniques*, 2010. **48**(6): p. 463-465.
  221. Kawarasaki, Y., et al., *Enhanced crossover SCRATCHY: construction and high-throughput screening of a combinatorial library containing multiple non-homologous crossovers*. *Nucleic Acids Res*, 2003. **31**(21): p. e126-e126.
  222. Kuo, S.C. and D.A. Lauffenburger, *Relationship between receptor/ligand binding affinity and adhesion strength*. *Biophys J*, 1993. **65**(5): p. 2191-2200.
  223. Heiple, J.M., et al., *Macrophages form circular zones of very close apposition to IgG-Coated surfaces*. *Cell Motil Cytoskel*, 1990. **15**(4): p. 260-270.
  224. Tolentino, T.P., et al., *Measuring diffusion and binding kinetics by contact area FRAP*. *Biophys J*, 2008. **95**(2): p. 920-930.
  225. Costantini, D.L., et al., *Trastuzumab-resistant breast cancer cells remain sensitive to the auger electron-emitting radiotherapeutic agent <sup>111</sup>In-NLS-trastuzumab and are radiosensitized by methotrexate*. *J Nucl Med*, 2008. **49**(9): p. 1498-1505.
  226. Xu, F., et al., *Radioiodinated antibody targeting of the HER-2/neu oncoprotein*. *Nucl Med Biol*, 1997. **24**(5): p. 451-459.
  227. Smith, K.G.C. and M.R. Clatworthy, *FcγRIIB in autoimmunity and infection: evolutionary and therapeutic implications*. *Nat Rev Immunol*, 2010. **10**(5): p. 328-343.

- 228. Zhang, X., et al., *Follicle-stimulating hormone peptide can facilitate paclitaxel nanoparticles to target ovarian carcinoma in vivo*. Cancer Res, 2009. **69**(16): p. 6506-6514.
- 229. Krombach, F., et al., *Cell size of alveolar macrophages: an interspecies comparison*. Environ Health Persp, 1997. **105**(Suppl 5): p. 1261-1263.
- 230. Pease III, L.F., et al., *Determination of protein aggregation with differential mobility analysis: application to IgG antibody*. Biotechnol Bioeng, 2008. **101**(6): p. 1214-1222.
- 231. Sondermann, P., R. Huber, and U. Jacob, *Crystal structure of the soluble form of the human Fc $\gamma$ -receptor IIb: a new member of the immunoglobulin superfamily at 1.7 Å resolution*. EMBO J, 1999. **18**(5): p. 1095-1103.